

University of Alberta

Bioactive Rosette Nanotubes



by

Mustapha. O. St. Jules

A thesis submitted to the Faculty of Graduate Studies and Research
in partial fulfillment of the requirements for the degree of

Master of Science

Department of Chemistry

Edmonton, Alberta

Fall 2008



Library and
Archives Canada

Published Heritage
Branch

395 Wellington Street
Ottawa ON K1A 0N4
Canada

Bibliothèque et
Archives Canada

Direction du
Patrimoine de l'édition

395, rue Wellington
Ottawa ON K1A 0N4
Canada

Your file Votre référence
ISBN: 978-0-494-47419-8
Our file Notre référence
ISBN: 978-0-494-47419-8

NOTICE:

The author has granted a non-exclusive license allowing Library and Archives Canada to reproduce, publish, archive, preserve, conserve, communicate to the public by telecommunication or on the Internet, loan, distribute and sell theses worldwide, for commercial or non-commercial purposes, in microform, paper, electronic and/or any other formats.

The author retains copyright ownership and moral rights in this thesis. Neither the thesis nor substantial extracts from it may be printed or otherwise reproduced without the author's permission.

AVIS:

L'auteur a accordé une licence non exclusive permettant à la Bibliothèque et Archives Canada de reproduire, publier, archiver, sauvegarder, conserver, transmettre au public par télécommunication ou par l'Internet, prêter, distribuer et vendre des thèses partout dans le monde, à des fins commerciales ou autres, sur support microforme, papier, électronique et/ou autres formats.

L'auteur conserve la propriété du droit d'auteur et des droits moraux qui protègent cette thèse. Ni la thèse ni des extraits substantiels de celle-ci ne doivent être imprimés ou autrement reproduits sans son autorisation.

In compliance with the Canadian Privacy Act some supporting forms may have been removed from this thesis.

Conformément à la loi canadienne sur la protection de la vie privée, quelques formulaires secondaires ont été enlevés de cette thèse.

While these forms may be included in the document page count, their removal does not represent any loss of content from the thesis.

Bien que ces formulaires aient inclus dans la pagination, il n'y aura aucun contenu manquant.

■ ■ ■
Canada

ABSTRACT

Nanotechnology has the potential to create many new materials and devices which can be utilized in a wide range of applications such as medicine, electronics, efficient energy production, enhanced food production and the list goes on. Construction of a synthetic molecular motif that possesses the hydrogen bonding faces of guanine (G) and cytosine (C) affords the formation of Rosette Nanotubes (RNTs) in a variety of solvents. Chemical functionalization of this G[^]C motif revealed that it can be utilized as a scaffold for designing biomaterials. Functionalization with various amino acids and hydrogels produced helical RNTs that show promising orthopedic applications.

This thesis will look at the synthesis and characterization of fluorescent RNTs, which will be used to study the feasibility of these systems to be internalized by cells and their ability to delivery biological cargo to cells (Chapter 2). Chapter 3 looks at the synthesis and characterization of a radioactive G[^]C precursor which will subsequently be used for the self-assembly of radioactive RNTs. This system will be used to investigate the biodistribution of RNTs. These systems may also be used to investigate the mechanism of cellular internalization and to gather general information about the toxicity of RNTs.

ACKNOWLEDGEMENT

first and foremost I would like to thank almighty GOD for keeping me healthy and strong through out the course of my studies. I would like to dedicate this thesis to my grandmother (Urica Roberts) who has encouraged and supported me in all of my endeavors.

Secondly, I would like to thank my research supervisor, Prof. Hicham Fenniri for his guidance, encouragement and understanding through out the duration of my masters. I would like to give special thanks to all the members of the Supramolecular Nanoscale Assembly Group (SNAG) especially Drs. Rachel Beingessner, Baker Jawabrah Al-Hourani, Andrew Myles and Mr. Martins Oderinde for the scientific insight and suggestions.

Finally, I would like thank some special individuals who have made my stay in this cold country as warm as the Caribbean sun: Mr. Kowlasar Misir, Ryan Rambarran, Rachel Rambarran, David Rambarran and Surya Rambarran.

TABLE OF CONTENTS

Chapter 1 Introduction to Supramolecular Chemistry and Organic Nanotubes

	page
1.1. Introduction to Supramolecular Chemistry: A Historical Perspective	1
1.2. Going Beyond: From Molecular to Supramolecular synthesis	2
1.3. Supramolecular Interactions	3
1.3.1. Hydrogen Bonding	4
1.3.2. $\pi - \pi$ Interaction	7
1.3.3. The Hydrophobic Effect	8
1.4. Concepts in Supramolecular Chemistry	10
1.4.1. Host-Guest Chemistry	11
1.4.2. Self-assembly	11
1.4.3. Preorganization and Complementarity	13
1.5. Inspiration: How Nature Utilizes Supramolecular Interactions	14
1.6. Self-assembly and Self-organization of Synthetic Molecular Motifs to Nanotubular Architectures	15
1.6.1. Helical Nanotubes	17
1.6.2. DNA Nanotubes	25
1.6.3. Nanotubes from Self-assembled Amphiphiles	26
1.6.4. Packing – Directed Self-assembly	28
1.6.5. Nanotubes from Linear Amphiphiles and Block	

Copolymers via Molecular Sculpting	28
1.6.6. Nanotubes from stacked Macrocycles	33
1.7. Self-assembling Nanotubes from Stacked Rosettes	37
1.7.1. The Beginning: G-quartet	38
1.8. Summary and Overview	45
1.9. Reference	47
Chapter 2	Fluorescent Rosette Nanotubes
2.1. Introduction	62
2.2. Results and Discussion	63
2.2.1. Synthesis of G ⁺ C Twinbase (39)	62
2.2.2. Synthesis of FITC G ⁺ C Twinbase (41)	65
2.2.3. Synthesis of Biotin-Streptavidin (FITC) labeled G ⁺ C Motif (45)	67
2.3. Microscopic Characterization of FITC RNTs	69
2.3.1. Microscopic Characterization of Biotin-Streptavidin RNTs	74
2.5. Conclusion and Future Work	78
2.6. Experimental Section	79
2.6.1. General Details	79
2.6.2. Synthetic Procedure	81
2.7. References.	97

Chapter 3 Radioactive Rosette Nanotubes

3.1.	Introduction	102
3.2.	Results and Discussion	104
3.2.1.	Synthesis of MAG ₃ (49)	104
3.2.2.	Conjugating MAG ₃ (49) to Twinbases (38)	105
3.2.3	Conjugating MAG ₃ (49) to Monobase G [^] C derivatives	108
3.3.	Microscopic characterization of unchelated RNTs (63)	112
3.4.	Conclusion and Future Work	117
3.5.	Synthetic Procedures	118
3.6.	References	128

List of Figures

	Page
1.1. Types of hydrogen bonds.	4
1.2. Schematic representation of double-, tetra-, and hexarosettes assemblies.	5
1.3. Jorgensen's secondary electrostatic model.	6
1.4. Different types of $\pi - \pi$ stacking interactions.	8
1.5. Cavitand host for alkyl chains.	11
1.6. Self-assembly of the Tobacco Mosaic Virus.	15
1.7. General strategies for the design of organic nanotubes based on hollow scaffolds and their self-assembly, stacks of macrocycles and rosettes, as well as cylindrical micelles and rolled bilayers sheet.	17
1.8. Gong's helical diarylamides of varying diameter depending on their mode of connectivity.	19
1.9. Moore's amphiphilic oligo (meta-phenyleneethylene)s, 7 , and model of the octadecamer (side chains are omitted for clarity).	20
1.10. Lehn's alternating 2',6'-diaminopyridine 2,6-pyridinedicarb-oxamide oligomer 8 , and favored kinked conformation due to H-bonding.	21
1.11. Meijer's helically folding ureidophthalimides 9 (DMAP).	21
1.12. Lehn's oligo(pyridine-alt-pyrimidine)s 10 and crystals structure of 13 mer ($n = 5$). CCDC-100440; N-atoms are black, C-atoms are gray, side chains are light, H-atoms are omitted for clarity.	22
1.13. Extending the helical diameter using the para-connected pyridazine heterocycle to afford oligo(pyridine-alt-pyridazine)s 11 . Model (N-atoms are black, C-atoms are gray, S-atoms are light, H-atoms and side chains are omitted for clarity) and freeze-fracture electron micrograph of 11 in CH_2Cl_2 (a) and pyridine (b) showing fiber network formation	

- with helical texture. 23
- 1.14. Self-assembly of vesicles and subsequent transformation into helical tubes in decane. 24
- 1.15. Side and top view of the hydrogen – bonded nanotubular structure formed by L – 1. 24
- 1.16. Self-assembly of DNA tiles into sheets and tubes. (A) structure of the double crossover tiles: arrowheads mark the 3' end of each oligonucleotide. The 6 nt single-stranded sticky ends on the α tile are complementary to those on the β tile; complementary shapes on the schematic representations of the tiles indicate complementary stick ends. The 5' biotin label on the β tile is represented by a black dot. (B) α and β tiles tessellate to form extended two-dimensional arrays. We propose that the fold and close upon themselves to form tubes, producing either alternating rings (C) or nested helices (D) of α and β tiles. 25
- 1.17. Schematic illustration of the different pathways of self assembly of an amphiphile from micellar bilayers in water (micelles, helical ribbons, nanotubes) as well as from inverse bilayers in toluene (micelles, multilayered vesicles, nanotubes) toward smooth tubular rods. 27
- 1.18. Variety of methods to yield nanotube structures: (1) chiral molecular self assembly; (2) packing-directed self-assembly based on an unsymmetrical bolaamphiphile; (3) self-assembly of a rod-coil copolymer into a nanotube; (4) nanotube formation from a triblock copolymer via a molecular sculpting process, which involves (f) self-assembly, (g) cross-linking of the shell, and (h) decomposition of the core by ozonolysis; (5) self-assembly or deposition of molecules inside the pore as a substrate. 27
- 1.19. Perec's wedge-shaped amphiphilic gallate **12** (*top*), cartoon illustrating assembly of amphiphile into layered tubes; Gin's analogue gallate **13** with H-bond-stabilized inner core and crosslinkable periphery (*bottom*). 29
- 1.20. Selected linear amphiphiles assembling into tubes: double-chain ammonium amphiphile (**14**), unsaturated double-chain phosphatidylethanolamine (**15**), diacetylenic aldonamide (**16**)

and aromatic glycolipid (17).	29-30
1.21. Stewart and Liu's approach to polymeric nanotubes based on block copolymer assembly followed by photocrosslinking of the poly (2-cinnamoyl ethyl methacrylate) (PCMA) shell and removal of the polyisoprene core by ozonolysis.	31
1.22. Self-assembly of PMOXA-PDMS-PMOXA (19) copolymers in solution.	31-32
1.23. Diagrammatic sketch of HBPO-star-PEO (left) and its self assembly into macroscopic tubes (right).	33
1.24. Schematic diagram of nanotube from assembly of cyclic D, L-peptides.	34
1.25. Stoddart's stacked cyclic oligosaccharides 21 and 22.	35
1.26. Phenolic functionalize PAM, 23, and its space filling model.	36
1.27. Strategy for the synthesis of cyclic comb like copolymers and their self-assembly. PS-DPELi, (1, 1-diphenylethylene) end-capped polystyryllithium; PI DPELi, (1,1-diphenylethylene) end-capped polyisoprenyllithium.	37
1.28. Cartoon depicting assembly of Rosette Nanotubes (RNTs).	37
1.29. Self assembly of G-quadruplex from 5'GMP.	38
1.30. Self association of G5 and isoG6 in the presence of cations to give hydrogen bonded G ₄ – quartets and isoG ₅ -pentamers.	39
1.31. Sessler's cation free G – quartet.	40
1.32. Modes of self- assembly of CA and M into rosettes and linear tapes.	40
1.33. Self-assembly of a bismelamine and bisisocyanurate into nanocylinders.	41
1.34. Kunitake's binary melamine-diimide system.	42
1.35. Molecular structures of OPVT3 and OPVT4.	42

1.36.	Fenniri's rosette forming pyrimido-pyrimidinedone motif, 24 (G [^] C base).	43
1.37.	Hierarchical self assembly of 25 into six member rosette and subsequently nanotubes (stained TEM (a) and TM-AFM (b) images).	44
1.38.	Structures of Momo- and Twinbase G [^] C motifs functionalize with lysine.	44
2.1	SEM (A and B) and TM-AFM (C and D) of 39 (0.025 mg.mL ⁻¹) in water immediately after preparation.	69
2.2	Representative SEM micrographs [(A) unstained (B) stained with ua] and TEM [C and D] micrographs of 41 in water, scale bar = 50 nm (E) UV-vis time study of 41 in water.	71
2.3.	Molecular modeling of 41 in water (F) graph showing the relative free energy of RNTs in water (G) Leonard Jones outer diameter of the rosette (H) model of the G [^] C motif of 41 and visual representation of a RNT.	73
2.4.	Representative SEM image of compound 45 (A) 1 mg.mL ⁻¹ in water after 2 days (B) 0.025 mg.mL ⁻¹ in DMSO immediately after preparation (C) 0.025 mg.mL ⁻¹ in DMSO after 2 h (D) 0.025 mg.mL ⁻¹ in DMSO after 1 week (E) time dependent UV-vis study of 45 in water.	75
2.5.	Representative TM-AFM micrographs of 45 (A and B with height profile inset), (C) SEM micrograph, stained with ua (D) TEM micrograph stained with ua. Scale bar = 50 nm	76
2.6.	Representative SEM micrographs of biotin RNTs complexed with streptavidin (FITC) in water – PBS buffer, pH = 7.4 (A & B) filtered sample (C & D) unfiltered sample.	77
3.1.	Scheme depicting the synthesis of radioactive RNTs.	103
3.2.	Steric interaction between twinbase and MAG ₃ -HBTU activated ester.	107
3.3.	Non-representative SEM micrograph of compound 63 in water (A) time dependent UV-vis study in water. (B) 1mg.mL ⁻¹ after 2 days. Representative SEM micrographs from a 0.05 mg.mL ⁻¹	

- in DMSO (C) after 3 days (D) after 1 week (E) after 1 week stained with ua. 112-113
- 3.4 Representative TM-AFM (F and G with height profile inset) and TEM micrographs (H and I) of compound **63** (0.05 mg.mL⁻¹ DMSO, 1 week old solution).Scale bar = 50 nm. 114
- 3.5. Molecular model of rosette and a RNT formed from radioactive labeled G[^]C motif (compound **64**). 116

List of Schemes

	page
1.1. Formation of a cyclodextrin nanotube by covalent capture of a polyrotaxane precursor. Treatment of the non-covalent assembly with epichlorin captures the cyclodextrins to yield a molecular tube that is unoccluded after removal of the polyethylene glycol thread	35
2.1. Large scale synthesis of the twinbase G [^] C motif, 39	65
2.2. Synthesis of the FITC functionalized twinbase G [^] C motif, 41	66
2.3. Synthesis of RNTs functionalized with biotin-streptavidin complex	68
3.1. Synthesis of mercaptotriglycine (MAG ₃) ligand, 49	104
3.2. Conjugation of MAG ₃ to twinbase 38	106
3.3. Conjugation of MAG ₃ to twinbases with amino linkers	108
3.4. Synthesis of the monobase G [^] C derivative of 54	109
3.5. Synthesis of radioactive nanotubes	110

LIST OF ABBREVIATIONS

AFM	Atomic Force Microscopy
Boc	<i>t</i> -Butyloxy carbonyl
(Boc) ₂ O	Di- <i>t</i> -Butyl dicarbonate
br	Broad
C	Carbon or Celsius
Calcd	Calculated
CD	Circular Dichroism
CHCl ₃	Chloroform
CH ₂ Cl ₂	Methylene Chloride
CH ₃ CN	Acetonitrile
CNT	Carbon Nanotube
Cbz	Carboxybenzyl
CDI	Carbonyldiimidazole
d	Doublet
Da	Dalton
DCC	Dicyclocarbodiimide
DCU	Dicyclohexylurea
DCE	1,2-Dichloroethane
DCM	Dichloromethane
dH ₂ O	Deionized water
DIEA	Diisopropylethylamine

DLS	Dynamic Light Scattering
DMAP	4- <i>N,N</i> -Dimethylaminepyridine
DMF	Dimethyl formamide
DMSO	Dimethylsulfoxide
DNA	Deoxyribonucleic acid
EA	Ethyl acetate
ESI	Electrospray Ionization
Et ₃ N	Triethylamine
Et ₂ O	Diethyl ether
FITC	Fluorescein isothiocyanate
G [^] C	Guanine – Cytosine
h	Hour
HATU	1-hydroxy-7-azabenzotriazole
H-bond	Hydrogen bonding
HCl	Hydrochloric acid
Hz	Hertz
Hex	Hexane
HR	High resolution
K ₂ CO ₃	Potassium Carbonate
<i>J</i>	Coupling constant
kDa	Kilo Daltons
kV	Kilovolts

L	Litres
LCMS	Liquid chromatography mass spectrometry
m	Multiplet
MeOH	Methanol
ML	Milliliters
mp	Melting point
MS	Mass spectrometry
NaHCO ₃	Sodium hydrogen carbonate
NaHB(OAc) ₃	Sodium triacetoxyborohydride
Na ₂ SO ₄	Sodium Sulfate
NH ₄ Cl	Ammonium chloride
NH ₂ OH.HCl	Hydroxylamine hydrochloride
NMR	Nuclear magnetic spectroscopy
NT	Nanotube
PAMs	Phenylacetylenes macrocycles
PEG	Polyethylene glycol
POCl ₃	Phosphorous oxychloride
ppm	Part per million
R _f	Retention factor
RNT	Rosette nanotube
rt	Room temperature
s	Singlet

SEM	Scanning Electron Microscopy
t	Triplet
TCT	2,4,6-Trichloro-1,3,5-triazine
TLC	Thin layer chromatography
TEM	Transmission electron microscopy
TFA	Trifluoroacetic acid
TFAA	Trifluoroacetic anhydride
THF	Tetrahydrofuran
TLC	Thin layer chromatography
TM-AFM	Tapping mode atomic force microscopy

Chapter 1: Introduction to Supramolecular Chemistry and Organic Nanotubes.

Supramolecular chemistry: 'Chemistry beyond the molecule', bearing on the organize entities of higher complexity that results from the association of two or more chemical species held together by intermolecular force.

1.1. Introduction to Supramolecular Chemistry: A Historical Perspective

Supramolecular chemistry deals with the study of non-covalent interactions such as hydrogen bonds, electrostatic, van der Waals, and π - π interactions and how these interactions are utilized in connecting molecular modules to form supramolecular structures. Supramolecular chemistry, as a discipline, dates back to the 1960s; however the fundamentals of the field goes back as far as Sir Humphrey Davy's discovery of chlorine calthrate hydrate, the inclusion of chlorine within a solid water lattice, in 1810.¹ Other basic concepts of this research area were developed by the likes of Joannes Diderik van der Waals, intermolecular forces (1893), Coordination chemistry by A.Werner in 1893,² the 'lock and key' principle of Nobel laureate Hermann Emil Fisher,³ and the recognition by Paul Ehrlich in 1906 that molecules donot act if they donot bind, *Corpora non agunt nisi fixate* ; in this way Erlich introduced the concept of biological receptors.

The field of supramolecular chemistry was firmly established by the 1987 Nobel laureates for chemistry Donald. J. Cram,⁴ Charles. J. Pedersen⁵ and Jean-Marie Lehn.⁶ Lehn have been dubbed as the 'father of supramolecular chemistry' for his enormous contribution to the field. He introduced "cryptands"- bicyclic host for binding ions, hosts with multiple binding sites, popularized the idea of self-assembly and produced some of the first good synthetic examples, elucidate what supramolecular chemistry is and what it may be used for in the future.⁷ As time passed, supramolecular chemistry became more sophisticated with researchers such as Rebek,⁸ Zimmerman,⁹ Wuest,¹⁰ Stoddart,¹¹ Diedrich,¹²

Rheinhoudt,¹³ Whitesides,¹⁴ Vogtle,¹⁵ Atwood,¹⁶ and others, making enormous contributions to the development of the discipline that is now supramolecular chemistry.

1.2. Going Beyond: From Molecular to Supramolecular Synthesis

A molecule is usually understood to be a stable collection of atoms connected by a continuous network of covalent bonds. The development of methods for the construction of these networks has been the central focus of organic chemistry, and the success of these methods have made possible the power, elegance, and utility of organic synthesis.¹⁷ The synthesis of Vitamin B₁₂,¹⁸ playtoxin,¹⁹ and other complex natural products demonstrate the extraordinary sophistication of this field. The advantage of this field is the ability to create arrays of covalently linked atoms in a well defined and controlled manner. Thus, molecular chemistry has proven to be extremely fruitful for the synthesis of molecules with molecular weights in the range of 100-3000 Da.²⁰ The synthesis of molecules such as vitamin B₁₂ required enormous manpower (~ 100 collaborators) and time (~ 10 years), and as such the construction of assemblies at the nanoscale level, 10–100 KDa, may be viewed as prohibited from a molecular synthetic standpoint.²¹ Thus, to construct systems at the nanoscale level, synthetic chemists must look for new approaches and embrace the novel concepts provided by supramolecular chemistry.

Supramolecular chemistry utilizes all the resources of molecular chemistry to design molecular components, however; supramolecular entities are only realized by the making and breaking of non-covalent bonds following an Aufbau strategy incorporated into the design of the molecular components.²² Supramolecular synthesis will allow us to move from simple to complex systems, onto living and thinking matter and ever up the ladder of complexity.

1.3. Supramolecular Interactions

Supramolecular aggregates are constructed by the cooperative effect of non-covalent interactions. Non-covalent forces are considerably weaker than covalent ones, which range from 150 kJ mol⁻¹ to 450 kJ mol⁻¹ for a single bond. Non-covalent bonds range from 2 kJ mol⁻¹ for dispersion interactions to 300 kJ mol⁻¹ for ion-ion interactions.¹ They can be divided into several different classes. Attractive or repulsive interactions are found when two partial charges interact either with opposite polarity (attraction) or with the same polarity (repulsion). Some of the most important non-covalent interactions are listed below;¹ however, only hydrogen bonding, hydrophobic and π - π interactions will be discussed here because these are most prevalent in supramolecular entities. For a more detailed discussion of non-covalent interactions see *Modern Physical Organic Chemistry* [ref. 23].

Interaction	strength(kJ mol ⁻¹)	example
Ion-ion	200-300	Tetrabutylammonium
Ion-dipole	50-200	chloride
Dipole-dipole	5-50	Sodium[15]crown-5
Hydrogen bonding	4-120	Acetone
Cation- π	5-80	Water
π - π	0-50	K ⁺ in benzene
van der Waals	< 5, may vary depending on surface.	Benzene and graphite Argon; packing in molecular crystals.
Hydrophobic/solvent effect.	Related to solvent-solvent interaction energy.	Cyclodextrin inclusion compounds.

Table 1: Summary of Supramolecular Interactions.

1.3.1. Hydrogen Bonding

The electrostatic model describes a hydrogen bond as a columbic interaction between a polar bond donor ($Dn^{\delta-} - H^{\delta+}$) and an acceptor atom ($:Ac^{\delta-}$). Due to their strength and high degree of directionality, hydrogen bonds are probably the most important non-covalent interactions used in the designing of supramolecular architectures. The strengths of hydrogen bonds range from 4-120 kJ mol^{-1} and can be divided into three categories. Those between 15 to 120 kJ mol^{-1} are considered to be very strong, those in the 21 to 59 kJ mol^{-1} range are moderate, and those in the 0 to 17 kJ mol^{-1} – the most common type of hydrogen bonds – are weak.^{1,23} Several factors determine the strength of hydrogen bonds, such as electronegativity, resonance, geometry, and the nature of the donor and acceptor. However, solvent effect plays the largest role in determining hydrogen bond strength. Direct hydrogen bonding between a donor and an acceptor is term as primary hydrogen bonding; it's attractive in nature. There are also secondary interactions between neighboring groups that can be attractive or repulsive in nature.

In supramolecular chemistry, synthetic organic modules are capable of forming extensive networks of hydrogen bonds through molecular recognition leading to supramolecular architectures.

The stability of these supramolecular architectures are directly dependent on the acidity and basicity of the donor and acceptor sites respectively, the number of hydrogen bonds

and the nature of the donor- acceptor geometric relationship.²⁴ The effect of acidity and basicity on the stability of supramolecular structures is somewhat limited because most systems utilize mostly oxygen and nitrogen atoms as their acceptor site and hydrogen atoms as the donor site. It should be noted that there

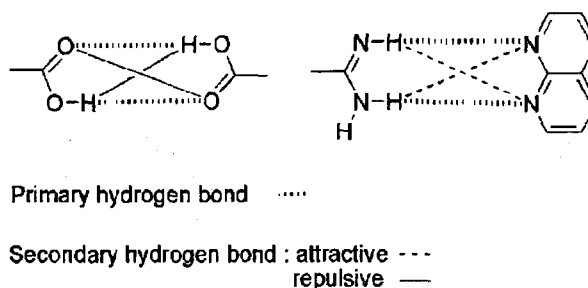


Figure 1.1. Types of hydrogen bonds

is not a general correlation between the number of hydrogen bonds and complex stability. However, Reinhoudt and coworkers showed how increasing the number of hydrogen bonds, by covalently linking rosettes, can increase the stability and rate of self-assembly of such systems (Fig. 1.2).²⁵ The relative thermodynamic stabilities of the hydrogen bonded rosettes can be obtained by the melting point index $I_{TM} = HB / (N-1)$, (HB = number of hydrogen bonds, N = number of components present in the assembly).²⁶ The geometry, more so the nature of the secondary interactions, has a profound effect on the stability of supramolecular structures. This is illustrated by comparing the association between diaminopyridine **1** and uracil **2** (equation 1) and guanine **3** and cytosine **4** (equation 2).

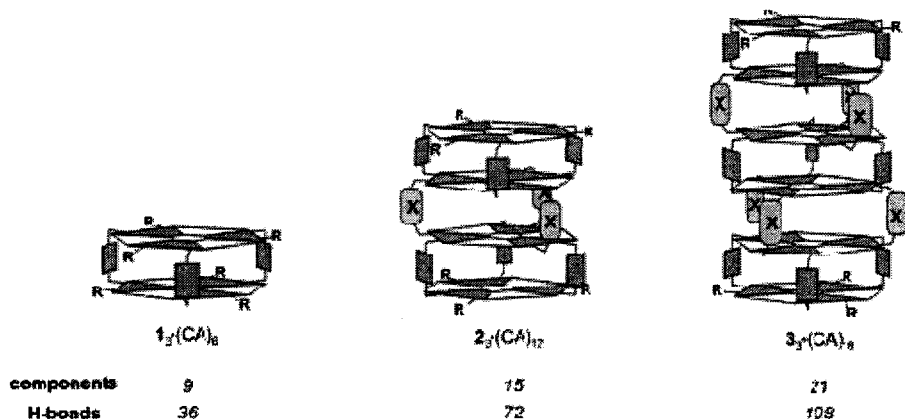
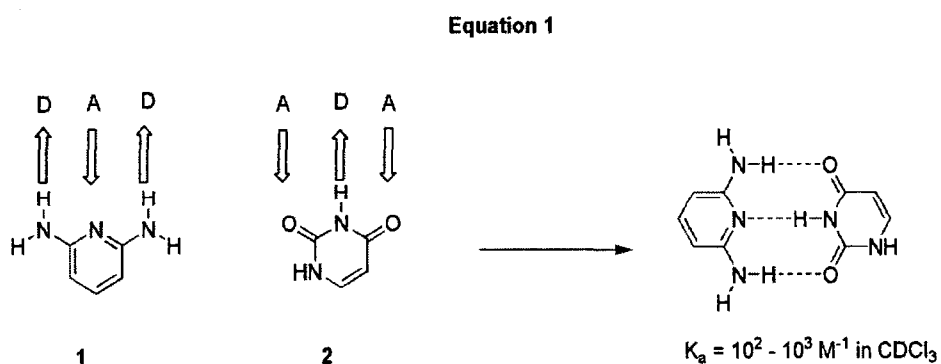
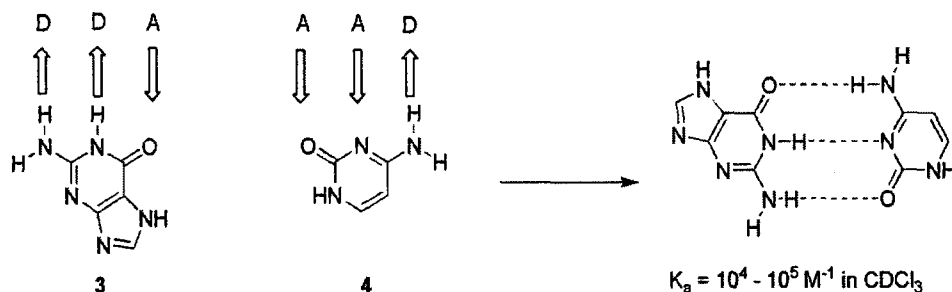


Figure 1.2. Schematic representation of double-, tetra-, and hexarosettes assemblies.



Equation 2



Jorgensen showed how secondary hydrogen bonding arising from different arrangements of hydrogen bond donor and acceptor groups affected the K_{assoc} of triply hydrogen bonded complexes.²⁷ Systems with the ADA•DAD hydrogen bonding array have four repulsive secondary interactions which weaken the binding (k_{assoc}) of such systems, while those that possess the AAA•DDD array have four attractive secondary interactions that strengthen binding.

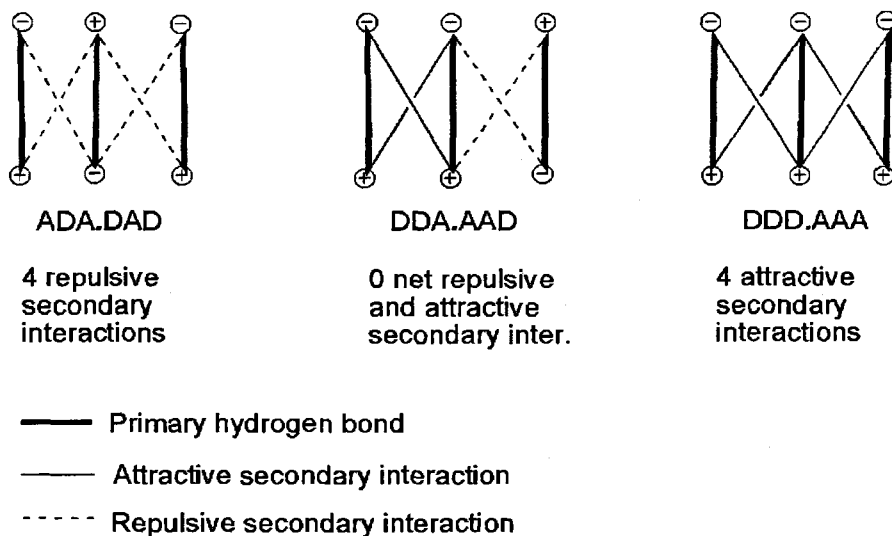


Figure 1.3. Jorgensen's secondary electrostatic model.²⁷

Zimmerman, testing the Jorgensen model, found that the thermodynamic stabilities of dimers with 0, 2 and 4 favorable secondary interactions had stability

constants of 10^2 , 10^3 - 10^4 and $>10^5$ respectively in chloroform, which was in agreement with Jorgensen model.²⁸ Secondary interactions that result from donor and acceptor atoms involved in hydrogen bonding have a destabilizing effect of $\sim 7 \text{ kJ mol}^{-1}$, whereas those interactions that have donor and acceptor atoms that are not involved in hydrogen bonding have a destabilizing effect of $\sim 11 \text{ kJ mol}^{-1}$.²⁹ With the advancement of computational approaches one will soon be able to measure the stability (absolute free energy) of self-assembled structures. However, by using experimental data and empirical relationships it is possible to qualitatively predict the stability of hydrogen bonded complexes.

1.3.2. π - π Interaction

Cation- π and π - π interactions are the two main types of interactions found in supramolecular systems. Cation- π interactions are prominent in organometallic chemistry and are not considered to be a non-covalent force.³⁰ The term π - π interaction is often misused in molecular recognition to mean π stacking, i.e., it is somehow favorable to stack two π systems directly on top of each other. However, the electrostatic potential surface of benzene clearly shows that this is not possible, since this will lead to adverse electrostatic repulsion due to the electron rich character of the π cloud.^{31a}

The two types of attractive π - π interaction are the edge-to-face (T-shape) and the face-to-face (slipped stacked). In the T-shape geometry a hydrogen atom of one ring interacts in a perpendicular fashion with the centre of another ring, while in the face-to-face arrangement parallel ring systems are separated by 3.5 \AA , are offset, and the interaction is between the centre of one ring and the corner of another (Fig 1.4). π interactions take advantage of the rich molecular orbitals of aromatic and vinyl systems. Determination of the strength and geometry of π - π interactions are based on the Hunter and Saunder model.³¹

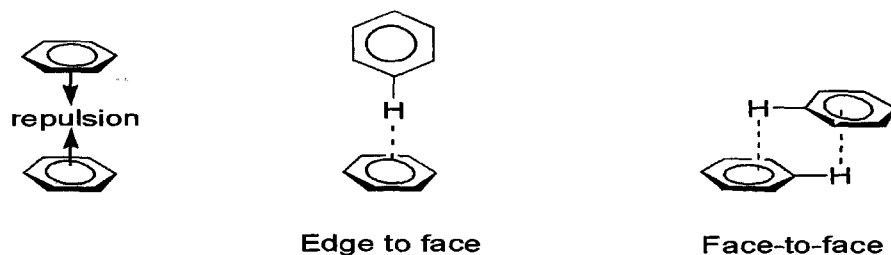


Figure 1.4. Different types of π - π stacking interactions.

The essence of the model is that it shows that π - π interactions are not due to electrostatic interaction between the two π systems, but rather when attractive interactions between π -electrons and the σ -framework outweigh π -electron repulsion. It also shows that π - π interaction is based upon polarize aryl hydrogen and π electrons interaction.^{31b} These π - π interactions play an important role in a wide variety of processes such as the stabilization of the double helical structure of DNA,³² the packing of aromatic molecules in crystals,³³ molecular recognition³⁴ and biomolecular self-aggregation.^{32,35} However, the most stable conformation is still a matter of serious debate and research due to the difficulties associated with extricating the contributions made from van der Waals and electron-donor interactions.

1.3.3. The Hydrophobic Effect

The hydrophobic effect is described simply as the exclusion or aggregation of nonpolar (organic) compounds in water.^{1,23} This simple definition can in no way begin to describe this complex phenomenon. Hydrophobic interactions are considered to be essential to many systems, be it micelles, vesicles, colloids, membrane and transport, self-organization, polymer interactions, protein folding and ligand binding, nucleic acids, drug action or water mediated organic reactions.^{36,37b} There are many models and interpretations as to the nature of the hydrophobic effect. This report will use the 'iceberg' model of Frank and Evans,^{37a} with an emphasis of keeping the discussion as simple as possible. The hydrophobic effect can be manifested in two ways: (1) the low solubility of

hydrocarbons in water, which can be measured by ΔG° for the transfer of organic molecules from the gaseous phase/hydrocarbon solution to water; (2) the tendency of organic molecules to aggregate or associate in water, which is typically measured by ΔG° of association/binding constants. The interactions between water molecules are very strong. Therefore creating a cavity in water by dissolving organic molecules would incur a significant enthalpic penalty, i.e., the breaking of hydrogen bonds. This penalty can be compensated for because there is little binding between hydrocarbons, which are nonpolar and polarizable, and polar water molecules; as a result these two would prefer to bind to their kind. The aforementioned factors are enthalpic in nature; however, close observation of the hydrophobic effect shows that its thermodynamics also has an entropic component.

Using the 'like dissolves like' paradigm, we know that hydrocarbons aggregate in water thus, if two hydrocarbon molecules are placed in water, ΔG° is favorable (< 0) for the non-covalent aggregation. However, it is often observed that ΔH° for the aggregation is small and sometimes even unfavorable (> 0), hence; ΔS° is favorable (> 0) leading to the conclusion that the hydrophobic effect is often entropically driven. The combination of two or more molecules would be considered entropically unfavorable. To explain, or rather rationalize, such behavior the 'iceberg' model is invoked.³⁸

The iceberg model in its simplest form states that when a nonpolar molecule is dissolved in water it modifies the water structure in the direction of greater crystallinity - the water so to speak builds a microscopic iceberg around it.³⁸ Water is not maximally hydrogen bonded as is the case with solid ice, which has a rigid structure with four hydrogen bonds. However, ice has a lower enthalpy than liquid water due to more hydrogen bonds and is thus entropically disfavored due to increase order. As stated earlier, it is unfavorable to dissolve hydrocarbons in water. To compensate for this, the local water structure around the solute becomes

more rigid by strengthening and increasing the number of hydrogen bonds. The near equal enthalpy, before and after dissolution, and clear loss of entropy explains why organic molecules have low solubility in water. When two or more hydrophobic molecules aggregate in water there is a reduction in surface area exposed to water, thus reducing the amount of 'ice-like' water. This is enthalpically unfavorable, but entropically favorable since more 'normal water' is produced, and so association is entropically driven.

The 'iceberg' model has been modified to be more quantitative in nature by using the flickering cluster model for liquid water proposed by Frank and Wen.³⁹ There are several other alternative models to the 'iceberg model' such as that reported by Miller and Hilderband,⁴⁰ which states that there is a loss of entropy upon solution of apolar gas without the formation of a rigid structure. There is also the model proposed by Howarth,⁴¹ who reported an interpretation of entropy of hydration of apolar compounds in terms of restricted motion of the hydrophobic parts of the solute molecule. Debate and research into the origin and nature of the hydrophobic effect is currently ongoing so as to gain a better understanding of this effect and more importantly, how it may be harnessed to build supramolecular structures.

1.4. Concepts in Supramolecular Chemistry

Supramolecular chemistry is truly multi-disciplinary in nature, drawing on principles from various fields such as chemical, biological and physical sciences, and engineering. As a result, an ever expanding degree of concepts are utilized to fabricate complex supramolecular architectures ranging from coordination chemistry to biological engineering to molecular machines. Only a few of the fundamental concepts will be elucidated here to give the reader some insight into what constitutes supramolecular chemistry.

1.4.1. Host - Guest Chemistry

Supramolecular chemistry can be broadly categorized into two areas: (1) host-guest chemistry and (2) self-assembly. Nobel laureate Donald Cram described a host as an organic molecule or ion whose binding sites converge in the complex.

The guest is any molecule or ion whose binding sites diverge in the complex. In these definitions, hosts are synthetic counterparts of the receptor sites of biological chemistry, and guests are the counterparts of substrates, inhibitors, or cofactors.⁴² The host – guest relationship requires a complementary stereoelectronic arrangement of binding sites in host and guest. A good representation of host-

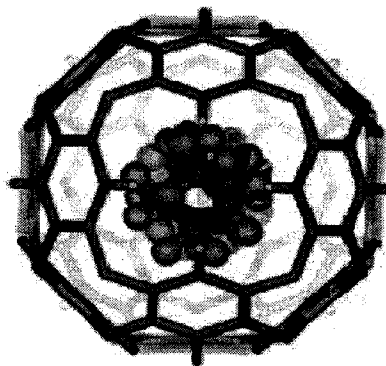


Figure 1.5. A cavitand host for alkyl chains.⁴⁴

guest chemistry is the metal-ligand complexes of coordination chemistry. Host species are divided into two categories: cavitands and clathrands. Cavitands may be described as hosts that have internal (intramolecular) cavities with specific binding sites – they act as host in both solution and solid state. A clathrand is described as a host that has extramolecular cavities, usually represented as a gap between host molecules, and exist only in the solid state.^{1,43}

1.4.2. Self-assembly

Self-assembly is the autonomous organization of components into patterns or structures without human intervention. Self-assembling processes are common throughout nature and technology. They involve components from the molecular to planetary weather system and many different type of interactions.⁴⁵ The hypothesis of self-assembly first arose from research in biological chemistry. Unraveling the complex nature of cells led to the concept that those structures were as a result of convergent assembly of smaller units.⁴⁶ The discipline of self-assembly is an area of active research, and its concepts and terminologies are ever

evolving. Lindsey produced an effective stratified framework of self-assembly in biological and chemical systems.⁴⁷

The term self-assembly is usually applied to systems in which the assembly is kinetically driven and completely reversible and replicable. This reversible characteristic of supramolecular structures imparts a unique feature to such systems, which is their ability to correct mistakes during assembly and gradually work their way to the most thermodynamically stable product. Any system that is capable of forming more than one product can be thought of as a *dynamic combinatorial library* – where the association and disassociation of these products are an ongoing process tending towards the most thermodynamically stable product. Thus, since self-assembly is an equilibrium process the position of equilibrium can be influenced by such parameters as heat, concentration, temperature etc.

Often self-assembled systems have more than one form of non-covalent interaction contributing to the stability of the system. In such systems the assembly process is dictated by optimizing the strongest interaction followed by the weaker ones. This type of assembly is usually referred to as *hierarchical self-assembly*: self-assembly comprising several separate levels or processes that cannot occur until the preceding one is complete.

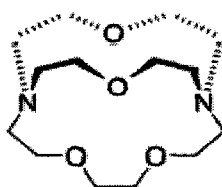
Because self-assembly tends toward the most thermodynamically stable product then both enthalpic and entropic factors are responsible for the final product. Self-assembled products are the result of favorable interactions, i.e., the process is enthalpically favourable. However, the process of aggregation is entropically unfavorable. The entropic cost is offset by the release of solvent molecules that were interacting with the molecular components that make up the aggregates of self-assembled systems - *solvophobic effect*. Generally, a system will assemble into a cyclic (discrete) architecture over an open oligomeric structure because its

enthalpic gain usually outweighs its entropic loss; this phenomenon is known as enthalpy-entropy compensation.⁴⁸

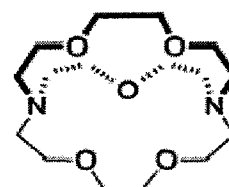
1.4.3. Preorganization and Complementarity

Complementarity plays an important role in biological and supramolecular systems. For example, the function of an enzyme: the active site of the enzyme is arranged in such way that it is functionally compatible with the substrate. Complementarity simply refers to a host and a guest that complement each other, whereby the host has binding sites that simultaneously contact and attract the binding sites of the guest without generating any internal strain or strong nonbonding repulsions.⁴⁹ Complementarity is shown by the two cryptands. Cryptand (1) selectively binds Li^+ over Na^+ by a factor of 4800, while cryptand (2) binds Na^+ over Li^+ by a factor of 440,000.

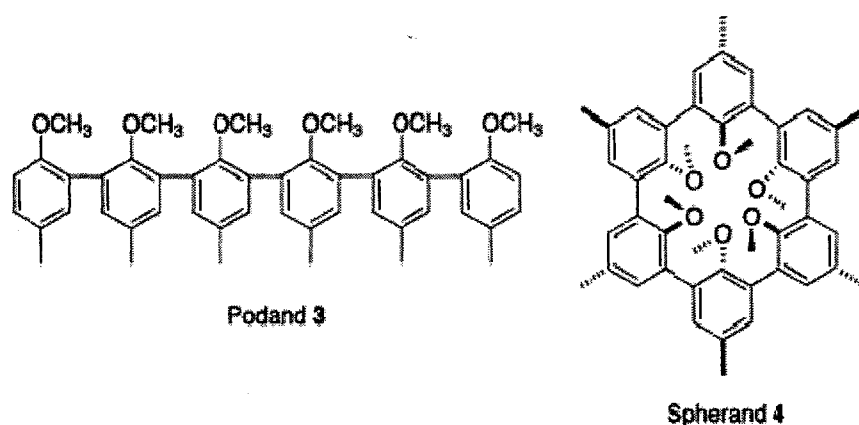
A host is said to be *preorganized* if its binding sites are in a well defined and complementary geometry with respect to that of the guest and it does not require a significant conformational change for binding. The more highly organized a host and guest are for binding, and the lower solvation prior to complexation, the more stable the complex will be. Preorganization is exemplified by the *macrocyclic effect*: this is where a host contains one or more large rings (macrocycles) with in its structure. These macrocyclic hosts are much more efficient at binding guests than their acyclic analogues because they are more rigid (entropically favorable) and any unfavorable enthalpic cost is prepaid during their synthesis.⁴⁹ Spherand 4 is much more preorganized than podand 3 because all the oxygen atoms are in the right orientation to bind cationic guest, whereas podand 3 would have to undergo conformational change for binding to occur.



Cryptand 1



Cryptand 2



1.5. Inspiration: How Nature Utilizes Supramolecular Interactions

The origins of supramolecular chemistry are deeply influenced by the ever evolving, ever inspiring, biological systems found in nature. One of the main goals of supramolecular chemistry is to synthesize abiotic, biomimetic analogues of biological systems that may be able to perform functions that are currently impossible.

The self-assembly of the α -helix of deoxyribonucleic acid (DNA), which carries the genetic information needed to create living organisms, is the most famous example of supramolecular chemistry being displayed in nature. The double helix of DNA is formed by the self-assembly of two strands via hydrogen bonding and π - π stacking interactions. The double helix shape of DNA minimizes contact of the nucleobase with the aqueous environment thereby optimizing internucleobase interaction while minimizing empty space in the interior. The nucleobases that make up DNA strands have complementary hydrogen bonding sites that cooperatively zip up into the famous double helix.

The concepts and interactions of supramolecular chemistry are prominently featured in the self-assembly of viruses, the most common being the Tobacco Mosaic Virus (TMV). The viral particle is made up of 2130 identical subunits,

each composing 150 amino acids, which form a helical sheet around a single strand of RNA, 6390 base pair in length. The virus is formed by the threading of the nucleic acid strand through two stacked protein discs, which have a templating effect for the helix formation. What makes the TMV remarkable is that it may be broken down into its components parts, and when remix under physiological conditions it will reassemble into a fully functional replica that is indistinguishable from the original.^{1,50}

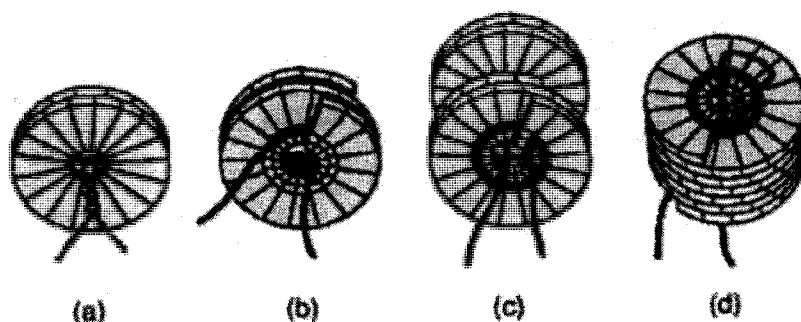


Figure 1.6. Self-assembly of the Tobacco Mosaic Virus.

1.6. Self-assembly and Self-organization of Synthetic Molecular Motifs to Nanotubular Architectures

Supramolecular chemistry has evolved into an area of vigorous interdisciplinary research that impinges on chemistry, biology, physics and engineering. Lehn, in 2002, added a functional definition: “supramolecular chemistry aims at developing highly complex chemical systems from components interacting by non-covalent intermolecular forces.”²²

Thus, in attempting to design ever more complex functional systems, supramolecular chemistry has led to the dawn of the nanotechnological era. Nanotechnology is broadly defined as the production of functional materials with features in the region of 0.1–500 nm in size, and is accomplished either through the top-down or bottom-up approaches.⁵² Traditional nanotechnology uses the top-down approach; however, this approach is becoming less feasible as the size

of devices become ever smaller. To realize the potential of nanotechnology, scientists have embraced the bottom-up approach which typically features some aspect of self-assembly.

The main goal of the nanotechnological era is to produce electronic devices that are continually being miniaturized. To this end, tubular nanoobjects are of essential importance because of their inherent geometric features that differentiate between defined inner and outer surfaces as well as termini giving rise to controllable spatial segregation. This property is associated with cylindrical dimensionality, which encodes both the directionality necessary for transport processes and the addressability needed for the generation of more complex architectures by self-assembly or rational manipulation.⁵³

Biological systems have made use of microtubules for a variety of functions such as transmembrane ion channels,⁵⁴ closed reaction chambers for protein degradation and protein folding,⁵⁵ and use of cytoskeletal microtubules as scaffolds.⁵⁶ Thus, biomimetic nanotubular structures can potentially perform a variety of tasks such as drug delivery, nanoreactors for analytical applications, insulated nanowires, catalysis, transporter of ionic and chiral species and light emitters for photonics.

This part of the introductory chapter will review literature that deals with the construction of organic nanotubes via covalent, but more so using non-covalent interactions, and highlight some possible applications of such materials. The primary focus of this section will be on the construction of these nanotubular architectures using synthetic molecular motifs. Carbon nanotubes⁵¹ and inorganic nanotubes will not be discussed here because their fabrication is not based on non-covalent interactions.

Tubular nanostructures are generated from the molecular information stored in chemical bonds, shape and linkage geometry, recognition sites and local solvophilicity and solvophobicity. Organic nanotubes can be constructed in one of the four following ways: (1) coiling of linear/helical precursors (2) stacking of macrocyclic rings (3) stacking of rosettes (4) amphiphilic assemblies (Fig 1.7).

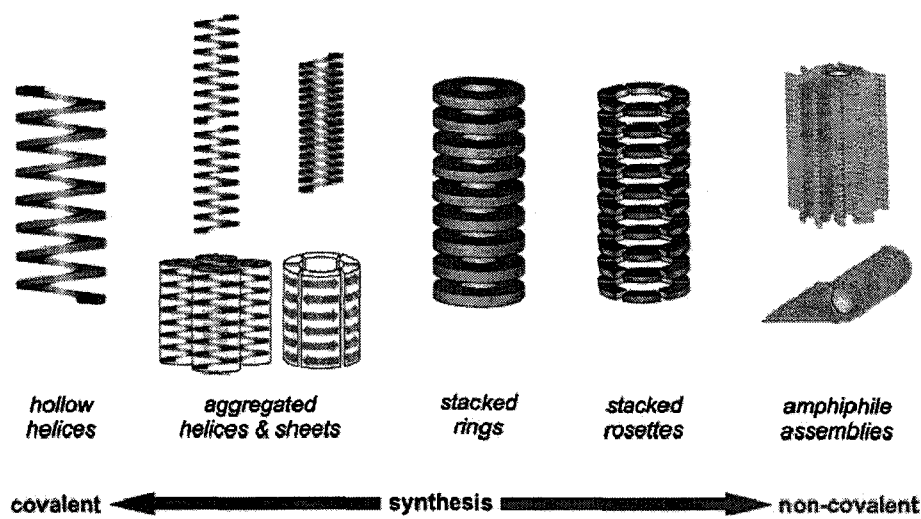


Figure 1.7. General strategies for the design of organic nanotubes based on hollow scaffolds and their self-assembly, stacks of macrocycles and rosettes, as well as cylindrical micelles and rolled bilayers sheets.

1.6.1. Helical Nanotubes

Biopolymers, proteins, deoxyribonucleic acid and polysaccharides are the building blocks of life. The precisely ordered stereostructures of biopolymers result from their intrinsic helical design, which is responsible for their function. In nature, oligonucleotide helices form the double stranded DNA which is responsible for storing and copying genetic information for the organization of life. Peptide helices perform a variety of biological tasks such as, selective chemical transporter through helical interior (gramicidin A),⁵⁷ mechanical strength via formation of supramolecular superhelical fibers (bundled collagen

cable),⁵⁸ and scaffolding - arrangement of different bacteriochlorophyll pigments in light harvesting complex II in bacteria.⁵⁹

The diverse biological functions that are conducted by a variety of naturally occurring motifs serve as inspiration for chemists to design artificial helices. Artificial helices can be used for molecular recognition (catalysis, separation and sensory functions), as scaffolds for the alignment of functional groups, chromophores, and for ordered molecular alignment in the solid phase such as that found in liquid crystalline materials.

Helical folding of biopolymers can result in one of two secondary conformations, an α or β -helix. Alpha helical structures do not have any internal cavity, running along the axis of the helix, because its inner walls are in van der Waals contact with each other. Beta helical structures are stabilized by β -sheet type hydrogen bonding and all amino acid side chains radiate outward, leaving an unoccluded central pore running the length of the helix axis. The number of residues per turn (helix periodicity) determines the average radius of the β -helix pore, thus making it an attractive scaffold for the preparation of tubular structures with tailored internal dimensions.⁶⁰

Gong and coworkers,⁶¹ showed how the internal diameter of helical meta-linked diarylamide **5** can be tuned by the continuous insertion of para-connectors. One turn of meta-linked diarylamide **5** consists of six repeating units and the hydrophilic internal cavity has a diameter of 8.2 Å. The alternating meta-/para-diarylamide **6** possess and increased diameter of ~ 25-30 Å. Adding another repeating unit in the para position yields an inner diameter of ~ 50 Å (Fig 1.8).

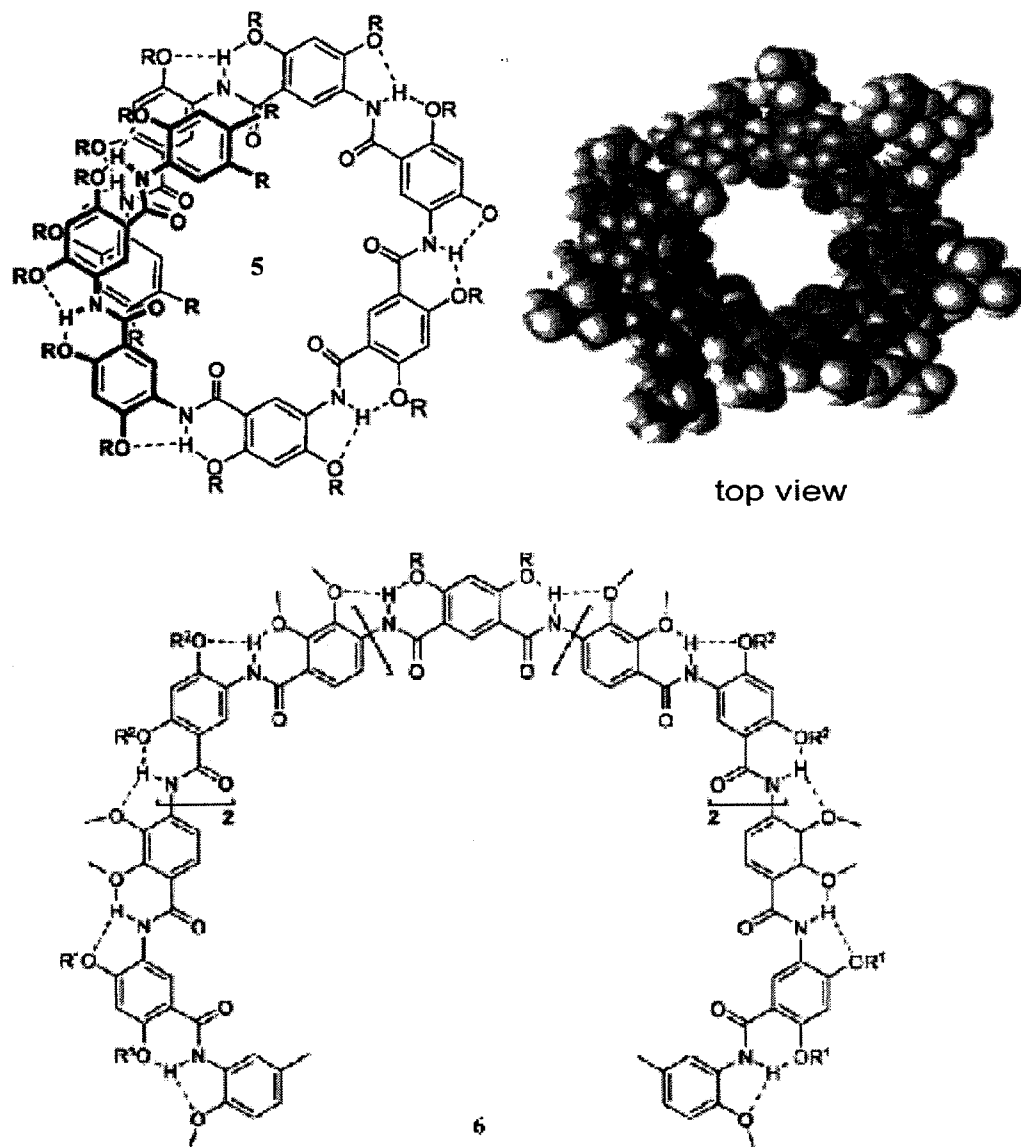


Figure 1.8. Gong's helical diarylamides of varying diameter depending on their mode of connectivity.⁶¹

Moore et al.⁶² have described the folding of non-biopolymers (foldamers) into helical conformations. Moore utilized his 'shape persistent' approach where meta-phenylacetylene subunits are coupled together to give oligophenylacetylenes that adopt helical conformations (Fig 1.9).

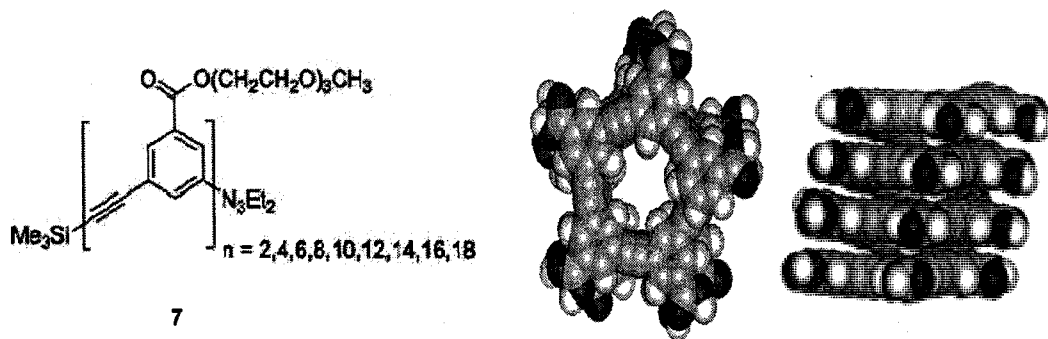


Figure 1.9. Moore's amphiphilic oligo (meta-phenyleneethynylene)s **7** and model of the octadecamer (side chains are omitted for clarity).⁶²

The helical secondary structures of *m*-oligophenylacetylenes in polar organic solvents is due to the meta connectivity of the backbone, π - π stacking interactions between aromatic moieties in adjacent turns, as well as segregation of the polar triglycine side chains and the non-polar phenylacetylene scaffold. The relative wide angle of turn (120°) prevents a closely packed core, resulting in a hollow coil that has a helical pitch of six and a cavity that is $\sim 7 \text{ \AA}$ in diameter.⁶³

Lehn et al.⁶⁴ were able to form a helical structure with an internal pore of 3.0 \AA using an alternating 2',6'-diaminopyridine 2,6-pyridinedicarboxamide oligomer (Fig 1.10). The helicity is derived from internal hydrogen bonding interactions between pyridine moieties and the amide group connecting them. The heptamer can dimerize to form double stranded helices that are stabilized primarily by additional aromatic stacking.

Meijer et al.⁶⁵ have shown that ureidophthalimide oligomers and polymers carrying chiral nonpolar side chains adopt helical conformations as a result of hydrogen bonding interactions between neighboring anti-oriented urea and 3,6-disubstituted phthalimide units, and π - π stacking between adjacent turns (Fig 1.11). The helix has a helical pitch of six to eight and internal cavity of $\sim 8\text{-}9 \text{ \AA}$ in diameter.

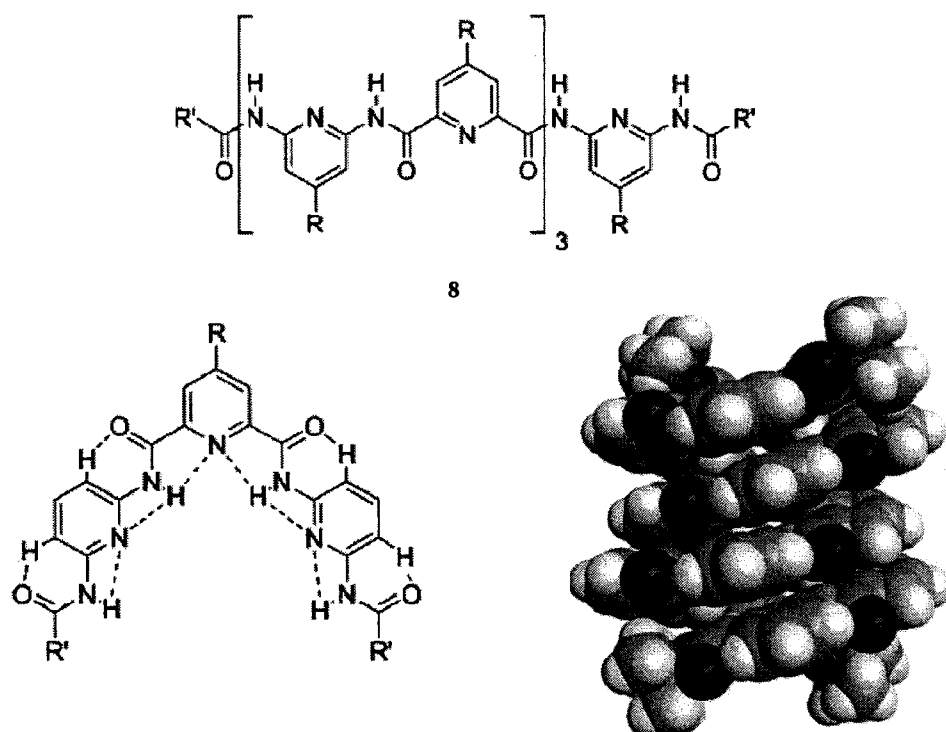


Figure 1.10. Lehn's alternating 2',6'-diaminopyridine 2,6-pyridinedicarboxamide oligomer **8**, and favored kinked conformation due to H-bonding.⁶⁴

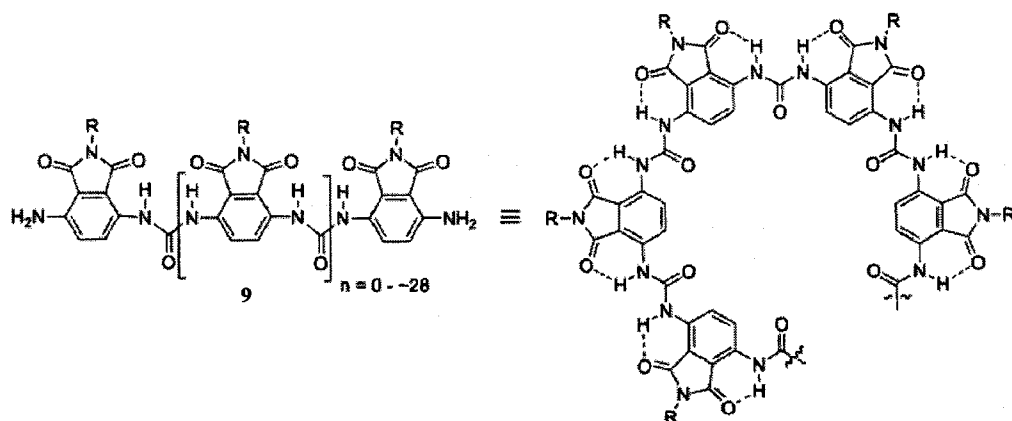


Figure 1.11. Meijer's helically folding ureidophthalimides **9** (DMAP).⁶⁵

In 1995, Lehn et al.⁶⁶ were able to form helical structures by using alternating pyridine-pyrimidine oligomers (Fig 1.12). The helical structure was derived from the ability of these oligomers to adopt a transoid conformation and the kinked meta connectivity between pyridine and pyrimidine units and intramolecular stacking between overlapping aromatic moieties. X-ray crystallography revealed the helical nature of these oligomers; it also showed that the nonadecamer had an internal cavity of 2.5 Å.

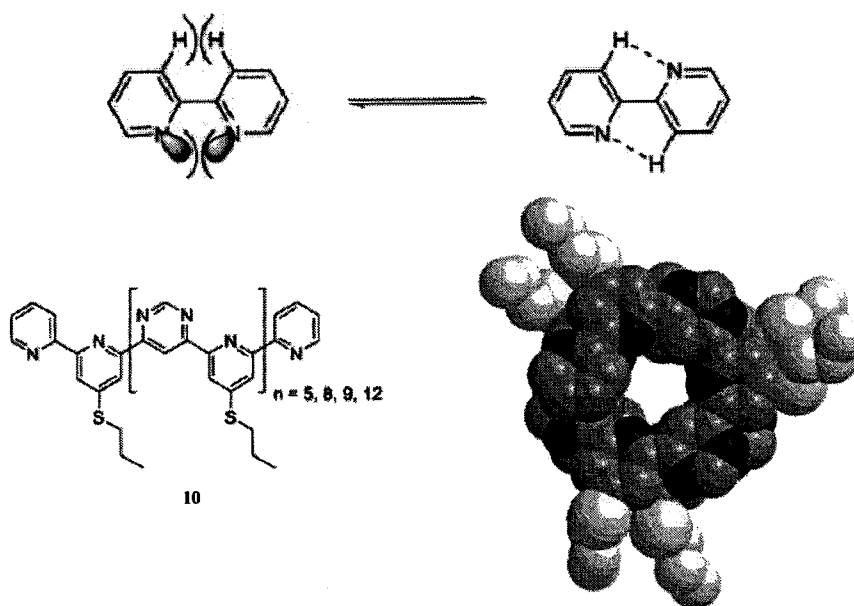


Figure 1.12. Lehn's oilgo (pyridine-alt-pyrimidine)s **10** and crystals structure of **13** mer ($n = 5$). N-atoms are black, C-atoms are gray, side chains are light; H-atoms are omitted for clarity.⁶⁶

By introducing para-connected building blocks (pyridazine) and carefully choosing the position of the heteroatoms, Lehn et al.⁶⁷ were able to increase the diameter of the helix. The oligo (pyridine-alt-pyridazine)s, **11**, had a helical pitch of twelve and a central cavity measuring $\sim 8-9$ Å in diameter.

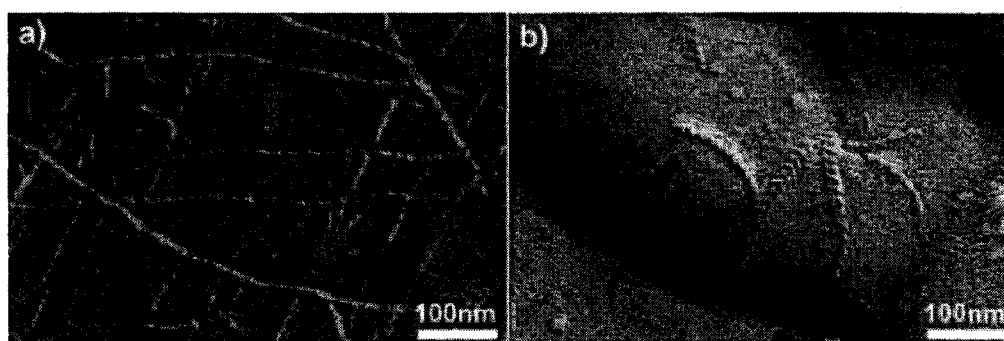
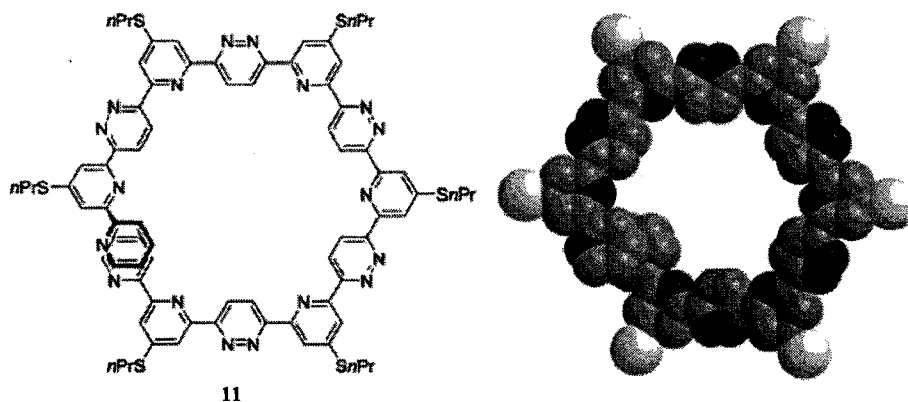


Figure 1.13. Extending the helix diameter using the para-connected pyridazine heterocycle to afford oligo (pyridine-alt-pyridazine)s **11**. Model (N-atoms are black, C-atoms are gray, S-atoms are light, H-atoms and side chains are omitted for clarity) and freeze-fracture electron micrographs of **11** in CH_2Cl_2 (a) and pyridine (b) showing fiber network formation with helical texture.⁶⁷

Ajayaghosh et al.⁶⁸ reported for the first time the assembly of helical nanotubes from vesicles during the sergeant-soldier coassembly of chiral oligo (p-phenyleneethynylene)s - OPEs and achiral OPEs (Fig 1.14). OPE 1 self-assembles in hydrocarbon solvents to form nanoparticles microspheres, while OPE 2 do not self-assemble. When 5-30 mol% of OPE 2 is mixed with OPE 1 coassembly into helical fibers occurs as revealed by chiral amplification using CD and UV-vis measurements. TEM analysis revealed that the helical fibers are tubular in nature with a diameter 50-90 nm.

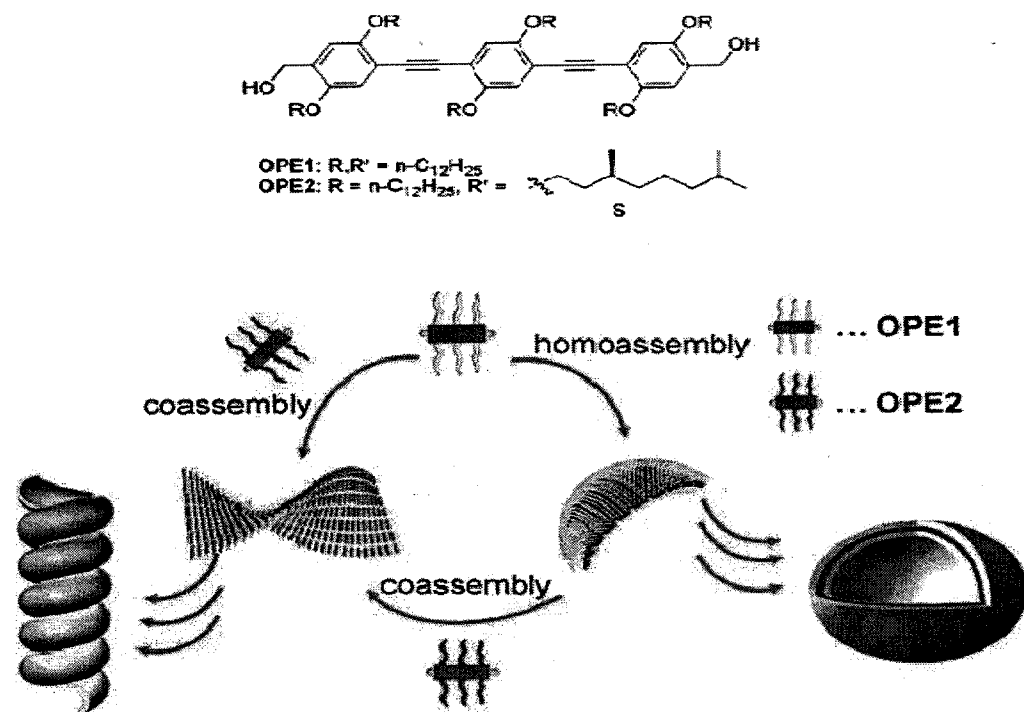


Figure 1.14. Self-assembly of vesicles and subsequent transformation into helical tubes in decane.⁶⁸

Sanders et.al.⁶⁹ reported that a new class of non-covalent polymers forms helical nanotubes in nonpolar solution and in the solid state. The dimerization of the carboxylic acids motifs (L-1) on the sides of the naphthalenediimide holds the nanotubes together. The inner diameter of the nanotubes average around 12.4 Å.

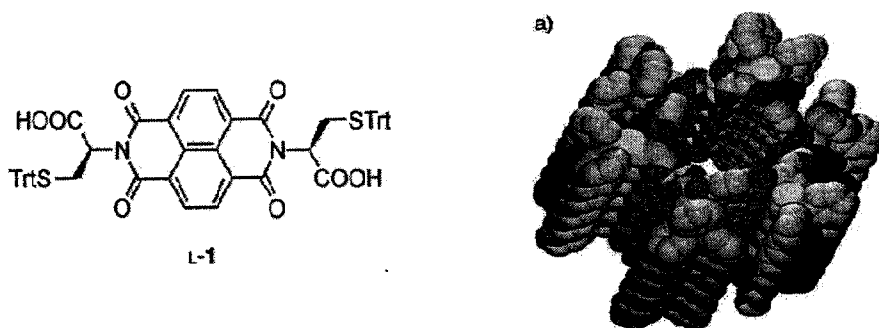


Figure 1.15. Side and top views of the hydrogen-bonded nanotubular structure formed by L-1.⁶⁹

1.6.1.2. DNA Nanotubes

DNA-based nanotechnology is currently being developed as a general assembly method for nanopatterned materials that may find use in electronics, sensors, medicine, and many other fields. The properties of the DNA double helix allows for the design of DNA complexes that are analogous to the abstract tiles of mathematical tilings.⁷⁰ Such DNA tiles can be programmed to self-assemble into a variety of two-dimensional (2D) arrays.⁷¹ Some early design of 2D arrays unexpectedly formed tubes.⁷² This has led to the development of several approaches for designing nanotubes from DNA tiles.⁷³

Figure 1.16 demonstrates one approach for designing helical nanotubes from DNA tiles from PAGE-purified DNA strands. These DNA tiles assemble to give two dimensional narrow ribbons that can curl and close onto themselves forming nanotubes with helical order.^{73b}

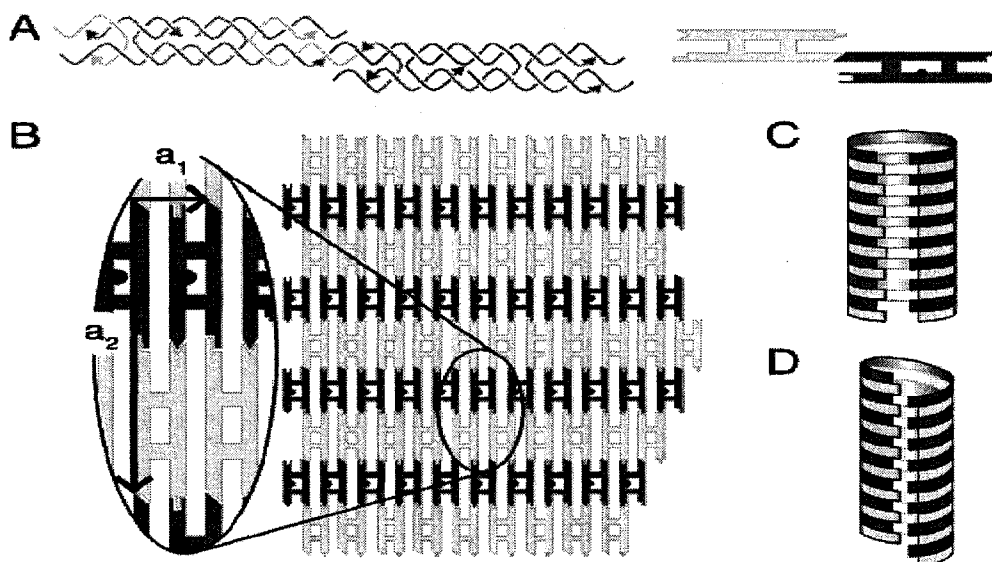


Figure 1.16. Self-assembly of DNA tiles into sheets and tubes. (A) structure of the double crossover tiles: arrowheads mark the 3' end of each oligonucleotide. The 6 nt single-stranded sticky ends on the α tile are complementary to those on the β tile; complementary shapes on the schematic representations of the tiles

indicate complementary stick ends. The 5' biotin label on the β tile is represented by a black dot. (B) α and β tiles tessellate to form extended two-dimensional arrays. It was proposed that the fold and close upon themselves to form tubes, producing either alternating rings (C) or nested helices (D) of α and β tiles.

DNA nanotubes have been used as templates for the growth of nanoscale conductors.^{74,73a} Other potential uses of DNA nanotubes are inspired by analogy with the roles of nanotubes and nanofilaments in living cells: as structural supports for the cytoskeleton (e.g., actin filaments), as tracks for the transport of microscopic cargo (e.g., microtubules conveying vesicles), and as moving parts for cellular motility (e.g., flagella). DNA nanotubes may eventually be engineered to mimic all these functions.

1.6.2. Nanotubes from Self-assembled Amphiphiles

Amphiphilic molecules of which soap is a typical example possess antagonistic hydrophilic and hydrophobic moieties in the same molecule. In aqueous media lipids self-assemble into diverse aggregated morphologies, depending on the molecular shape and lipid conditions such as lipid concentration, electrolyte concentration, pH, and temperature.⁷⁵ Manipulation of the aforementioned parameters can be used to some degree to control the self-assembly of amphiphiles into Lipid Nanotubes (LNTs).

The self-assembly of lipid bilayers into LNTs is a complex process, however; Shimizu et.al.⁷⁶ highlighted the following methods for lipid nanotube formation (Fig 1.18). The scope of this review is to highlight a few examples of the most popular methods used for self-assembly of lipid nanotubes; for a more comprehensive review the reader is referred to reference [76].

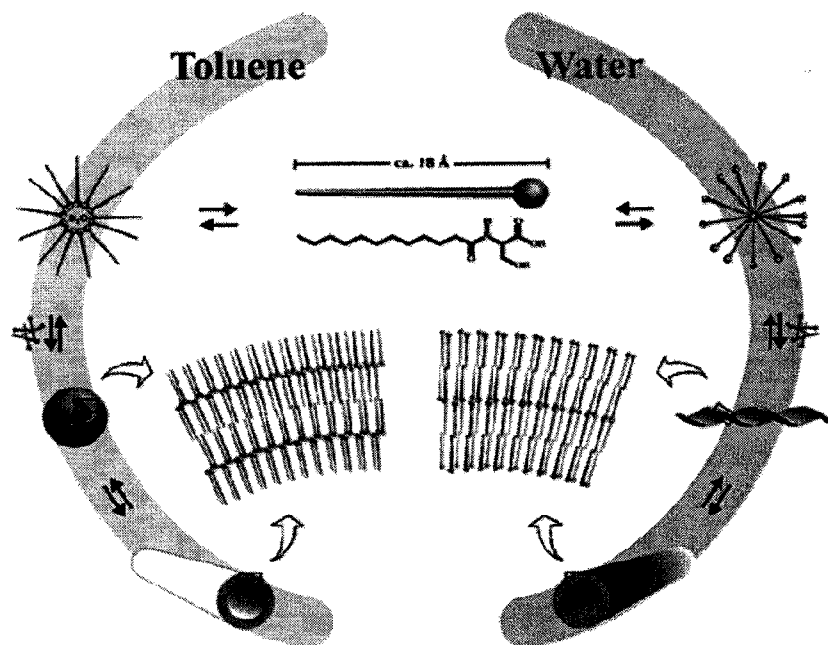


Figure 1.17. Schematic illustration of the different pathways of self-assembly of an amphiphile from micellar bilayers in water (micelles, helical ribbons, nanotubes) as toward smooth tubular rods.

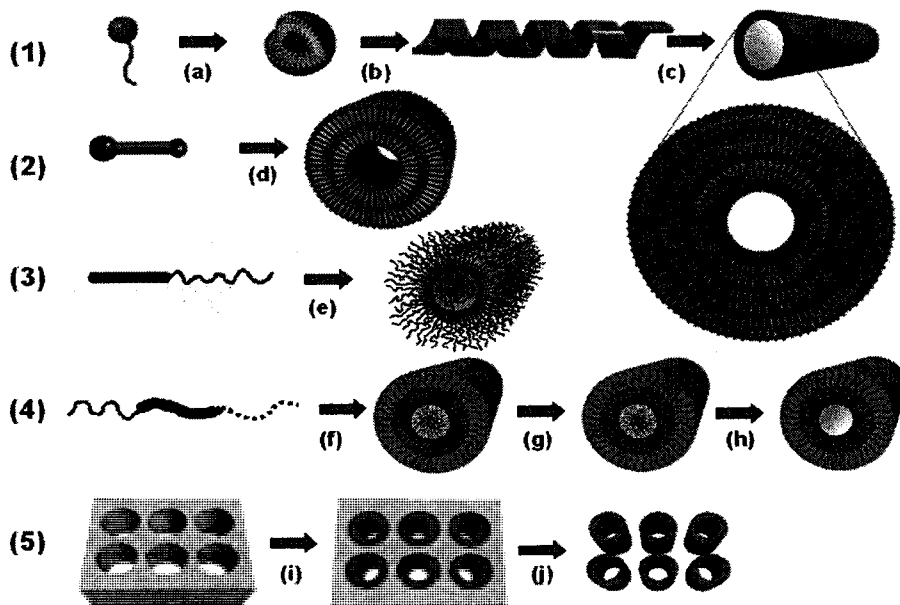


Figure 1.18. Variety of methods to yield nanotube structures: (1) chiral molecular self-assembly; (2) packing-directed self-assembly based on an unsymmetrical

bolaamphiphile; (3) self-assembly of a rod-coil copolymer into a nanotube; (4) nanotube formation from a triblock copolymer via a molecular sculpting process, which involves (f) self-assembly, (g) cross-linking of the shell, and (h) decomposition of the core by ozonolysis; (5) self-assembly or deposition of molecules inside the pore as a substrate.

1.6.2.1. Packing – Directed Self-assembly

Wedge, tapered, or sector shaped amphiphiles have a tendency to assemble into hollow cylindrical structures in solution or suspension and inverted hexagonal phase with tubular channels in the liquid crystal state. Polar head groups form the inner periphery of the tubes, while the disordered tail form the outer periphery and thus isolate the tubes from each other. Inspired by the Tobacco Mosaic virus, Perc et.al.⁷⁷ synthesized taper-shape dendritic amphiphiles **12**, based on gallic acid, which form five and six membered discotic assemblies that further stack into columns (Fig 1.19). The carboxylic acid serves as the hydrophilic head at the interior of the assembly, while the fluorocarbon attached to small aromatic branches generates a hydrophobic exterior.

Building on the work of Perc, Gin and coworkers designed analogous taper shape gallic acid salt monomers with polymerizable olefin, diolefin or acrylate units allowing for crosslinking without affecting the column inner void. The hydrogen bonding motifs in compound **13** further stabilize the columnar phase (Fig 1.19).⁷⁸

1.6.2.2. Nanotubes from Linear Amphiphiles and Block Copolymers via Molecular Sculpting

Bolaamphiphiles: molecules that have two polar head groups separated by a hydrophobic linker also self-assemble into nanotubes. Some bolaamphiphiles that self-assemble into nanotubes are double chain ammonium salts,⁷⁹ unsaturated double chain phosphatidylcholines,⁸⁰ aromatic glycolipids, and aldoamines (Fig.1.20).⁸¹

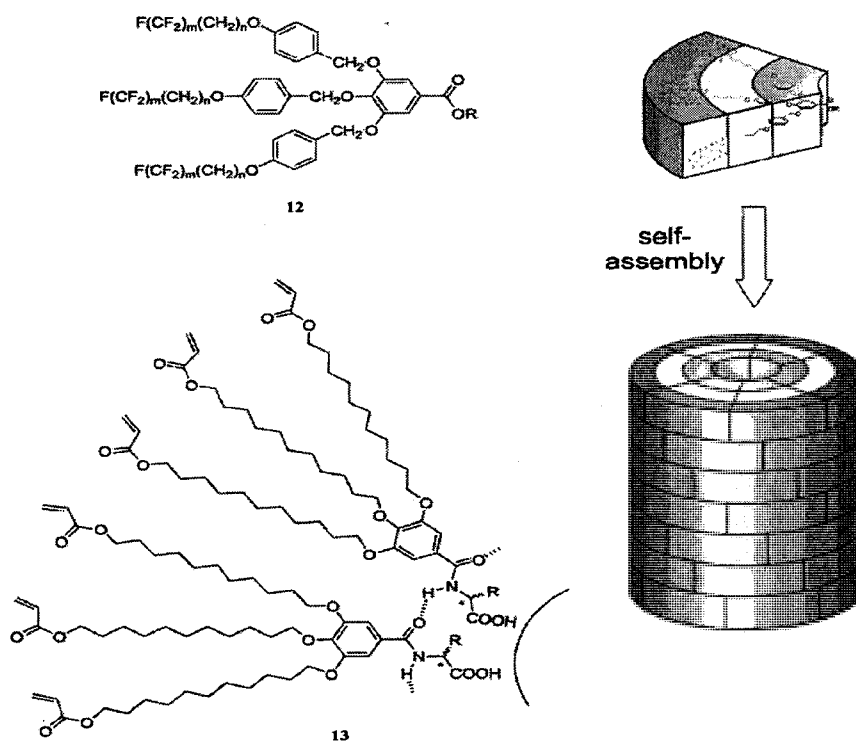
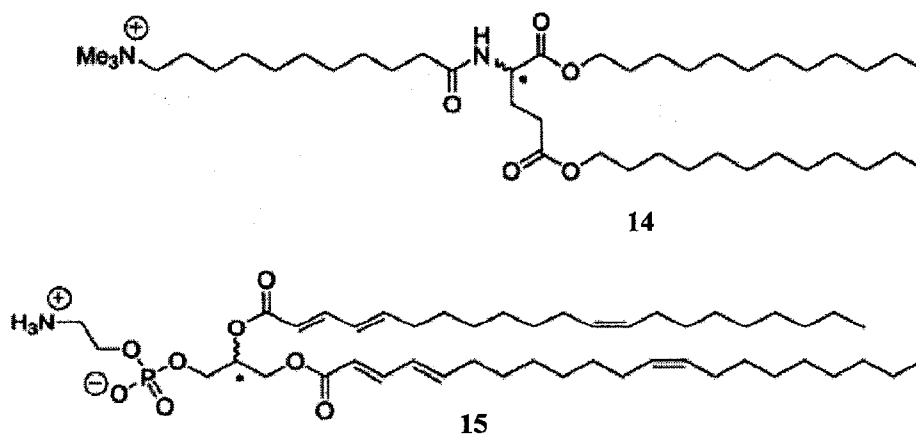


Figure 1.19. Perc's wedge-shaped amphiphilic gallate **12** (*top*), cartoon illustrating assembly of amphiphile into layered tubes; Gin's analogue gallate **13** with H-bond stabilized inner core and crosslinkable periphery (*bottom*).⁷⁷



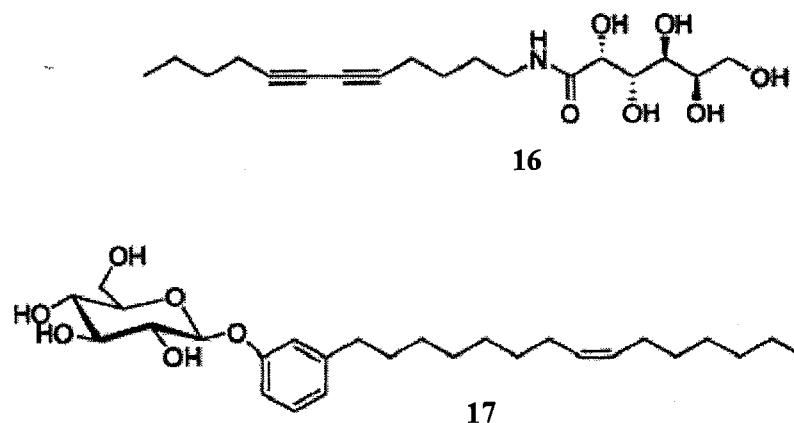
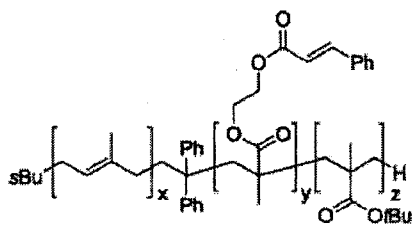


Figure 1.20. Selected linear amphiphiles assembling into tubes: double-chain ammonium amphiphile (14), unsaturated double-chain phosphatidylethanolamine (15), diacetylenic aldonamide (16) and aromatic glycolipid (17).⁷⁹

The introduction of di- and tri- block copolymers serving as amphiphiles have resulted in large tubular structures. Diblock copolymers such as polystyrene-block-poly(ethyleneoxide) or poly(ethyleneoxide)-block-poly(ethylene) formed tubular bilayers that aggregate in solution.⁸² An excellent example of making polymeric nanotubes was demonstrated by Stewart and Liu (Fig 1.21),⁸³ they made use of the so called ‘molecular sculpting’ of cross-linked nanofibers. The triblock copolymer [polyisoprene-block-poly (2-cinnamonyl ethyl methacrylate)-block-poly (tert-butyl acrylate), PI-b-PCEMA-b-PtBA] **18** self-assembled into cylindrical micelles in solution. Subsequent photocross linking of the PCEMA shell and subsequent removal of the PI internal core via ozonolysis resulted in nanotube formation. TEM and uptake of the guest rhodamine B provided evidence of a hollow cylindrical structure. Using a mixing ratio of 130:130:80 repeating units lead to cylindrical micelles having dimensions of 79 nm in diameter and a few microns in length.



18

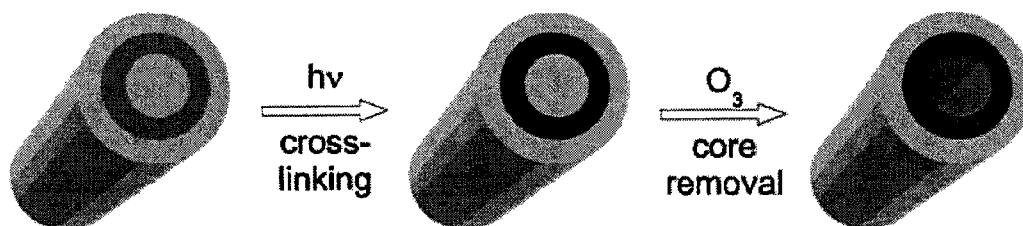
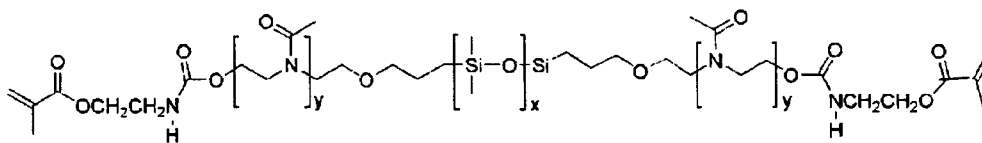


Figure 1.21. Stewart and Liu's approach to polymeric nanotubes based on block copolymer assembly followed by photocrosslinking of the poly (2-cinnamoyl ethyl methacrylate) (PCMA) shell and removal of the polyisoprene core by ozonolysis.⁸³

Meire and coworkers⁸⁴ were also able to form nanotubes from amphiphilic ABA triblock macromonomers. Amphiphilic poly (2-methyloxazoline-block-dimethylsiloxane-block-2-methyloxazoline) - PMOXA-B-PDMS-B-PMOXA-triblock copolymers form polymeric nanotubes via film rehydration. TEM showed that the mixture contained a mixture of vesicles and nanotubes, with nanotubes diameter being uniform at ~ 40 nm in length.



19

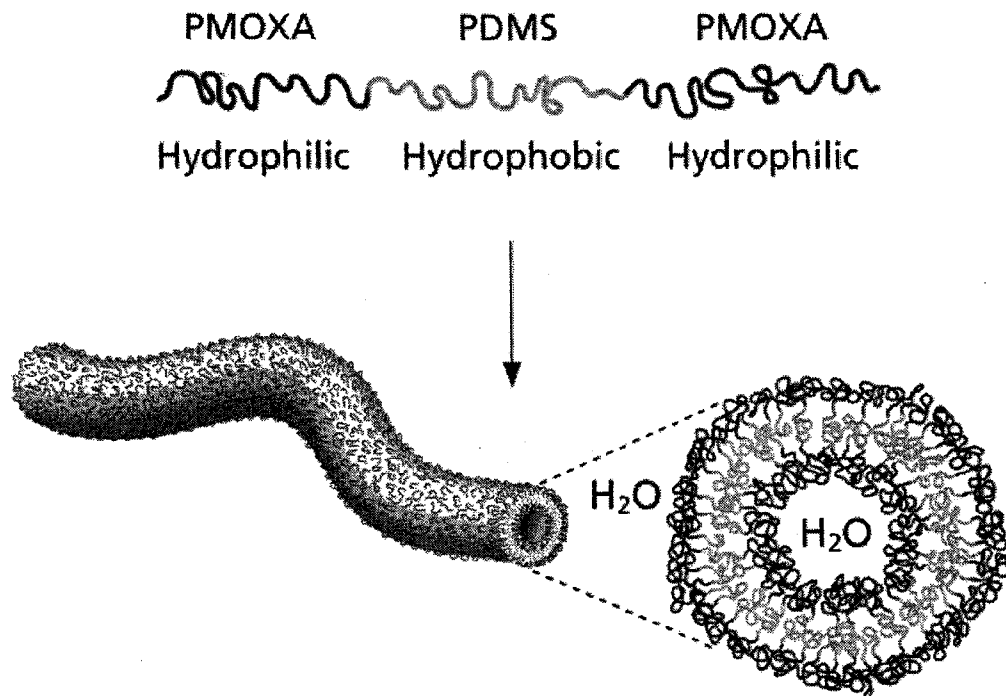


Figure 1.22. Self-assembly of PMOXA-PDMS-PMOXA (19) copolymers in solution.⁸⁴

The addition of an amphiphilic multiarm copolymer (HPBO-star PEO) to selective solvents resulted in macroscopic tubes with centimeter length and millimeter diameter and are visible to the naked eye (Fig 1.23).⁸⁵ The diameter of the tubes approached 1 mm and the average length was about 1.5 cm. Optical microscopy revealed that the tubes are multiwalled in nature, with most of the tubes having similar inner diameters, uniform wall thickness, and almost equal distance between two neighboring walls.

Exquisite nanotubes can be synthesized via rational design of amphiphilic monomers that produce tubular morphologies. The self-assembly process takes place via a bottom-up approach. LNTs can be used as templates for the synthesis of nanowires via metallization. The hollowness of nanotubes make them suitable for medical,⁸⁶ industrial,⁸⁷ as well as filtration and purification applications.⁸⁸

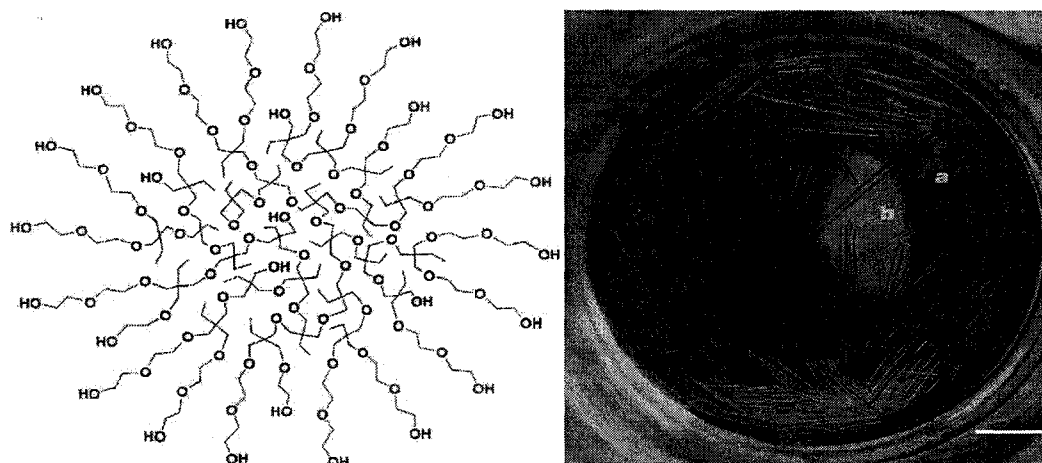


Figure 1.23. Diagrammatic sketch of HBPO-star-PEO (left) and its self-assembly into macroscopic tubes (right).⁸⁵

1.6.3. Nanotubes from Stacked Macrocycles

Another way of creating nanotubes is through self-assembly or stacking of macrocyclic rings. In this design process covalent bonds determine the inner and outer diameters, while non-covalent interactions determine the length of the nanotube. This design methodology is not quite as prominent in nature as it is in the designing of artificial systems.

Tubular ensembles have been realized by the stacking of cyclic D, L- α -peptides. Gadhiri et.al⁸⁹ reported that the formation of rod shape crystals with high aspect ratios were formed upon the controlled acidification of basic solutions of the octapeptide, **20**, cyclo-[(L-Gln-D-Ala-L-Glu-D-Ala)₂-]. Each crystal contained hundreds of tightly packed nanotubes. The use of TEM, cryo-TEM, electron diffraction and molecular modeling revealed that the tubular stack has an inner diameter of 7 Å (Fig 1.24).

One advantage of using cyclic D, L-peptides to construct nanotubes is that the external surface properties and internal diameter of the nanotube can be

rigorously controlled by changing the amino acid side chain and varying the size of the ring, respectively. The dodecamer, cyclo-[(L-Gln-D-Ala-L-Glu-D-Ala)₃], was assembled to give microcrystalline aggregates with an expanded diameter of 13 Å.^{89b}

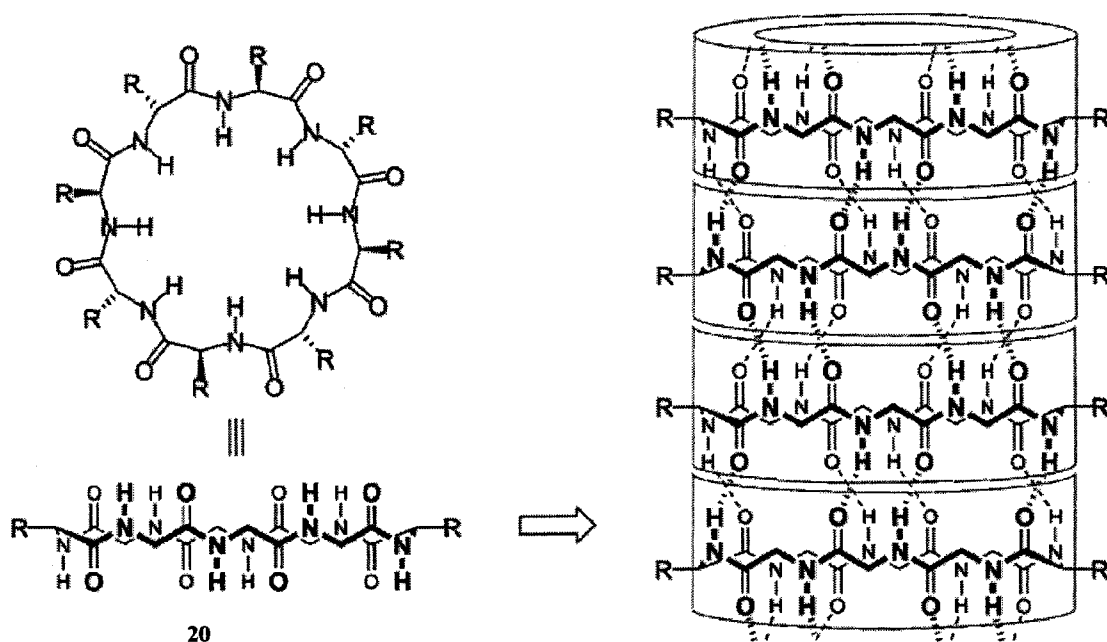
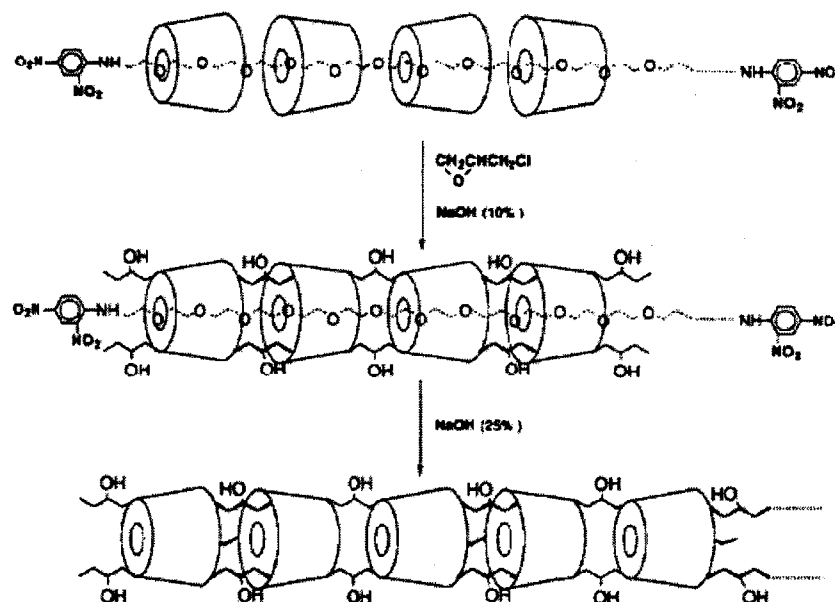


Figure 1.24. Schematic diagram of nanotube from assembly of cyclic D, L-peptides.⁸⁹

Harada et. al.⁹⁰ reported the ability of carbohydrates to form nanotubes. A cyclodextrin polyrotaxane was prepared by threading a single polyethylene glycol bisamine (PEG-BA) through several cyclodextrin units, then stoppering the end with dinitrofluorobenzene (Scheme 1.1). The rotaxane assembly was then cross linked using the dielectrophile epichlorohydrin, destoppered and purified by gel filtration to afford polymeric nanostructure.

Stoddart and coworkers,⁹¹ were able to synthesize a series of cyclodextrin analogues from protected disaccharide precursors (Fig. 1.25). X-ray crystallography showed that cyclic oligosaccharides **21**, having alternating (1→4)

- linked α -D- and α -L-rhamnopyranose residues, and **22**, having alternating (1 \rightarrow 4) – linked α -L-rhamnopyranose and mannopyranose residues stacked in a head-to-tail fashion to form tubular channels with diameters of ~ 10 Å.



Scheme 1.1 Formation of a cyclodextrin nanotube by covalent capture of a polyrotaxane precursor. Treatment of the non-covalent assembly with epichlorin captures the cyclodextrins to yield a molecular tube that is unoccluded after removal of the polyethylene glycol thread.⁹⁰

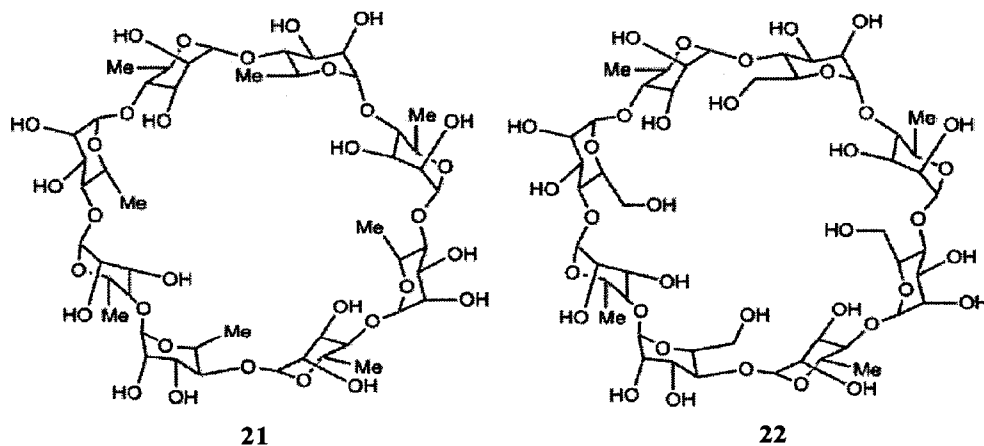


Figure 1.25. Stoddart's stacked cyclic oligosaccharides **21** and **22**.⁹¹

Moore and coworkers, utilizing their meta-connected phenylacetylenes, have been able to create a variety of macrocycles (PAMs), some of which stack to create columnar architectures (Fig 1.26).⁹² Using macrocycle **23** they were able to show that it forms hexagonally closed-packed, two dimensional hydrogen bonded networks that form layers that stack, while approximately maintaining the alignment between the internal void to afford extended channels with diameters of $\sim 9 \text{ \AA}$.⁹³ Other researchers such as Schlüter⁹⁴ and Höger⁹⁵ have been able to create columnar aggregates using phenyl base macrocycles.

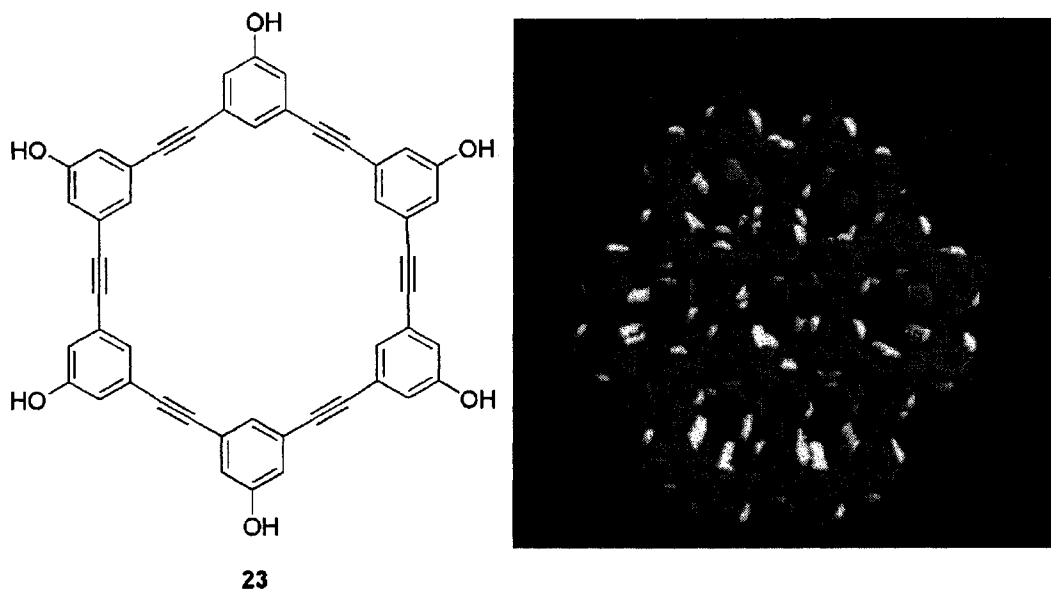


Figure 1.26. Phenolic functionalize PAM, **23**, and its space filling model.⁹²

In 2008, Schappacher and Deffieux reported the design of large polymeric macrocycles that assembled into supramolecular tubes.⁹⁶ The polymeric macrocycles were synthesized from a triblock copolymer, ABC, via intramolecular coupling of A and C (Fig. 1.27). The chloroethyl vinyl ether monomer, block B, was decorated with polystyrene or randomly distributed polystyrene or polyisoprene to produce macrocyclic brushes that self-assembled into cylindrical tubes with diameters of about 100 nm and 700 nm in length.

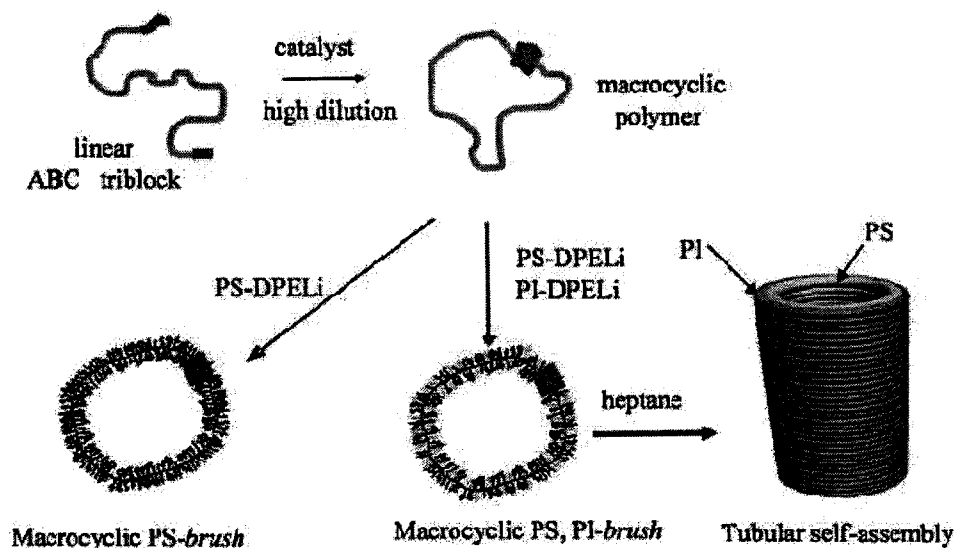


Figure 1.27. Strategy for the synthesis of cyclic comb like copolymers and their self-assembly. PS-DPELi, (1,1-diphenylethylene) end-capped polystyryllithium; PI DPELi, (1,1-diphenylethylene) end-capped polyisoprenyllithium.⁹⁶

1.7. Self-assembling Nanotubes from Stacked Rosettes

The three preceding methods of assembling nanotubes are not as sophisticated, nor do they employ the whole gamut of non-covalent interactions, as does the assembly of rosettes into nanotubes. The rosette is a macrocycle that is constructed from disc like segments via molecular recognition processes, usually through built-in hydrogen bonding sites.

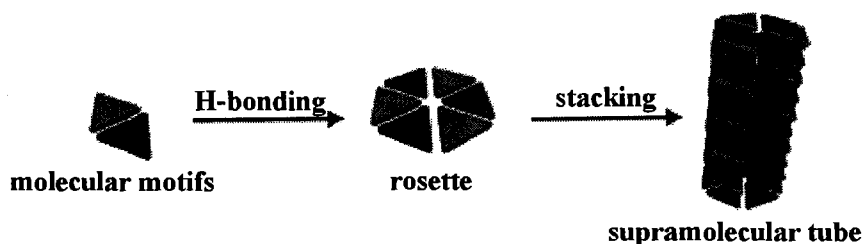


Figure 1.28. Cartoon depicting assembly of Rosette Nanotubes (RNTs).

The utilization of non-covalent interactions such as aromatic π - π stacking and solvophobic effects allows rosette macrocycles to stack forming supramolecular tubes with internal cavities running along the axis of the tubes. The sophistication of this approach lies in the hierarchical nature of the assembly.

1.7.1. The Beginning: G – quartet

Gellert et al., over 40 years ago, reported that 3' guanylic acid and 5'guanylic acid (GMP) form layers of hydrogen bonded tetramers, which may be stacked onto each other to give a cylindrical structure with a central cavity.⁹⁷ These tetrameric structures formed by 5'GMP are termed as *G-quartets* and are formed by eight hydrogen bonds between the Hoogsteen and Watson – Crick faces of neighboring bases. Na⁺ and K⁺ ions were shown to be important for templation and stabilization of G-quartets.⁹⁸ The G-quartet can stack on top of each other to form cylindrical structures know as G-quadruplexes (Fig 1.29). The sugar moiety of the nucleobase was shown to induce and amplify supramolecular chirality.

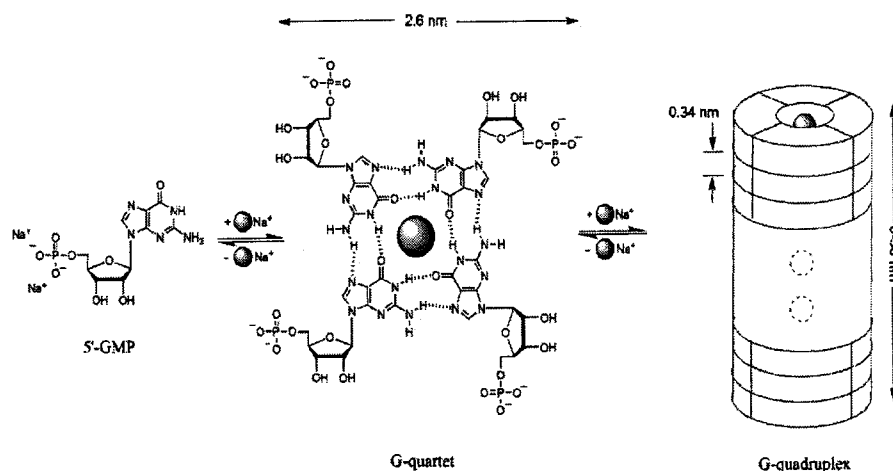


Figure 1.29. Self-assembly of G – quadruplex from 5'GMP.⁹⁸

Small structural changes in the guanosine motif can have a drastic effect on the self-assembly and the resulting supramolecular structure. IsoGuanine (IsoG6), an

isomer of guanine, self-assembles into a decamer that is made of two IsoG6 pentamers that sandwich the templating cation. The donor and acceptor sites of G5 are at an angle of 90° , while those of IsoG6 are at an angle of 110° , hence; G5 forms tetramers and IsoG6 forms pentamers (Fig 1.30).⁹⁹

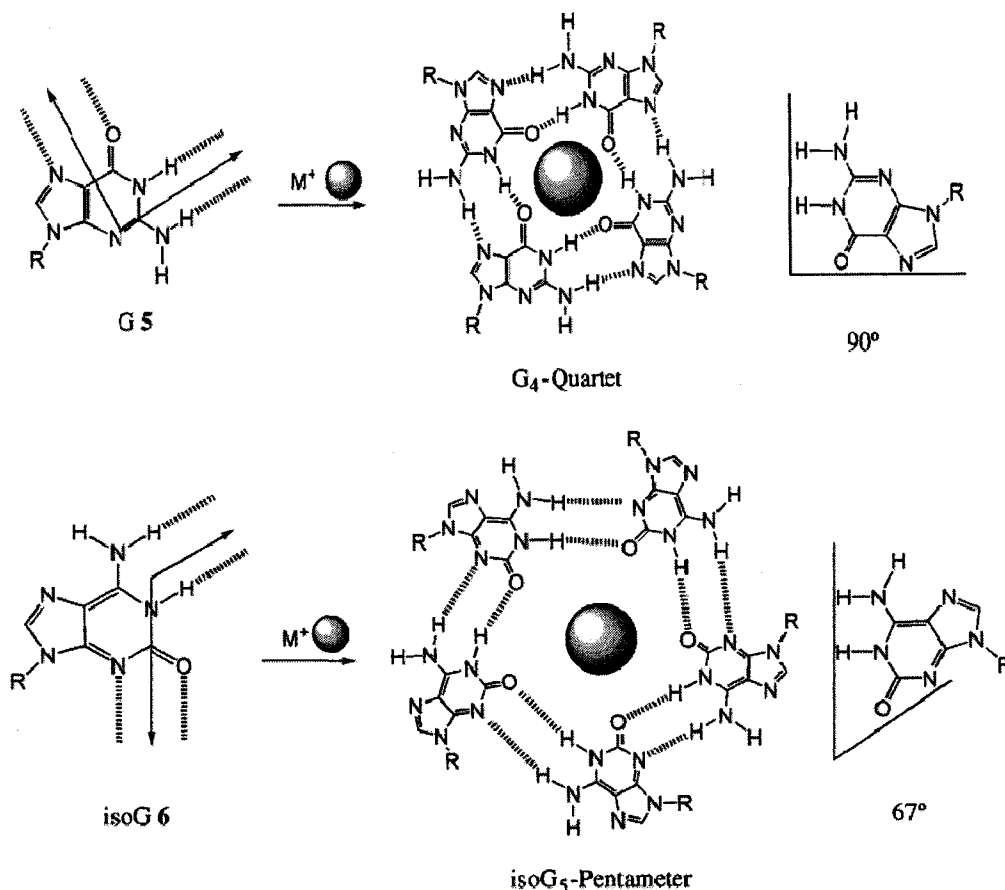


Figure 1.30. Self association of G5 and isoG6 in the presence of cations to give hydrogen bonded G_4 -quartets and isoG5-pentamers.⁹⁹

The nature of the cation determines the size of the supramacrocycle formed. Using K^+ ions, Davis et al.¹⁰⁰ showed that tetrameric rosettes can be formed from iso-guanine; they also found that Ba^{2+} formed G-hexadecamer and decamer for guanine and Iso-guanine respectively.

Sessler et al.¹⁰¹ showed that a guanine dimethylaniline analogues self-assemble into G-quartets without the assistance of a templating/stabilizing cation. This is

made possible by attaching a dimethylaniline unit to C8 of the purine, which makes it a sterically hindered nucleoside which favours G-quartet formation as opposed to ribbon formation.

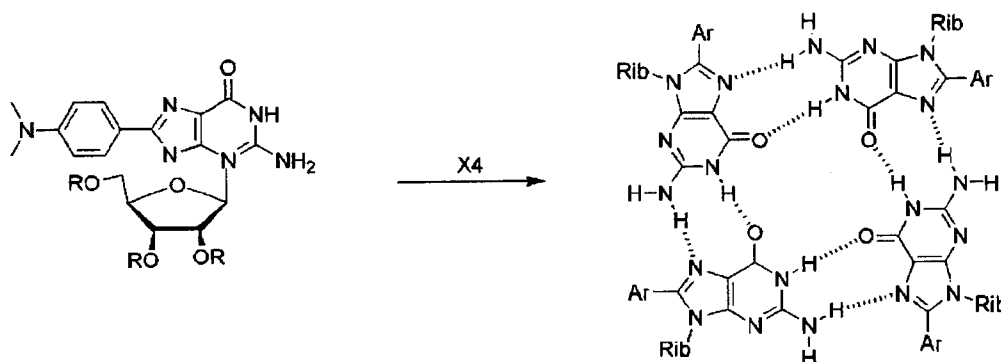


Figure 1.31. Sessler's cation free G – quartet.¹⁰¹

This work demonstrates how synthetic chemistry can be utilized to design unnatural nucleobases to generate supramolecular structures. The G-quadruplexes and IsoG decamers of guanine have potential applications in nanomedicine, supramolecular catalysis, artificial ion channels, nanotechnology, nanowires, nanotubes and liquid crystals.^{51,98}

Whitesides and coworkers,¹⁷ introduced the melamine (M) – cyanuric acid (CA) hydrogen bonding motif that forms supramolecular rods with diameters of $\sim 5 \text{ \AA}$ via the stacking of rosette like assemblies. The melamine – cyanuric acid subunits can form tapes and rosette structures with the later being preferentially formed by peripheral crowding of the subunits (Fig 1.32).

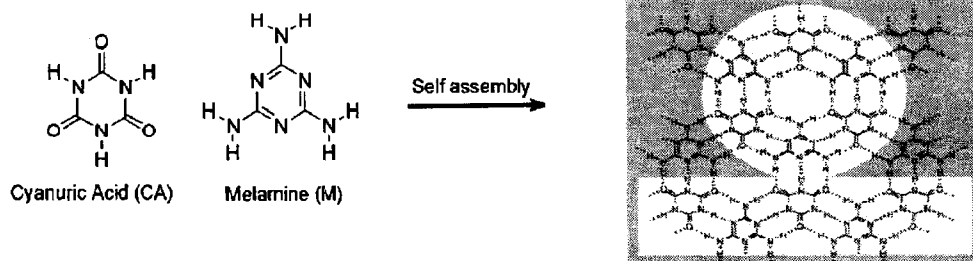


Figure 1.32. Modes of self-assembly of CA and M into rosettes and linear tapes.

Employing the idea of peripheral crowding of CA and M Whitesides et al. were able to self-assemble cylindrical structures, with diameters of 5 nm, using complementary building blocks of bisisocyanurates and bismelamines.¹⁰² The self-assembly was driven by the solvophobic effect and hydrogen bonding between complementary motifs. Preorganization of the molecular motifs by covalent linkage to aromatic groups ensured that the units adopted a face-to-face orientation which favored rosette formation (Fig 1.33).

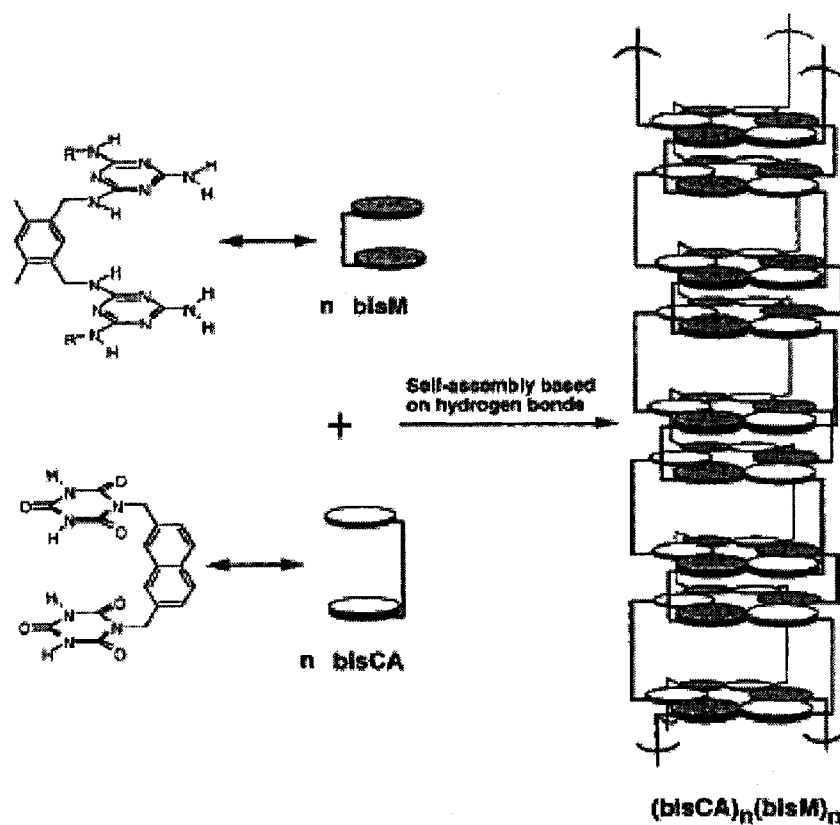


Figure 1.33. Self-assembly of a bismelamine and bisisocyanurate into nanocylinders.¹⁰²

Kunitake et al.¹⁰³ were able to form columnar aggregates, with large diameters, by replacing cyanuric acid with naphthalenedicarboxoimide and melamine with dialkylmelamine. The diameter of the columnar aggregate was ~ 4 nm and they further aggregated into fibers because of the amphiphilic nature of the dialkylmel-

aine.

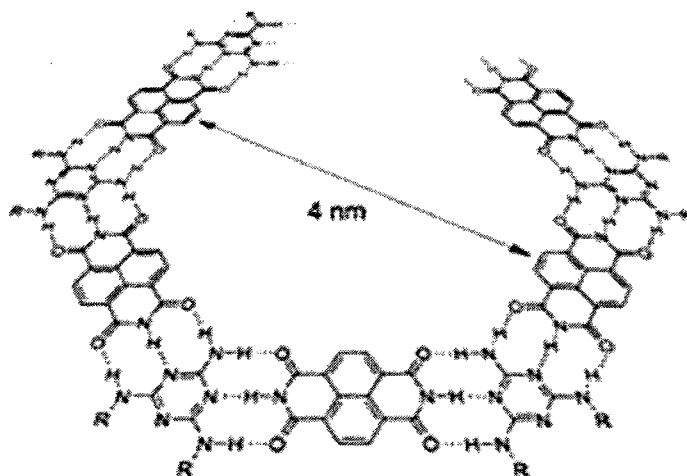


Figure 1.34. Kunitake's binary melamine-diimide system.

Chiral π -conjugated hexameric rosettes were formed from two oligo-(p-phenylenevinylene) diaminotriazine precursors (Fig 1.35). **OPVT 3** and **OPVT 4**. These rosettes subsequently self-assembled into chiral tubular structures as revealed by SANS (small angle neutron scattering), AFM (atomic force microscopy), UV-vis and CD spectroscopy. The tubes have an average internal diameter of 1 nm and length exceeding 185 nm in solution and 10 μm when cast on a solid substrate.¹⁰⁴

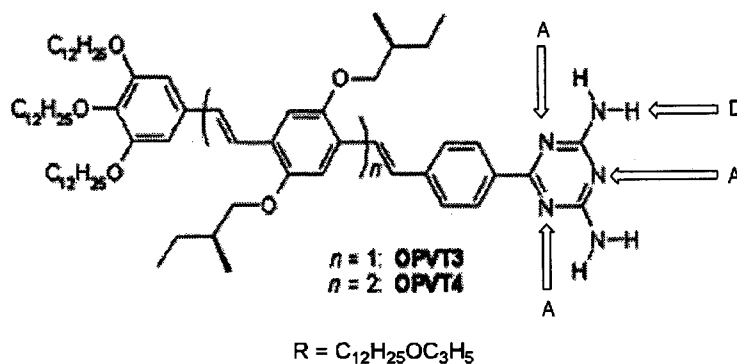


Figure 1.35. Molecular structures of **OPVT3** and **OPVT4**.¹⁰⁴

Our research group have been utilizing a pyrimido-pyrimidinedione motif **24** (Fig.1.36.), which has self complementary guanine-cytosine hydrogen bonding

faces (G⁺C base) capable of forming rosettes. These rosettes are composed of six G⁺C bases, which are held together by 18 hydrogen bonds, and has an internal channel whose diameter measured 1.1 nm in length. These rosettes then stack, via π - π interactions, to produce tubular structures which are kinetically stable even though they are maintained by non-covalent interactions.¹⁰⁵ By varying the nature of the R group, we can create nanotubular architectures where the respective R group is expressed on the outer surface of the tube.¹⁰⁶ Self-assembly of rosette nanotubes in water is driven by the solvophobic effect.

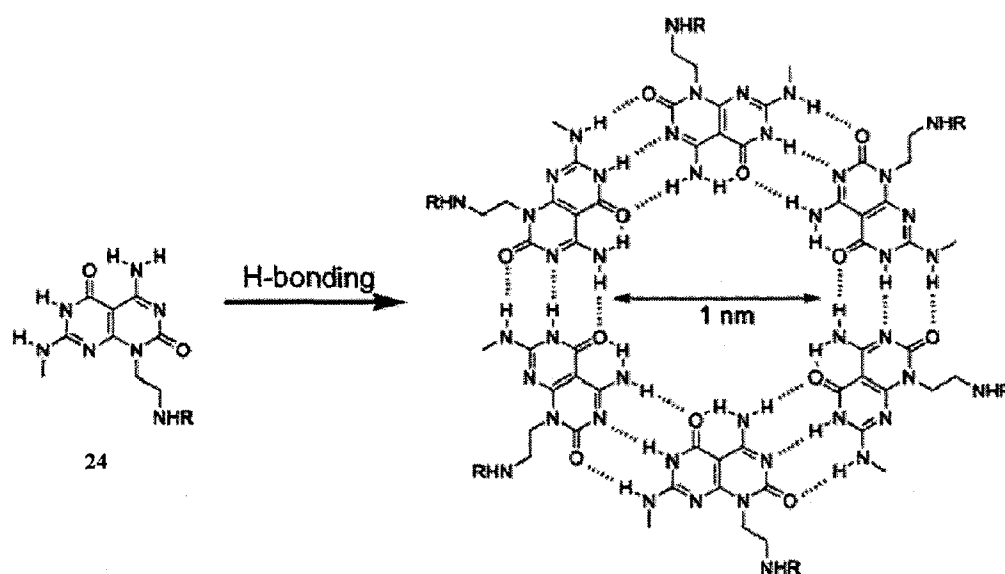


Figure 1.36. Fenniri's rosette forming pyrimido-pyrimidinedone motif, **24** (G⁺C motif).¹⁰⁵

Utilizing a prochiral crown ether functionalized G⁺C motif **25**, we were able to form helical rosette nanotubes (HRNTs) via chiral induction.^{107a} Supramolecular chirality inversion was also observed when HRNTs were assembled in methanol and subsequently treated with small amounts of water.^{107b.}

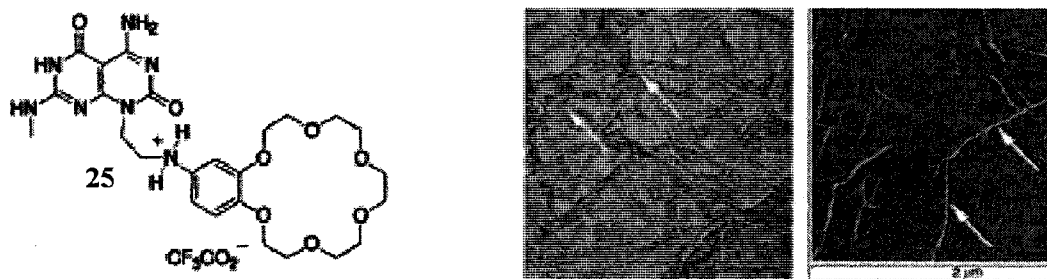


Figure 1.37. Hierarchical self-assembly of **25** into six member rosette and subsequently nanotubes (stained TEM (a) and TM-AFM (b) images).

Tuning the stability and hierarchical organization of HRNTs was demonstrated by varying the functional group density (steric) of R and net electrostatic charge. We found that the higher the net charge, the less stable are the HRNTs, and that nanotubes made from twin bases are thermodynamically more stable than those made from single G⁺C motifs, and this is directly related to preorganization and less sterics of the twin base.¹⁰⁸

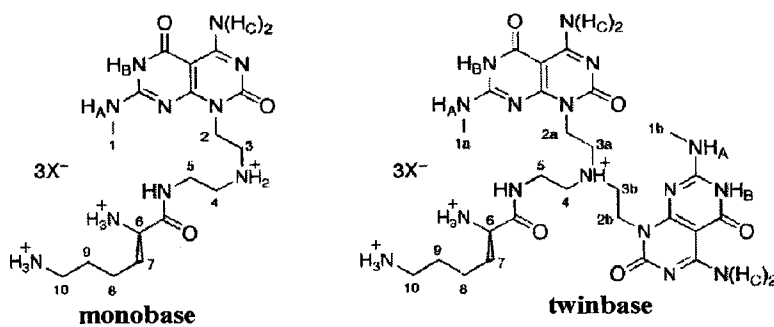


Figure 1.38. Structures of mono- and twinbase G⁺C motifs functionalized with lysine.

Lysine functionalized HRNTs (HRN-K1) coated with titanium enhanced osteoblast adhesion at concentration as low as 5 $\mu\text{g} / \text{mL}$. Research has shown that HRNTs are excellent scaffolds for the designing of biomaterials because of their

tuneability, and to this end they have been functionalized with different amino acids and hydrogels to investigate their feasibility for orthopedic applications.¹⁰⁹

The potential applications of nanotubular objects are indeed numerous; however, there are some fundamental problems that must be solved before the true potential of such systems can be realized. In order to create functional materials from rosette nanotubes our research group has addressed, and is currently addressing; some of these fundamental problems. We are conducting research that will provide us with deeper insight into the process of self-assembly and disassembly, increasing tubular stability, and determining the exact sites of protonation within the G⁺C motif. Investigation into ways of controlling the length and increasing the inner diameter of the G⁺C motif is currently being look at for potential use in host-guest chemistry, transportation, storage and templation applications. However, by far the most important application is to use our nanotubes for biological applications.¹¹⁰

1.8. Summary and Overview

As the burgeoning, multidisciplinary scientific field of nanotechnology comes of age, it promises to revolutionize the way in which science is conducted, and from which amazing benefits will be derived for all mankind. Supramolecular chemistry is one of the sub-disciplines that has, and will continue, to contribute to the expansion of nanotechnology. One of the areas that nanotechnology promises to revolutionize is the treatment, monitoring and diagnosis of diseases – nanomedicine; this is because of the size and supramolecular structures of nanoparticles.¹¹¹ Whitesides stated that chemistry will, and is, playing a major role in nanotechnology; because chemistry is (and has always been) the ultimate nanotechnology. Chemists make new forms of matter by joining atoms together with bonds.¹¹² Thus, synthetic organic chemists will play a major role in the future developments of nanotechnology.

This scope of this thesis is to provide a preliminary insight into the role of nanotubes, specifically RNTs, to the development of nanotechnology. Chapter 1 introduced some core concepts of supramolecular chemistry, a major driving force behind nanoscience/nanotechnology and a non-exhaustive review of different synthetic nanotubular motifs. Chapter 2 focuses on the synthesis and characterization of fluorescent RNTs for investigations into the possibility of cellular internalization and the delivery of biological cargo into cells. Chapter 3 looks at the synthesis and characterization of a G^C motif labeled with a radioactive metal chelator. Subsequent labeling will provide radioactive RNTs that will be used to determine the *in vivo* biodistribution of RNTs under physiological conditions.

1.9. References

1. J. Steed, D. Turner and K. J. Wallace "Core concepts in supramolecular chemistry and nanochemistry," Wiley, **2005**.
2. A. Werner: *Zeitschr. Anorg. Chem. Ges.* 27, 2985 (**1894**).
3. E. Fischer, "Effekt der zuckerkonfiguration auf die enzymwirkung," *Ber. Duetch. Chem.* **1894**, 27, 2984.
4. D. J. Cram, T. Kaneda, R. C. Helgeson, and G. M. Lein, "Spherands - Ligands whose binding of cations relieves enforced electron-electron repulsions," *J. Am. Chem. Soc.*, **1979**, 101, 6752.
5. Charles J. Pedersen, "Cyclic polyethers and their complexes with metal salts," *J. Am. Chem. Soc.* **1967**, 89, 2495.
6. B. Dietrich, J. M. Lehn and J. P. Sauvage, "Diaza-polyoxa-macrocycles and macrobicycles," *Tett. Lett.* **1969**, 10, 34, 2885.
7. Jean-Marie Lehn, "Supramolecular chemistry: concepts and perspectives," VCH, New York, **1995**.
8. (a) J. Rebek, Jr., "Molecules in quarantine," *Nature*, **2006**, 444, 557. (b) A. Gissot and J. Rebek, Jr., "A functionalized, deep cavitand catalyzes the aminolysis of a choline derivative," *J. Am. Chem. Soc.* **2004**, 126, 7424.
9. S. C. Zimmerman, K. W. Saionz, and B. Zeng, "Chemically bonded stationary phases that use synthetic hosts containing aromatic binding clefts: HPLC analysis of nitro-substituted polycyclic aromatic hydrocarbons," *Proc. Natl. Acad. Sci. USA.* **1993**, 90, 1190.
10. M. Simard, D. Su and J. D. Wuest, "Use of hydrogen bonds to control molecular aggregation. Self-assembly of three-dimensional networks with large chambers," *J. Am. Chem. Soc.* **1991**, 113, 4696.
11. (a) R. Ballardini, V. Balzani, M. T. Gandolfi, L. Prodi, M. Venturi, D. Philip, H. G. Ricketts and J. Fraser Stoddart, "A photochemically driven molecular machine," *Angew. Chem. Int. Ed. Engl.* **1993**, 32, 1301. (b) B. Y. Bunimovich, E. Johnston-Halprin, E. DeIonno, Y. Luo, B. A. Sheriff,

- K. Xu, Y. S. Shin, H.- R. Tseng, J. F. Stoddart, J. R. Heath, "A 160-kilobit molecular electronic memory patterned at 10^{11} bits per square Centimeter," *Nature*. **2007**, 445, 414.
12. W. L. Jorgensen, T. B. Nguyen, E. M. Sanford, I. Chao, K. N. Houk, and F. Diederich, "Enhanced view of structure and binding for cyclophane-arene complexes through joint theoretical and experimental study," *J. Am. Chem. Soc.* **1992**, 114, 4003.
13. (a) K. D. Schierbaum, T. Weiss, E. U. Thoden van Veizen, J. F. J. Engbersen, D. N. Reinhoudt, and W. Göpel, "Molecular recognition by self-assembled monolayers of cavitand receptors," *Science*. **1994**, 265, 1413. (b) L. J. Prins, F. De Jong, P. Timmerman and D. N. Reinhoudt, "An enantiomerically pure Hydrogen-bonded Assembly," *Nature*. **2000**, 408, 181.
14. (a) J. Aizenberg, A. J. Black, and G. M. Whitesides, "Control of crystal nucleation by patterned self-assembled monolayers," *Nature*. **1999**, 398, 495. (b) H. O. Jacobs and G. M. Whitesides, "Submicrometer patterning of charge in thin film lectrets," *Science*. **2001**, 291, 1763.
15. C. Yamamoto, Y. Okamoto, T. Schmidt, R. Jäger, and F. Vögtle, "Enantiomeric resolution of cycloenantiomeric rotaxane, topologically chiral catenane, and pretzel-shaped molecules: Observation of pronounced circular dichroism," *J. Am. Chem. Soc.* **1997**, 119, 10547.
16. J. L. Atwood, L. J. Barbour, and A. Jerga, "Storage of methane and freon by interstitial van der Waals confinement," *Science*. **2002**, 296, 2367.
17. G. M. Whitesides, E. E. Simanek, J. P. Mathias, C. T. Seto, D. Chin, M. Mammen, and D. M. Gordon, "Noncovalent synthesis: Using physical-organic chemistry to make aggregates," *Acc. Chem. Res.* **1995**, 28, 37.
18. R. B. Woodward, "The total synthesis of vitamin B₁₂," *Pure and Appl. Chem.* **1973**, 33, 145.
19. R. W. Armstrong, J.-M. Beau, S. H. Cheon, W.J. Christ, H. Fujioka, W.-H. Ham, L. D. Hawkins, H. Jin, S. Ho Kang, Y. Kishi, M. J. Martinelli, W.

- W. McWhorter, Jr., M. Mizuno, M. Nakata, A. E. Stutz, F. X. Talamas, M. Taniguchi, J. A. Tino, K. Ueda, Jun-ichi Uenishi, J. B. White, and M. Yonaga, "Total synthesis of a fully protected playtoxin carboxylic acid," *J. Am. Chem. Soc.* **1989**, 111, 7525.
20. K. C. Nicolaou, E. J. Sorensen, "Classics in total synthesis," VCH, New York, **1996**.
21. J-M. Lehn, "Supramolecular Chemistry- Scope and perspectives, molecules, supermolecules and molecular devices (Nobel lecture)," *Angew. Chem. Int. Ed. Engl.* **1988**, 27, 89.
22. J-M. Lehn, "Towards Complex Matter: Supramolecular chemistry and self-organization," *Proc. Natl. Acad. Sci USA.* **2002**, 99, 8, 4763.
23. E. V. Anslyn and D. A. Dougherty, "Modern physical organic chemistry," Univ. Science Book, **2005**.
24. S. C. Zimmerman and P. S. Corbin, "Heteroaromatic modules for the self-assembly using multiple hydrogen bonds," *Struc. and Bond.* **2000**, 66, 64.
25. (a) L. J. Prins, E. E. Neuteboom, V. Paraschiv, M. Crego-Calama, P. Timmerman, and D. N. Reinhoudt, "Kinetic stabilities of double, tetra-, and hexarosette hydrogen-bonded assemblies," *J. Org. Chem.* **2002**, 67, 4808. (b) M. G. J. Ten- cate, M. Omerovic, G. V. Oshovsky, M. Crego-Calama, and D. N. Reinhoudt, "Self-assembly and stability of double nanostructures with biological functionalities," *Org. Biomol. Chem.* **2005**, 3, 3727. (c) V. Paraschiv, M. Crego-Calamas, R. H. Fokkens, C. J. Padberg, P. Timmerman, and D. N. Reinhoudt, "Nanostructures via noncovalent synthesis: 144 hydrogen bonds bring together 27 components," *J. Org. Chem.* **2001**, 66, 8297.
26. M. Mammen, E. E. Simanek, and G. M. Whitesides, "Predicting the relative stabilities of multiparticle hydrogen-bonded aggregates based on the number of hydrogen bonds and the number of particles and measuring these stabilities with titrations using dimethyl sulfoxide," *J. Am. Chem. Soc.* **1996**, 118, 12614.

27. (a) W. L. Jorgensen and J. Pranata, "Importance of secondary interactions in triply hydrogen bonded complexes: Guanine-Cytosine vs Uracil-2,6-diaminopyridine," *J. Am. Chem. Soc.* **1990**, 112, 2008. (b) J. Pranata, S. G. Wierschke and W. L. Jorgensen, "OPLS potential functions for nucleotide bases. Relative association constants of hydrogen-bonded base pairs in chloroform," *J. Am. Chem. Soc.* **1991**, 113, 2810.
28. (a) T. J. Murray and S. C. Zimmerman, "New triply hydrogen bonded complexes with highly variable stabilities," *J. Am. Chem. Soc.* **1992**, 114, 4010. (b) D. C. Sherrington and K. A. Taskinen, "Self-assembly in synthetic macromolecular systems via multiple hydrogen bonding interactions," *Chem. Soc. Rev.* **2001**, 30, 83.
29. F. H. Beijer, R. P. Sijbesma, J. A. J. M. Vekemans, E. W. Meijer, H. Kooijman, and A. L. Spek, "Hydrogen-bonded complexes of diaminopyridines and diaminotriazines: Opposite effect of acylation on complex stabilities," *J. Org. Chem.* **1996**, 61, 6371.
30. C. Elschenbroich, "Organometallics: A concise introduction," 3rd Edt, VCH, Weinheim, Germany, **2006**.
31. (a) C. A. Hunter and J. K. Saunders, "The nature of the π - π interactions," *J. Am. Chem. Soc.* **1990**, 112, 5525. (b) C. A. Hunter, "Molecular recognition of p-benzoquinone by macrocyclic Host," *J. Chem. Soc. Chem. Commun.* **1991**, 749.
32. W. Saenger, "Principles of nucleic acid structure," Springer-Verlag; New York, **1984**, 132.
33. A. Sygula, F. R. Fronczek, R. Sygula, P. W. Rabideau, and M. M. Olmstead, "A double concave hydrocarbon buckycatcher," *J. Am. Chem. Soc.* **2007**, 129, 3842.
34. A. Petitjean, R. G. Khoury, N. Kyritsakas, and J-M. Lehn, "Dynamic devices. Shape switching and substrate binding in ion-controlled nanomechanical molecular tweezers," *J. Am. Chem. Soc.* **2004**, 126, 6637.

35. B. Alberts, "Molecular biology of the cell," **1989**, Garland, New York, Ed. 2, 84.
36. (a) P. A. Grieco, Ed., "Organic Synthesis in Water," Thomson science: London, **1998**. (b) C. J. Li and T. H. Chan, "Organic reactions in aqueous media," Wiley: New York, **1997**. (c) J. B. F. N. Engberts and M. J. Blandamer, "Understanding organic reactions in water: from hydrophobic encounters to surfactant aggregates," *Chem. Commun.* **2001**, 18, 1701.
37. (a) N. T. Southall, K. A. Dill, and A. D. J. Haymet, "A view of the hydrophobic effect," *J. Phys. Chem. B.* **2002**, 106, 521. (b) W. Blokijl and J. B. F. N. Engberts, "Hydrophobic effects. Opinions and facts," *Angew. Chem. Int. Ed. Engl.* **1993**, 32, 1545.
38. M. S. Frank and M. W. Evans, "Free volume and entropy in condensed systems III. Entropy in binary liquid mixtures; partial molal entropy in dilute solutions; structure and thermodynamics in aqueous electrolytes," *J. Chem. Phys.* **1945**, 13(11), 507.
39. (a) G. Némethy, H. A. Scheraga, "Structure of water and hydrophobic bonding in proteins. I. A model for the thermodynamic properties of liquid water," *J. Chem. Phys.* **1962**, 36, 3382. (b) G. Némethy and H. A. Scheraga, "Structure of water and hydrophobic bonding in proteins. II. Model for the thermodynamic properties of aqueous solutions of hydrocarbons," *J. Chem. Phys.* **1962**, 36, 3401. (c) G. Némethy, "Hydrophobic interactions," *Angew. Chem. Int. Ed. Engl.* **1967**, 6, 195. (d) H. S. Frank and W-Y Wen, "Ion-solvent interaction. Structural aspect of ion-solvent interaction: A suggested picture of water structure," *Discuss. Faraday Soc.* **1957**, 24, 133.
40. K. W. Miller and J. H. Hildebrand, "Solution of inert gas in water," *J. Am. Chem. Soc.* **1968**, 90, 3001.
41. O. W. Howarth, "Reassessment of hydrophobic bonding," *J. Chem. Soc. Faraday Trans. 1*, **1975**, 71, 2303.

42. (a) D. J. Cram, "Preorganization from solvents to spherands," *Angew. Chem. Intl. Ed. Engl.* **1986**, 25, 1039. (b) D. J. Cram, "The design of molecular hosts, guests, and their complexes (Nobel Lecture)," *Angew. Chem. Intl. Ed. Engl.* **1988**, 27, 1009.
43. (a) J. Atwood and J. W. Steed, 'Supramolecular chemistry', John Wiley and Sons, **2000**. (b) J. W. Steed, "Supramolecular chemistry: Definition," *Encyclopedia of Supramolecular Chemistry*, **2004**, 1, 1, 1401.
44. B. W. Purse and J. Rebek, Jr., "Self-fulfilling cavitands: Packing alkyl chains into small spaces," *Proc. Natl. Acad. Sci. USA*. **2006**, 103, 2530.
45. G. M. Whitesides and B. Grzybowski, "Self-assembly at all scales," *Science*. **2002**, 295, 2418.
46. D. J. Kushner, "Self-assembly of biological structures," *Bacteriol. Rev.* **1969**, 33, 302.
47. (a) J. S. Lindsey, "Self-assembly in Synthetic routes to Molecular Devices. Biological principles and chemical perspectives: a review," *New J. Chem.* **1991**, 15, 153. (b) J. A. Thomas, "Self-assembly: Definition and kinetic and thermodynamic consideration," *Encyclopedia of Supramolecular Chemistry*. **2004**, 1: 1, 1248.
48. (a) D. H. Williams; M. S. Westwell, "Aspect of weak interaction," *Chem. Soc. Rev.* **1998**, 27, 57. (b) L. Liu, Q-X Guo, "Isokinetic relationship, isoequilibrium relationship, enthalpy-entropy compensation," *Chem. Rev.* **2001**, 101, 673.
49. (a) D. J. Cram and J. M. Cram, "Container molecules and their guest." In monographs in supramolecular chemistry; J. F. Stoddart, ed., Royal society of Chemistry: Cambridge, **1990**, 39. (b) J. C. Sherman, "Preorganization and complementarity," *Encyclopedia of Supramolecular Chemistry*. **2004**, 1:1, 1158.
50. A. Klug, "From macromolecules to biological assemblies (Nobel Lecture)," *Angew. Chem. Intl. Ed. Engl.* **1983**, 22, 565.

51. S. Iijima, "Helical microtubules of graphitic carbon," *Nature*. **1991**, 354, 56.
52. Bottom - up - approach: the synthesis of nanoscale structures and devices by chemically building up from the molecular level. Top-down approach: the use of microfabrication techniques that reduce bulk matter into smaller components to form nanoscale features or objects.
53. S. Hetch, "Functional organic nanotubes from hollow scaffolds," *Synthetic Met.* **2004**, 147, 37.
54. B. Eisenberg, "Ionic channels in biological membranes: Natural nanotube," *Acc. Chem. Res.* **1998**, 31, 117.
55. S. Rye, S. G. Burston, W. A. Fenton, J. M. Beechem, Z. Xu, P. B. Sigler and A. L. Horwich, "Distinction actions of cis and trans ATP within the double ring of the chaperonin GroEL," *Nature*. **1997**, 388, 792.
56. M. Borgnia, S. Nielsen, A. Engel and P. Agre, "Cellular and molecular biology of the aquaporin water channels," *Ann Rev of Biochemy*. **1999**, 68, (1), 425.
57. R. R. Ketchum and W. Hu, T. A. Cross, "High-resolution conformation of gramicidin A in a lipid bilayer by solid-state NMR," *Science*. **1993**, 261, 1457.
58. D. S. Jackson and M. E. Grant, "The collagen triple helix," *Nature*. **1974**, 249, 406.
59. G. McDermott, S. M. Prince, A. A. Freer, A. M. Hawthornthwaite-Lawless, M. Z. Papiz, R. J. Cogdell, and N. W. Isaacs, "Crystal structure of an integral membrane light-harvesting complex from photosynthetic bacteria," *Nature*. **1995**, 374, 517.
60. P. De Santis, S. Morosetti, and R. Rizzo, "Conformational analysis of regular enantiomeric sequences," *Macromolecules*. **1974**, 7, 52.
61. (a) J. Zhu, R. D. Parra, H. Zeng, E. Skrzypczak-Jankun, X. C. Zeng, and B. Gong, "A new class of folding oligomers: Crescent oligoamides," *J. Am. Chem. Soc.* **2000**, 122, 4219. (b) B. Gong, H. Zeng, J. Zhu, L. Yuan,

- Y. Han, S. Cheng, M. Furukawa, R. D. Parra, A. Y. Kovalevsky, J. L. Mills, E. Skrzypczak-Jankun, S. Martinovic, R. D. Smith, C. Zheng, T. Szyperski, and X. Cheng Zeng, "Creating nanocavities of tunable sizes: Hollow helices," *Proc. Natl. Acad. Sci. USA*. **2002**, 99, 11583.
62. (a) J. C. Nelson, J. G. Saven, J. S. Moore, and P. G. Wolynes, "Solvophobic driven folding of nonbiological oligomers," *Science*. **1997**, 277, 1793. (b) D. J. Hill, M. J. Mio, R. B. Prince, T. S. Hughes, and J. S. Moore, "A field guide to foldamers," *Chem. Rev.* **2001**, 101, 3893.
63. K. Matsuda, M. T. Stone, and J. S. Moore, "Helical pitch of *m*-phenylene ethynylene foldamers by double spin labeling," *J. Am. Chem. Soc.* **2002**, 124, 11836.
64. V. Berl, I. Huc, R. G. Khoury, and J-M Lehn, "Helical molecular programming: folding of oligopyridine-dicarboxamides into molecular single helices," *Chem. Eur. J.* **2001**, 7, 2798 (b) V. Berl, I. Huc, R. G. Khoury, and J-M Lehn, "Helical molecular programming: Supramolecular double helices by dimerization of helical oligopyridine-dicarboxamide strands," *Chem. Eur. J.* **2001**, 7, 2810. (c) V. Berl, I. Huc, R. G. Khoury, and J-M. Lehn, "Interconversion of single and double helices formed from synthetic molecular strands," *Nature*. **2000**, 407, 720.
65. J. J. van Gorp, J. A. J. M. Vekemans and E. W. Meijer, "Facile synthesis of a chiral polymeric helix; folding by intramolecular hydrogen bonding," *Chem. Commun.* **2004**, 60.
66. (a) G. S. Hanan, J-M. Lehn, N. Kyritsakas and J. Fischer, "Molecular helicity: A general approach for helicity induction in a polyheterocyclic molecular strand," *Chem. Soc. Chem. Commun.* **1995**, 765. (b) D. M. Bassani, J-M. Lehn, G. Baum, and D. Fenske, "Designed self-generation of an extended helical structure from an achiral polyheterocyclic strand," *Angew. Chem. Int. Ed. Engl.* **1997**, 36, 1845. (c) M. Ohkita, J-M. Lehn, G. Baum, and D. Fenske, "Helicity coding: Programmed molecular self-organization of achiral nonbiological strands into multiturn helical

- superstructures: Synthesis and characterization of alternating pyridine-pyrimidine oligomers,” *Chem. Eur. J.* **1999**, 5, 3471.
67. L. A. Cuccia, J-M. Lehn, J-C. Homo, and M. Schmutz, “Encoded helical self-organization and self-assembly into helical fibers of an oligoheterocyclic pyridine - pyridazine molecular strand,” *Angew. Chem. Int. Ed. Engl.* **2000**, 39, 233.
68. A. Ajayaghosh, R. Varghese, S. Mahesh, and V. K. Praveen, “From vesicles to helical nanotubes: A sergeant-and-soldiers effect in the self-assembly of oligo (*p*-phenyleneethynylene)s,” *Angew. Chem. Int. Ed. Engl.* **2006**, 45, 7729.
69. G. Dan Panto, P. Pengo, and J. K. M. Sanders, “Hydrogen-bonded helical organic nanotubes,” *Angew. Chem. Int. Ed. Engl.* **2006**, 46, 194.
70. B. Grunbaum and G. C. Shephard, “Tilings and patterns,” W. H. Freeman and Company: New York, **1987**.
71. (a) C. Mao, W. Sun, and N. C. Seeman, “Designed two-dimensional DNA holliday junction arrays visualized by atomic Force Microscopy,” *J. Am. Chem. Soc.* **1999**, 121, 5437. (b) T. H. LaBean, H. Yan, J. Kopatsch, F. Liu, E. Winfree, J. H. Reif, and N. C. Seeman, “Construction, analysis, ligation, and self-assembly of DNA triple crossover complexes,” *J. Am. Chem. Soc.* **2000**, 122, 1848. (c) D. Liu, M. Wang, Z. Deng, R. Walulu, and C. Mao, “Tensegrity: Construction of rigid DNA triangles with flexible four-arm DNA junctions,” *J. Am. Chem. Soc.* **2004**, 126, 2324.
72. E. Winfree, F. R. Liu, L. A. Wenzler, and N. C. Seeman, “Design and self-assembly of two-dimensional DNA crystals,” *Nature.* **1998**, 394, (6693), 539.
73. (a) D. Liu, S. H. Park, J. H. Reif, and T. H. LaBean, “DNA nanotubes self-assembled from triple-crossover tiles as templates for conductive nanowires,” *Proc. Natl. Acad. Sci. USA.* **2004**, 101, 717. (b) J. C. Mitchell, J. R. Harris, J. Malo, J. Bath, and A. J. Turberfield, “Self-assembly of chiral DNA nanotubes,” *J. Am. Chem. Soc.* **2004**, 126, 16342. (c) P. W. K.

- Rothmund, A. Ekani-Nkodo, N. Papadakis, A. Kumar, D. K. Fygenon, and E. Winfree, "Design and characterization of programmable DNA nanotubes," *J. Am. Chem. Soc.* **2004**, 126, 16344. (d) P. O'Neill, P.W. K. Rothmund, A. Kumar, and D. K. Fygenon, "Sturdier DNA nanotubes via ligation," *Nano Lett.* **2006**, 6, 1379.
74. (a) H. Yan, S. Ha Park, G. Finkelstein, J. H. Reif, and T. H. LaBean, "DNA-templated self-assembly of protein arrays and highly conductive nanowires," *Science.* **2003**, 301, 1882.
75. J. N. Israelachivili, "Intermolecular and surface forces," Academic press: New York, **1985**.
76. T. Shimizu, M. Masuda, and H. Minamikawa, "Supramolecular nanotube architectures based on amphiphilic molecules," *Chem. Rev.* **2005**, 105, 1401.
77. V. Percec, C.-H. Ahn, G. Ungar, D. J. P. Yearley, M. Möller and S. S. Sheiko, "Controlling polymer shape through the self-assembly of dendritic side-groups," *Nature*, **1998**, 391, 161.
78. (a) D. L. Gin, W. Gu, B.A. Pindzola, and W-J. Zhou, "Polymerized lyotropic liquid crystal assemblies for materials applications," *Acc. Chem. Res.* **2001**, 34, 973. (b) W. Zhou, W. Gu, Y. Xu, C. S. Pecinovsky, and D. L. Gin, "Assembly of acidic amphiphiles into inverted hexagonal phases using an L-alanine based surfactant as a structure-directing agent," *Langmuir.* **2003**, 19, 3638.
79. N. Nakashima, S. Asakuma, and T. Kunitake, "Optical microscopic study of helical superstructures of chiral bilayer membranes," *J. Am. Chem. Soc.* **1985**, 107, 59.
80. W. Srisiri, T. M. Sisson, D. F. O'Brien, K. M. McGrath, Y. Han, and S. M. Grune, "Polymerization of the inverted hexagonal phase," *J. Am. Chem. Soc.* **1997**, 119, 4866.

81. J. H. Fuhrhop, P. Schnieder, E. Boekema, and W. Helfrich, "Lipid bilayer fibers from diastereomeric and enantiomeric *N*-octylaldonamides," *J. Am. Chem. Soc.* **1988**, 110, 2861.
82. (a) K. Yu and A. Eisenberg, "Bilayer morphologies of self-assembled crew-cut aggregates of amphiphilic PS-*b*-PEO diblock copolymers in solution," *Macromolecules.* **1998**, 31, 3509. (b) M. Antonietti and S. Förster, "Vesicles and liposomes: A self-assembly principle beyond lipids," *Adv. Mater.* **2003**, 15, 1323.
83. S. Stewart and G. Liu, "Block copolymer nanotubes," *Angew. Chem. Int. Ed. Engl.* **2000**, 39, 340.
84. J. Grumelard, A. Taubert and W. Meier, "Soft nanotubes from amphiphilic ABA triblock macromonomers," *Chem. Commun.* **2004**, 1462.
85. D. Yan, Y. Zhou, and J. Hou, "Supramolecular self-assembly of macroscopic tubes," *Science.* **2004**, 33, 65.
86. D. D. Lasic, "Liposomes in gene delivery," CRC press: Boca Raton, FL, **1997**.
87. D. D. Archibald and S. Mann, "Self-assembled microstructures from 1,2-ethanediol suspensions of pure and binary mixtures of neutral and acidic biological galactosylceramides," *Chem. Phys. Lipid.* **1994**, 69, 51.
88. J. I. M. Schnur, R. Price, and A. S. Rudolph, "Biologically engineered microstructures: Controlled release applications," *J. Controlled Release*, **1994**, 28, 3.
89. (a) M. R. Ghadiri, J. R. Granja, R. A. Milligan, D. E. McRee and N. Khazanovich, "Self-assembling organic nanotubes based on a cyclic peptide architecture," *Nature.* **1993**, 366 324. (b) N. Khazanovich, J. R. Granja, D. E. McRee, R. A. Milligan, and M. R. Ghadiri, "Nanoscale tubular ensembles with specified internal diameters. Design of a self-assembled nanotube with a 13 - ANG pore," *J. Am. Chem. Soc.* **1994**, 116, 6011.

90. A. Harada, J. Li and M. Kamachi, "Synthesis of a tubular polymer from threaded cyclodextrins," *Nature*. **1993**, 364, 516.
91. (a) P. R. Ashton, C. L. Brown, S. Menzer, S. A. Nepogodiev, J. F. Stoddart, and D. J. Williams, "Synthetic cyclic oligosaccharides: Syntheses and structural properties of a cyclo[(1→4) - α - L-rhamnopyranose- (1→4)- α -D-manopyranosyl] trioside and-tetraoside," *Chem. Eur. J.* **1996**, 2, 580. (b) P. R. Ashton, S. J. Cantrill, G. Gattuso, S. Menzer, S. A. Nepogodiev, A. N. Shipway, J. F. Stoddart, and D. J. Williams, "Achiral cyclodextrin analogues," *Chem. Eur. J.* **1997**, 3, 1299. (c) G. Gattuso, S. Menzer, S. A. Nepogodiev, J. F. Stoddart, and D. J. Williams, "Carbohydrate nanotubes," *Angew. Chem. Int. Ed. Engl.* **1997**, 36, 1451.
92. (a) J. K. Young and J. S. Moore In: P. J. Stang, F. Diederich (eds), "Modern acetylene chemistry." VCH, Weinheim, Germany, **1995**, 415. (b) J. S. Moore, "Shape persistent molecular architectures of nanoscale dimension," *Acc. Chem. Res.* **1997**, 30, 402.
93. D. Venkataraman, S. Lee, J. Zhang and J. S. Moore, "An organic solid with wide channels based on hydrogen bonding between macrocycles," *Nature*. **1994**, 371, 591.
94. P. Müller, I. Usón, V. Hensel, A. D. Schlüter, and G. M. Sheldrick, "Crystal structure of a cyclotetraicosaphenylene," *Helv. Chim. Acta.* **2003**, 84, 778.
95. S. Höger, D. L. Morrison, and V. Enkelmann, "Solvent triggering between conformational states in amphiphilic shape-persistent macrocycles," *J. Am. Chem. Soc.* **2002**, 124, 6734.
96. M. Schappacher and A. Deffieux, "Synthesis of macrocyclic copolymer brushes and their self-assembly into supramolecular tubes," *Science*. **2008**, 319, 1512.
97. (a) M. Gellert, M. Lipsett and D. Davies, "Helix formation by guanylic acid," *Proc. Natl. Acad. Sci. USA.* **1962**, 48, 12, 2013. (b) T. J. Davis. "G

- Quartet 40 years later: from 5' – GMP to molecular biology and supramolecular chemistry,” *Angew. Chem. Int. Ed.* **2004**, 43, 6, 668.
98. T. J. Pinnavaia, C. L. Marshall, C. M. Mettler, C. L. Fisk, H. T. Miles, and E. D. Becker, “Alkali metal ion specificity in the solution ordering of a nucleotide, 5'-guanosine monophosphate,” *J. Am. Chem. Soc.* **1978**, 100, 3625.
99. (a) A. Wong, R. Ida, Lea Spindler, and G. Wu, “Disodium guanosine 5'-monophosphate self-associates into nanoscale cylinders at pH 8: A combined diffusion NMR spectroscopy and dynamic light scattering study,” *J. Am. Chem. Soc.* **2005**, 127, 6990. (b) W. A. Harell and J. T. Davis, “Self-assembly: Guanine nucleobase,” *Encyclopedia of Supramolecular Chemistry*. **2006**, 1:1, 1.
100. (a) X. D. Shi, J. C. Fettinger, M. M. Cai, and J. T. Davis, “Enantiomeric self recognition: Cation-templated formation of homochiral isoguanine pentamers,” *Angew. Chem. Int. Ed.* **2000**, 39, 3124. (b) M. M. Cai, X. D. Shi, V. Sidorov, D. fabris, Y. F. Lam, and J. T. Davis, “Cation directed self-assembly of lipophilic nucleosides: The Cation’s central role in the structure and dynamics of a hydrogen-bonded assembly,” *Tetrahedron*. **2002**, 58, 661.
101. J. L. Sessler, M. Sathiosatham, K. Doerr, V. Lynch, and K. A. Abboud, “A G-quartet formed in the absence of a templating metal cation: A New 8-(*N,N*-dimethylaniline) guanosine derivative,” *Angew. Chem. Int. Ed.* **2000**, 39, 1300.
102. I. S. Choi, X. Li, E. E. Simanek, R. Akaba, and G. M. Whitesides, “Self-assembly of hydrogen-bonded polymeric rods based on the cyanuric acid-melamine lattice,” *Chem. Mater.* **1999**, 11, 684.
103. N. Kimizuka, T. Kawasaki, K. Hirata, and T. Kunitake, “Tube-like nanostructures composed of networks of complementary hydrogen bonds,” *J. Am. Chem. Soc.* **1995**, 117, 6360.

104. P. Jonkheijm, A. Miura, M. Zdanowska, F. J. M. Hoeben, S. De Feyter, A. P. H. J. Schenning, F. C. De Schryver, and E. W. Meijer, " π -conjugated oligo-(*p*-phenylenevinylene) rosettes and their tubular self-assembly," *Angew. Chem. Int. Ed. Engl.* **2004**, 43, 74.
105. H. Fenniri, Bo-Liang Deng, A. E. Ribbe, K. Hallenga, J. Jacob, and P. Thiyagarajan, "Entropically driven self-assembly of multichannel rosette nanotubes," *Proc. Natl. Acad. Sci. USA.* **2002**, 99, 6487.
106. H. Fenniri, P. Mathivanan, K. L. Vidale, D. M. Sherman, K. Hallenga, K. V. Wood, and J. G. Stowell, "Helical rosette nanotubes: Design, self-assembly, and characterization," *J. Am. Chem. Soc.* 2001, **123**, 3854.
107. (a) H. Fenniri, Bo-Liang Deng, and A. E. Ribbe, "Helical rosette nanotubes with tunable chiroptical properties," *J. Am. Chem. Soc.* **2002**, 124, 11064. (b) R. S. Johnson, T. Yamazaki, A. Kovalenko, and H. Fenniri, "Molecular basis for water-promoted supramolecular chirality inversion in helical rosette nanotubes," *J. Am. Chem. Soc.* **2007**, 129, 5735.
108. J. G. Moralez, J. Raez, T. Yamazaki, R. K. Motkuri, A. Kovalenko, and H. Fenniri, "Helical rosette nanotubes with tunable stability and hierarchy," *J. Am. Chem. Soc.* **2005**, 127, 8307.
109. (a) A. Chun, J.G. Moralez, T. J. Webster, and H. Fenniri, "Helical rosette nanotubes: A biomimetic coating for orthopedics?" *Biomaterials.* **2005**, 26, 7304. (b) A. Chun, J. G. Moralez, T. J. Webster, and H. Fenniri, "Helical rosette nanotubes: A more effective orthopaedic implant material," *Nanotechnology.* **2004**, 15, S234.
110. C. R. Martin and P. Kholi, "The emerging field of nanotube biotechnology," *Nature Reviews Drug Discovery.* **2003**, 2, 29.
111. Y. Liu, H. Miyoshi and M. Nakamura, "Nanomedicine for drug delivery and imaging: A promising avenue for cancer therapy and

diagnosis using targeted functional nanoparticles,” *Int. J. Cancer*, **2007**, 120, 2527.

112. G. M. Whitesides, “Nanoscience, Nanotechnology and chemistry”, *Small*, **2005**, 2, 172.

Chapter 2: Fluorescent labeled RNTs.

2.1. Introduction

Research into the delivery and targeting of therapeutic and diagnostic agents with nanoparticles represents the forefront of nanomedicine because the efficiency of drug delivery is a direct function of particle size.¹ Several nanoparticle based technologies are already commercially available and in clinical use, such as liposomal formulations for cancer therapy, colloidal gold for *in vitro* diagnostics, and magnetic nanoparticles for *in vivo* imaging.² The pursuit of new types of molecular transporters is an active area of research, due to the high impermeability of cell membranes to foreign substances and the need for intracellular delivery of molecules for drug, gene, or protein therapeutics.³

Carbon nanotubes, in particular single wall carbon nanotubes (SWNTs), have received much attention in this area of research because of their unique physico-chemical properties.⁴ CNTs are used for *in vivo* delivery of drugs,⁵ proteins, peptides,⁶ nucleic acid,⁷ *in vivo* tumour imaging,⁸ gene transfer and gene silencing.⁹ However, concerns about the potential toxicity of SWNTs have been raised,¹⁰ and this is directly related to their insolubility, which can lead to bioaccumulation, and the presence of residual toxic transition metal catalysts that remain from the manufacturing process.

In light of the potential biomedical applications of CNTs as well as the toxicological concerns about CNTs, we sought to further investigate the biomedical potential of our water soluble, metal-free organic nanotubes (RNTs).¹¹ To this end, we synthesized the twinbase G[^]C motif, **38** (Scheme 2.1), which was then functionalized with fluorescein isothiocyanate (FITC) to explore the feasibility of cellular uptake of RNTs and the mechanism by which such an uptake would occur.¹² Furthermore, we wished to develop a general procedure for the tracking of RNTs by coassembling small amounts of the fluorescent G[^]C

motif, **41**, with other G[^]C motifs thus producing RNTs that are tagged with the fluorophore. Functionalization of RNTs with the biotin-streptavidin complex was pursued to assess the possibility of delivering large biological cargoes under *in vivo* conditions into cells. Self-assembly of our nanotubes was studied using scanning electron microscopy (SEM), transmission electron microscopy (TEM), tapping mode-atomic force microscopy (TM-AFM), ultraviolet-visible spectroscopy (UV-vis) and molecular modelling, and cellular uptake was investigated using fluorescence microscopy.

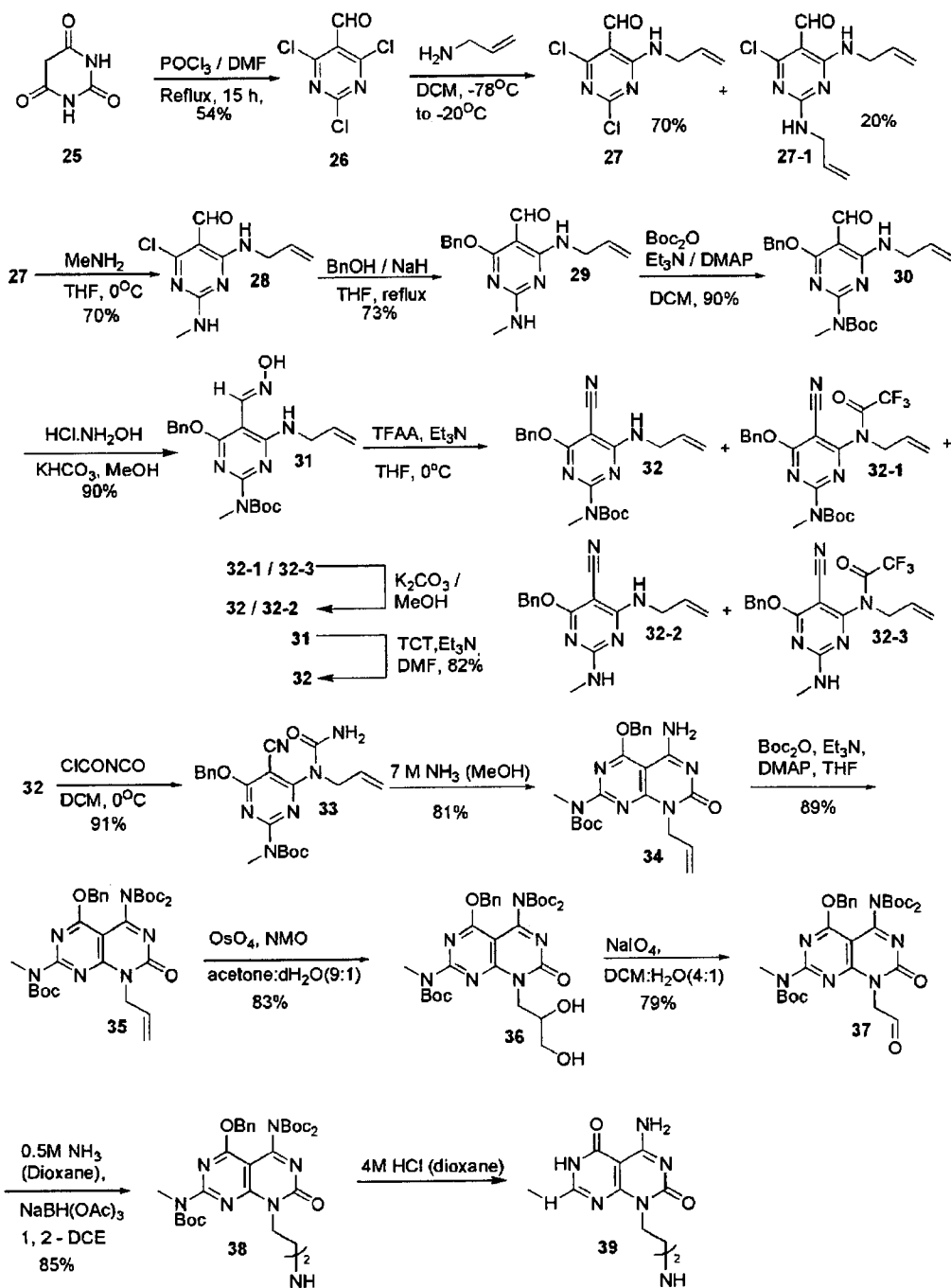
2.2. Results and Discussion

2.2.1. Synthesis of G[^]C Twinbase (39)

Our research group focuses on the synthesis of RNTs by self-assembling a bicyclic G[^]C motif possessing the Watson-Crick donor-donor-acceptor of guanine and the acceptor-acceptor-donor hydrogen bonding sites of cytosine.¹³ Our research,¹⁴ along with others,¹⁵ has shown that the more preorganized a molecular motif is, the more thermodynamically stable are its rosettes, and in our case the more thermodynamically stable will be our NTs. In order to synthesize a more preorganized G[^]C motif, we decided to link two G[^]C aldehyde, **37**, covalently by reductive amination with ammonia to give **38**. The twinbase motif is more preorganized than the monobase because it forms twin rosettes that are held together by 36 H-bonds compared to 18 for the monobase.¹⁴ The secondary amino group of **38** can be used to functionalize the twinbase motif, thus affording RNTs that are more thermodynamically stable than their monobase counterparts.

To successfully prepare the twinbase G[^]C motif, **38**, we first had to synthesize the aldehyde, **37** (Scheme 2.1), which has been reported by our group.¹³ The synthesis of **37** was done on a scale of 150 grams (1.17 mol Barbituric acid) with one minor exception. It was reported that the oxime, **31**, was dehydrated with trifluoroacetic anhydride (TFAA) to afford the nitrile **32**, with a yield of 79%. The scale up of

this step was not as successful as was reported, in that the desired nitrile **32**, along with the Boc deprotected amine **32-2**, and two trifluoroacetamide side products (**32-1** and **32-3**) were detected by LCMS. The trifluoroacetamide side products were converted to their free amines by treatment with K_2CO_3 in methanol¹⁶ to give the nitrile **32** and the secondary amine **32-2** with yields of 51 and 11%, respectively. This step was optimised by treating the oxime **31** with 2,4,6-trichloro-1,3,5-triazine (TCT) which produced the desired compound, **32**, in a yield of 86%.¹⁷ The synthesis of the **37** was then completed as previously reported. The synthesis of the twinbase, **39**, was completed by reacting the aldehyde **37** with excess ammonia to afford **38**, the protected precursor of **39**, in a yield of 85%. Deprotection of **38** with 4 M HCl afforded the corresponding hydrochloride salt **39**.

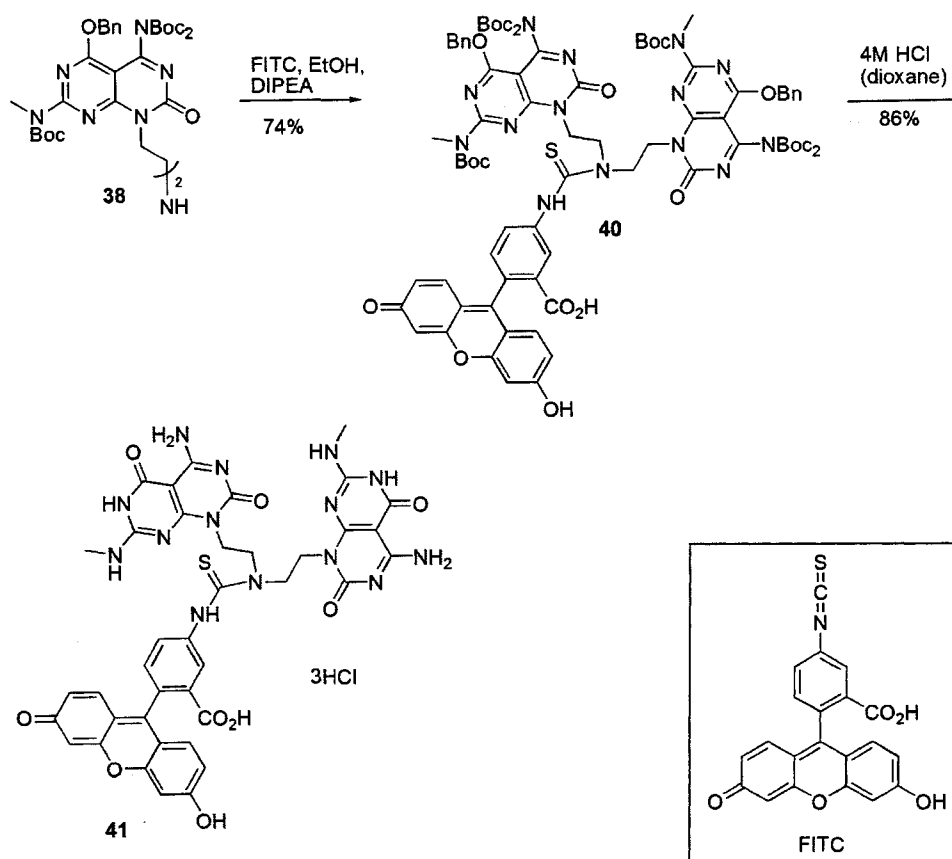


Scheme 2.1. Large scale synthesis of the twinbase G[^]C motif, 39.

2.2.2. Synthesis of FITC G[^]C Twinbase (41)

Many hydrophobic compounds of low molecular weight are known to diffuse freely through low-polarity cell membranes.¹⁸ Our low molecular weight,

hydrophobic, bicyclic G[^]C motif undergoes a hierarchical self-assembly process under physiological conditions to form a six-member supramacrocycle (rosette) that is substantially more hydrophobic than the molecular G[^]C motif. The hydrophobicity is enhanced further when these rosettes stack to form RNTs, thus we decided to investigate the possibility of cellular internalization of our RNTs. To this end, we functionalized the twinbase G[^]C motif (**38**) with the fluorescent dye, FITC; thus generating FITC labeled RNTs upon self-assembly.



Scheme 2.2. Synthesis of the FITC functionalized twinbase G[^]C motif, **41**.

Scheme 2.2 illustrates the synthesis of the FITC functionalized G[^]C twinbase, **41**. By coupling FITC and compound **38** in the presence of Hunig's base the protected G[^]C-FITC conjugate, **40**, was obtained in a yield of 74%. Global deprotection of **40** with 4 M HCl afforded the target compound, **41**, in a yield of 86%.

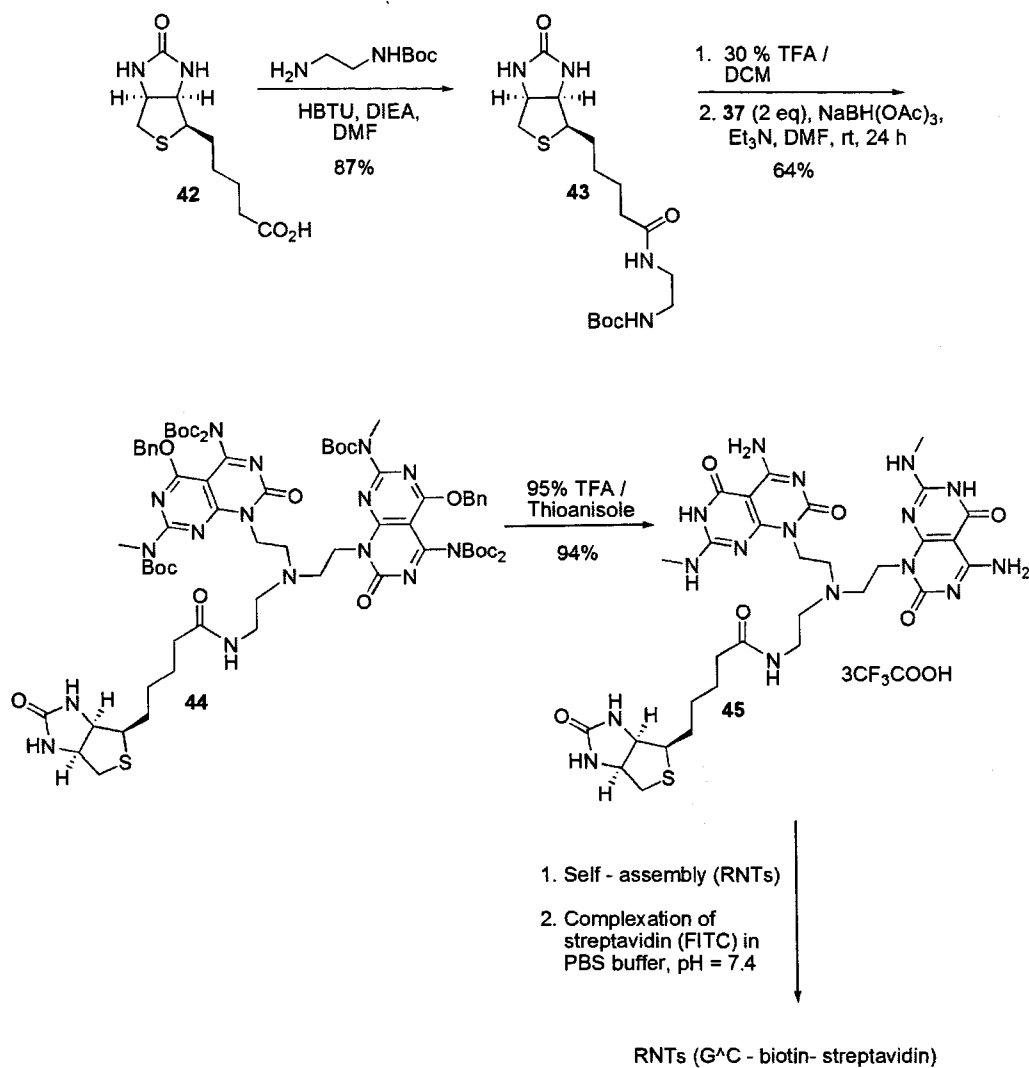
2.2.3. Synthesis of Biotin-Streptavidin (FITC) labeled G[^]C motif (45)

The effectiveness of therapeutics and cellular probes depends critically on the efficient delivery of molecules into living cells. The poor cellular penetration of many small molecules and macromolecules such as proteins and nucleic acids requires the development of new strategies for cellular penetration. Researchers have shown that cellular uptake can be enhanced by covalently or non-covalently attaching the molecular cargo to cationic, hydrophobic or amphipathic polymers, or hydrophobic lipids.³ An area that is receiving a lot of attention is the use of nanotubes as biocompatible transporters. In light of this, we decided to study the possibility of using our RNTs for the cellular transportation of molecular cargo.

RNTs for molecular transportation were synthesized by functionalizing the G[^]C twinbase motif with D-(+)-biotin (vitamin H) and self-assembling this adduct into RNTs. The NTs were then complexed with the protein streptavidin, which was tagged with the fluorophore FITC, to produce biotin-streptavidin-RNTs. The protein streptavidin was chosen because of its large size (~53 KDa), strong binding affinity for biotin ($K_d \sim 100$ fM) and its known clinical application in anticancer therapies.¹⁹

The synthesis of **43** (Scheme 2.3) began by coupling *N*-Boc diaminoethane to the carboxylic acid group of D-(+)-biotin using HBTU and Hunig's base to afford **43**. The purification of **43** was somewhat challenging in that it was insoluble in most common organic solvents, except for DMF and DMSO, and it remained at the baseline of the TLC plate (silica gel) when eluted with 20% MeOH/CH₃CN.

However, it was purified by precipitation with Et₂O. Compound **43** was then treated with 30% TFA/DCM for 4 h, and then precipitated with Et₂O to produce a viscous gum, which was then dissolved in DMF and coupled to **37** under reductive amination conditions to afford **44** in a yield of 64%. Compound **44** was then globally deprotected with TFA to afford the TFA salt **45** in 94% yield. This synthesis benefited tremendously from the experimental work conducted in Chapter 3.



Scheme 2.3. Synthesis of RNTs functionalized with a biotin-streptavidin complex.

2.3. Microscopic Characterization of FITC RNTs

The self-assembly of compound **39** into RNTs was investigated by dissolving 1.0 mg of compound **39** in 1.0 mL of dH₂O (pH = 4.73) and then taking 25 μ L of this solution and diluting it to 1.0 mL with dH₂O (pH = 5.21). The formation of rosette nanotubes was instantaneous (Fig 2.1.A & B), and TM-AFM measurements indicated that they have an average diameter of 2.0 ± 0.2 nm (Fig 2.1.C & D). This demonstrated that the twinbase, compound **39**, is capable of forming RNTs in water, thus making it an ideal scaffold for the synthesis of RNTs that can be functionalized for biological applications.

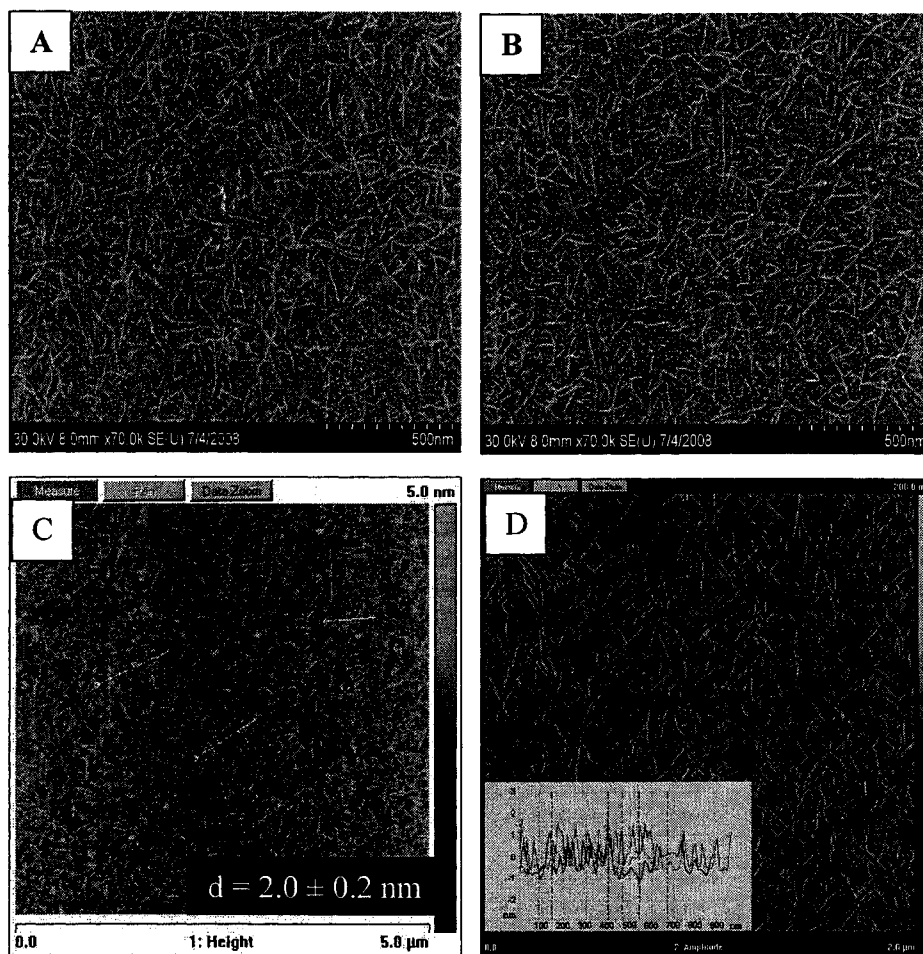


Figure 2.1. SEM (A and B) and TM-AFM (C and D) of **39** ($0.025 \text{ mg}\cdot\text{mL}^{-1}$) in water immediately after preparation.

After observing that compound **39** was capable of forming RNTs instantaneously in water, we set out to covalently functionalize compound **38**, the protected precursor of **39**, with fluorescein-5'- isothiocyanate (FITC). The fluorophore FITC was chosen because of its highly electrophilic isocyanate moiety, but more importantly because of its high photostability i.e. low degree of photobleaching. It was anticipated that the aryl moieties of FITC would enhance the rate of self-assembly and stability of RNTs via π - π stacking interactions and the hydrophobic effect. There were some concerns about how the non-polar character of FITC would affect the solubility of the target compound, because it is known to have a very low solubility in water, less than 0.1 mg.mL^{-1} .²⁰ However, because the concentration of FITC conjugates can be determined by UV-vis analysis of standard FITC solutions under basic condition we decided to proceed.²¹

As suspected, FITC greatly reduced the solubility of the target (compound **41**) in water, with a 1 mg.mL^{-1} solution having limited solubility, even after heating to boiling. This solution did not form tubes instantaneously as compound **39** did, but after aging for one week, tubes were observed all over the carbon grid (Fig 2.2.A & B). TEM samples were prepared from this solution and negatively stained with uranyl acetate. The average measured diameter of the FITC functionalized RNTs was found to be $5.2 \pm 0.1 \text{ nm}$, while the calculated diameter from molecular modeling was slightly less at 5.1 nm (Fig 2.3.G). The self-assembly of this system was also studied using UV-vis spectroscopy. The UV-vis profile of the G⁺C motif is similar to that of the DNA bases, with maxima at 238 and 287 nm.¹⁴ The UV-vis spectrum of **41** exhibits these two maxima and a third one at $\sim 485 \text{ nm}$, which comes from the FITC component. A hypochromic effect was observed when compound **41** was monitored over a one week period. This hypochromic effect indicates that the RNTs are being self-assembled via π - π stacking interactions of rosettes. A similar effect is observed when DNA base pairs stack.²² π - π interactions are responsible for holding the RNTs together.

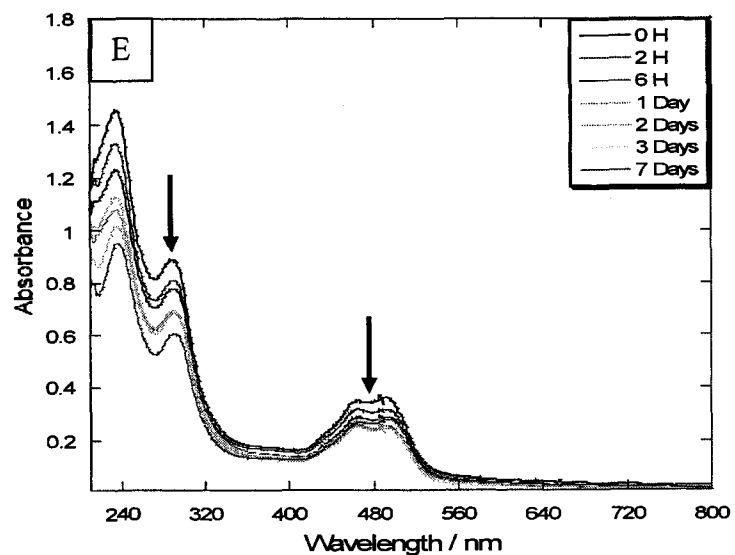
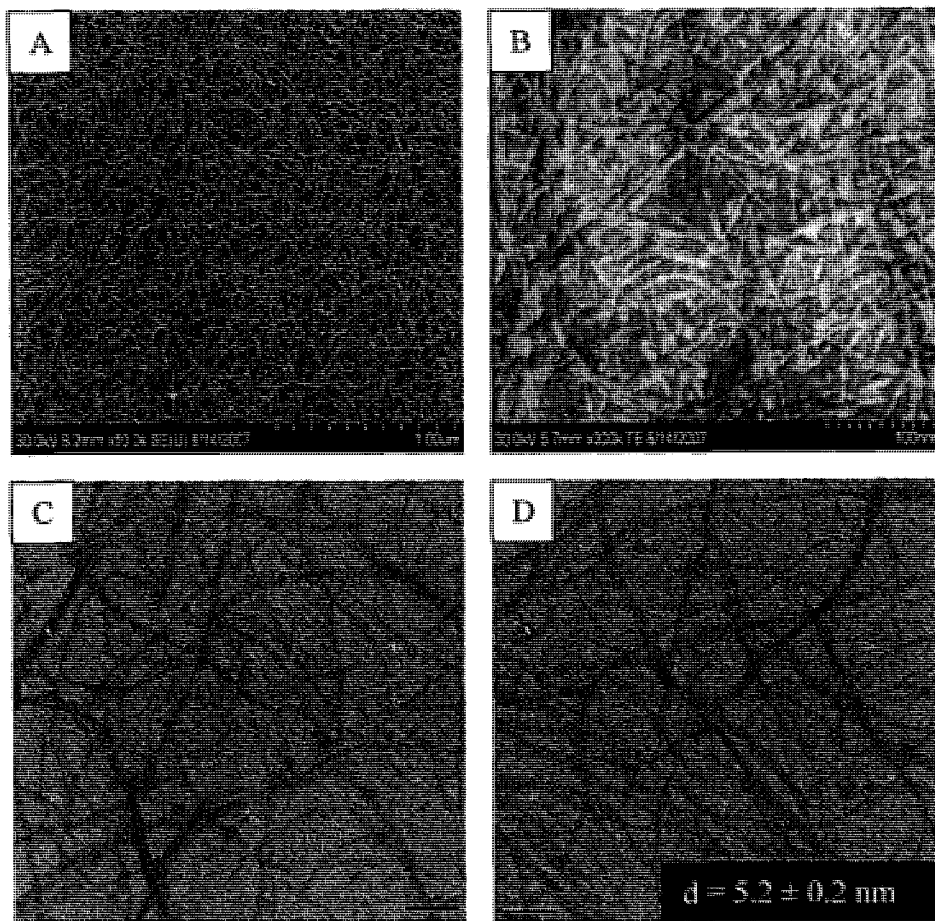


Figure 2.2. Representative SEM micrographs [(A) unstained (B) stained with ua] and TEM [C and D] micrographs of 41 in water, scale bar = 50 nm (E) UV-vis time study of 41 in water.

Molecular modeling of the FITC conjugated G⁺C motif was performed using Macromodel 8.5, so as to estimate its theoretical outer diameter in water and to check whether theories of solvation and association free energies support the observed self-assembly of the motif as revealed by SEM and UV-vis. A conformational search was conducted on the motif by rotating the FITC moiety, and subsequently constructing RNTs based on these different conformations. The relative free energies of the resulting RNTs was determined. The most stable RNT in water was shown to have a relative free energy of 0 Kcal.mol⁻¹ regardless of how many rosettes make up the nanotube (Fig. 2.3.F).

To obtain the structural and thermodynamic parameters of solvation in water, the three-dimensional reference interaction site model (3D-RISM) integral equation complemented with the Kovalenko-Hirata closure approximation was applied.²³ The 3D-RISM-KH integral equation theory of molecular solvation explicitly and properly accounts for the effect of chemical specificities of the RNTs, water and counter ions, in particular the association effects on the solvation structure and thermodynamics. This theoretical method based on the first principles of statistical mechanics provides a detailed microscopic insight into the organization of solution molecules both outside and inside the nanotube, and their role in nanotube formation.²⁴

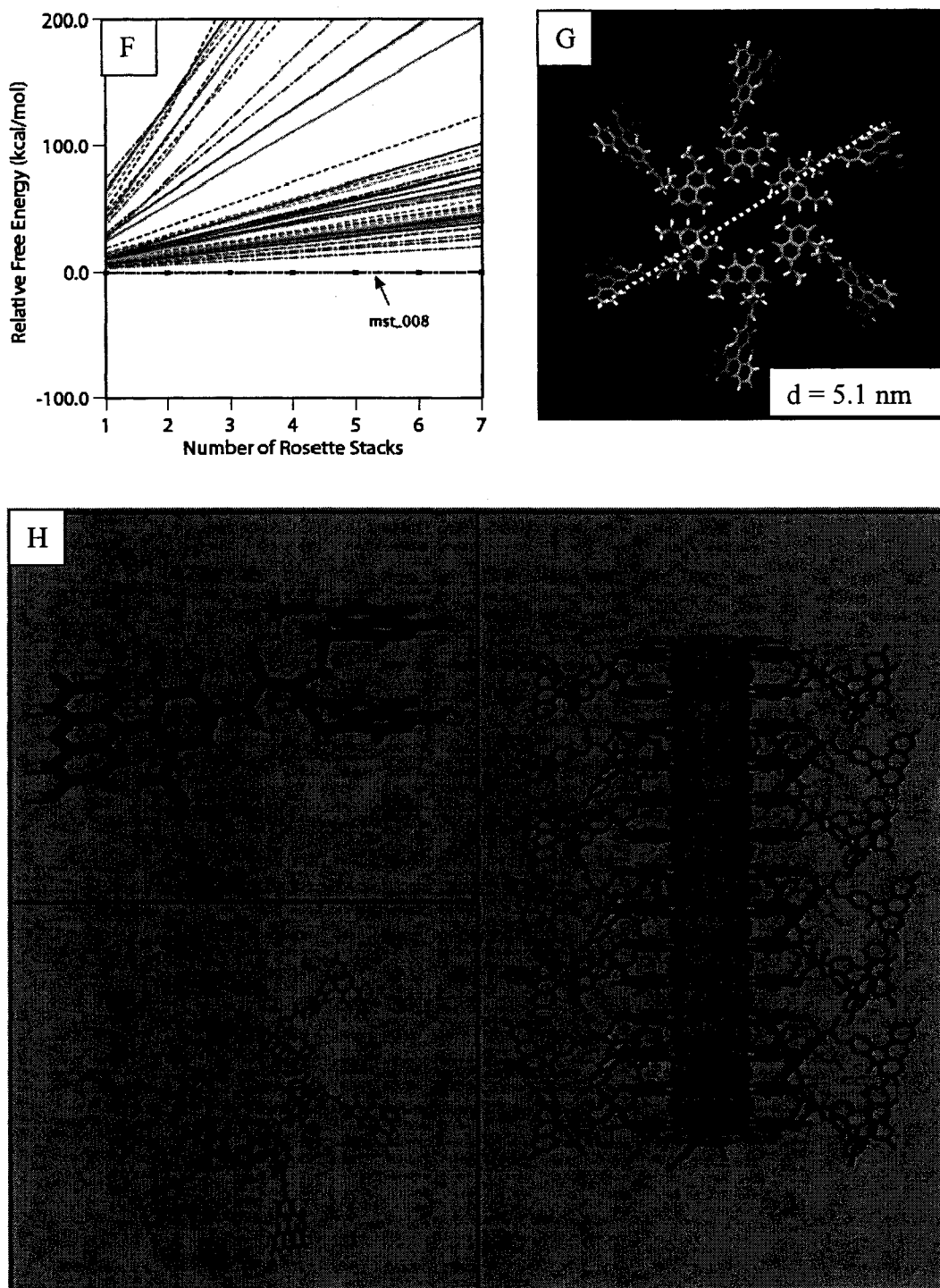


Figure 2.3. Molecular modeling of **41** in water (F) graph showing the relative free energy of RNTs in water (G) Leonard Jones outer diameter of the rosette (H) model of the G[^]C motif of **41** and visual representation of a RNT.

2.3.1. Microscopic Characterization of Biotin-Streptavidin RNTs

The self-assembly of the biotin functionalized G[^]C motif, compound **45**, was studied by dissolving 1 mg in 1 mL of water (limited solubility) and 1 mg in 1 mL of DMSO (completely soluble). The dissolution of **45** in water resulted in a suspension. Deposition of this mixture after 2 days onto a TEM carbon grid revealed that RNTs had formed (Fig. 2.4.A); however most of the tubes were obscured by undissolved particulate matter. Dissolution of 1 mg of **45** in 1 mL water (heated and sonicated), followed by filtration through 0.2 μ m Whatman filter (nonsterile PVFD membranes) revealed that NTs were not formed after 2 days. SEM analysis of the 1 mg / mL DMSO solution showed that it was a better solvent for NT formation, thus it was used to self-assemble NTs for the purpose of characterization. Thus, 25 μ L of a 1 mg.mL⁻¹ DMSO solution was diluted to 1 mL with DMSO and studied over a one week period. Figure 2.4. (B – D) clearly shows the growth of RNTs over that one week period. The NTs formed in DMSO after one week are shorter than those formed in water after 2 days. This may be due to the fact that water is more polar than DMSO; hence, π - π stacking of the hydrophobic faces of the G[^]C motifs are more prevalent in water,¹³ resulting in longer tube formation. The self-assembly of compound **45** in water was studied over a two day period using UV-vis spectroscopy. The UV-vis spectrum revealed the two characteristic absorbance maxima of the G[^]C motif at 238 and 287 nm, and a hypochromic effect which is indicative of π - π stacking between rosettes. Our research has shown that chirality can be express at the supramolecular level (supramolecular chirality) when the G[^]C motif was functionalized with a L-lysine.^{13b,25} Thus, CD studies were conducted over six weeks to determine whether compound **45** RNTs expressed supramolecular chirality. Contrary to our expectations, they were CD-silent in both water and DMSO. This may be due to the fact that the chiral centre of biotin is too removed from the G[^]C motif to influence the rosette into a preferred conformation.

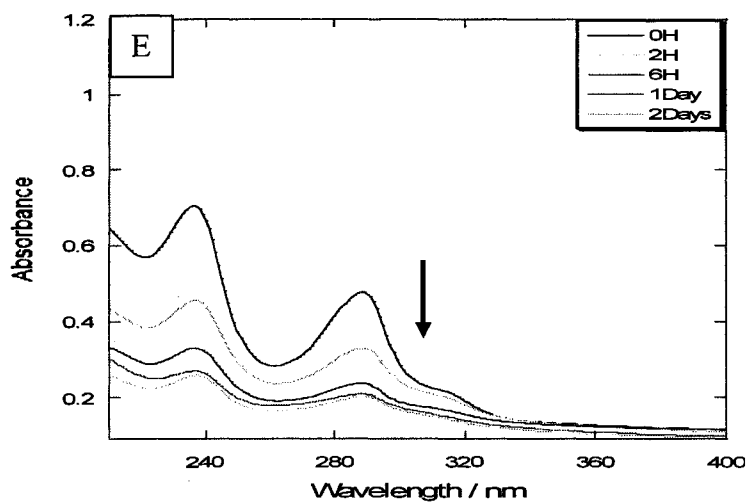
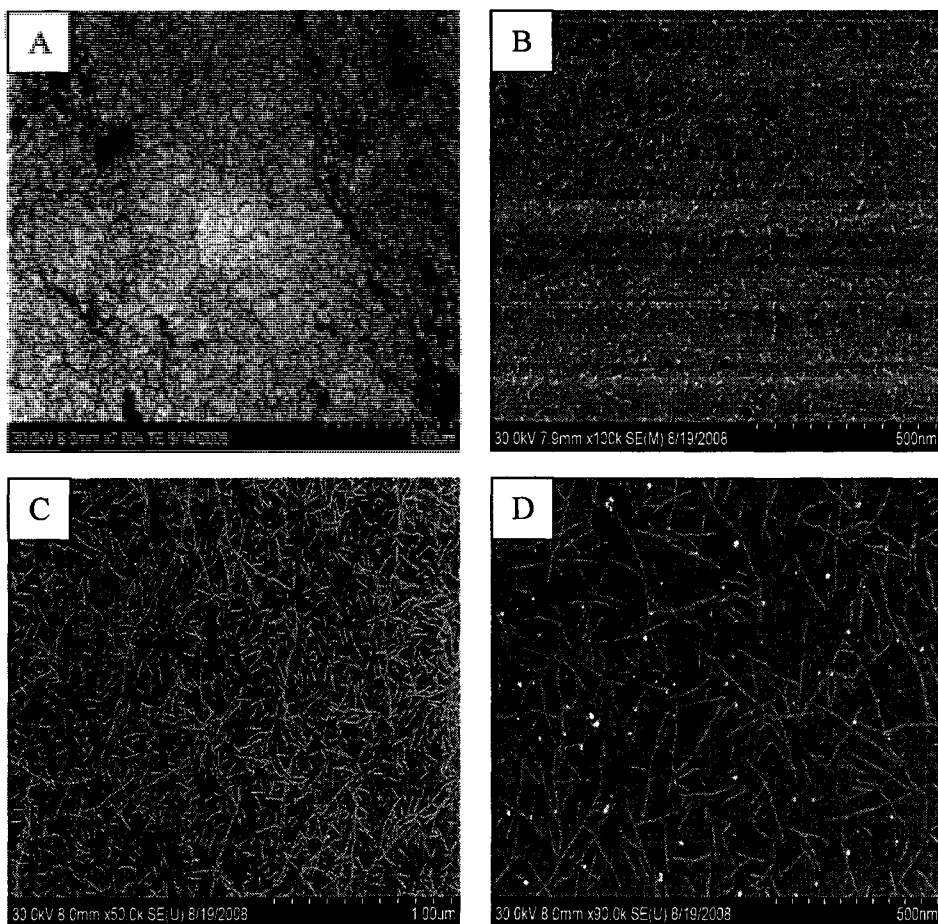


Figure 2.4. Representative SEM image of compound **45** (A) 1 mg.mL^{-1} in water after 2 days (B) 0.025 mg.mL^{-1} in DMSO immediately after preparation (C) 0.025 mg.mL^{-1} in DMSO after 2 h (D) 0.025 mg.mL^{-1} in DMSO after 1 week (E) time dependent UV-vis study of **45** in water.

Rosettes of compound **45** were shown to have average outer diameters of 3.2 ± 0.2 nm and 3.7 ± 0.2 nm from TM-AFM and TEM measurements respectively. TM-AFM diameter measurements are usually slightly lower than TEM measurements because of compression from the AFM tip.²⁶ However, the diameter (Fig 2.5.A) is consistent with the height profile (inset fig B) obtained from TM-AFM images of single rosettes. The TEM images show that all the NTs derived from **45** have the same outer hydrodynamic diameter.

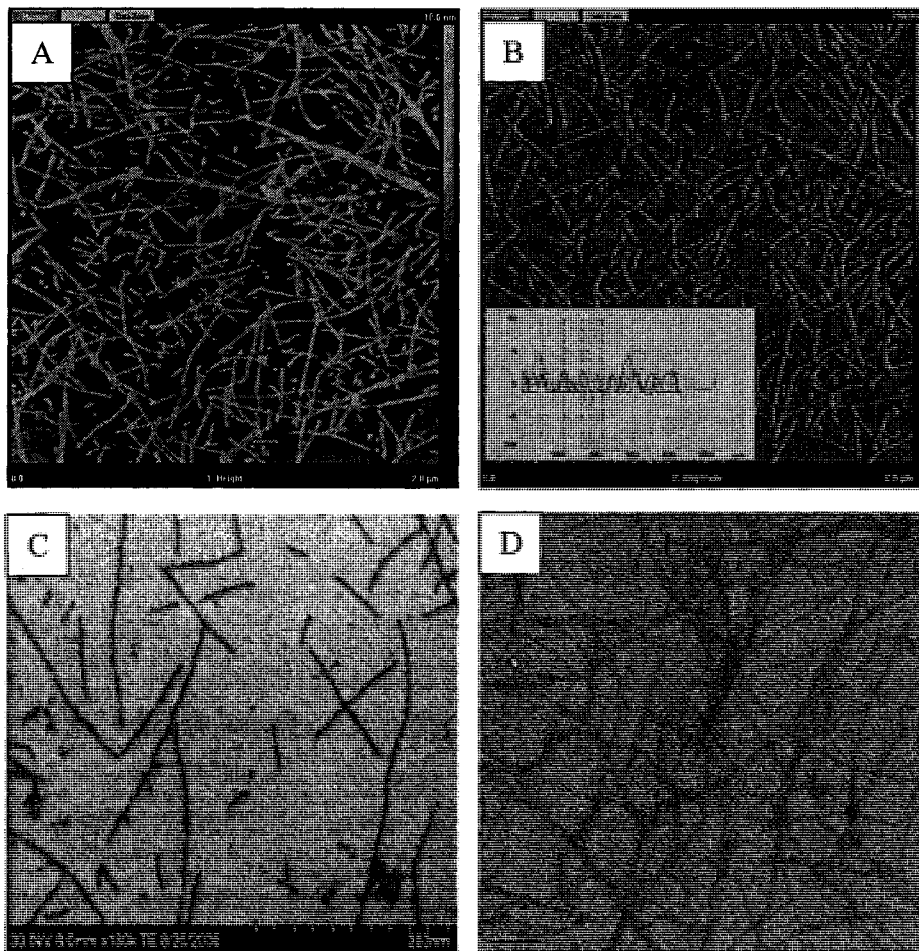


Figure 2.5. Representative TM-AFM micrographs of **45** (A and B with height profile inset), (C) SEM micrograph, stained with ua (D) TEM micrograph stained with ua. Scale bar = 50 nm

Complexation of streptavidin onto biotin-RNTs was carried out by diluting 500 μL of a $0.5 \text{ mg}\cdot\text{mL}^{-1}$ water solution to 1 mL with PBS buffer, pH = 7.4. To this mixture was added 20 μL of a streptavidin PBS buffer solution ($1 \text{ mg}\cdot\text{mL}^{-1}$); 0.5

mL of this solution was filtered through a 100 KDa cut off filter (Amicon ultra – 4) to remove excess streptavidin.²⁷

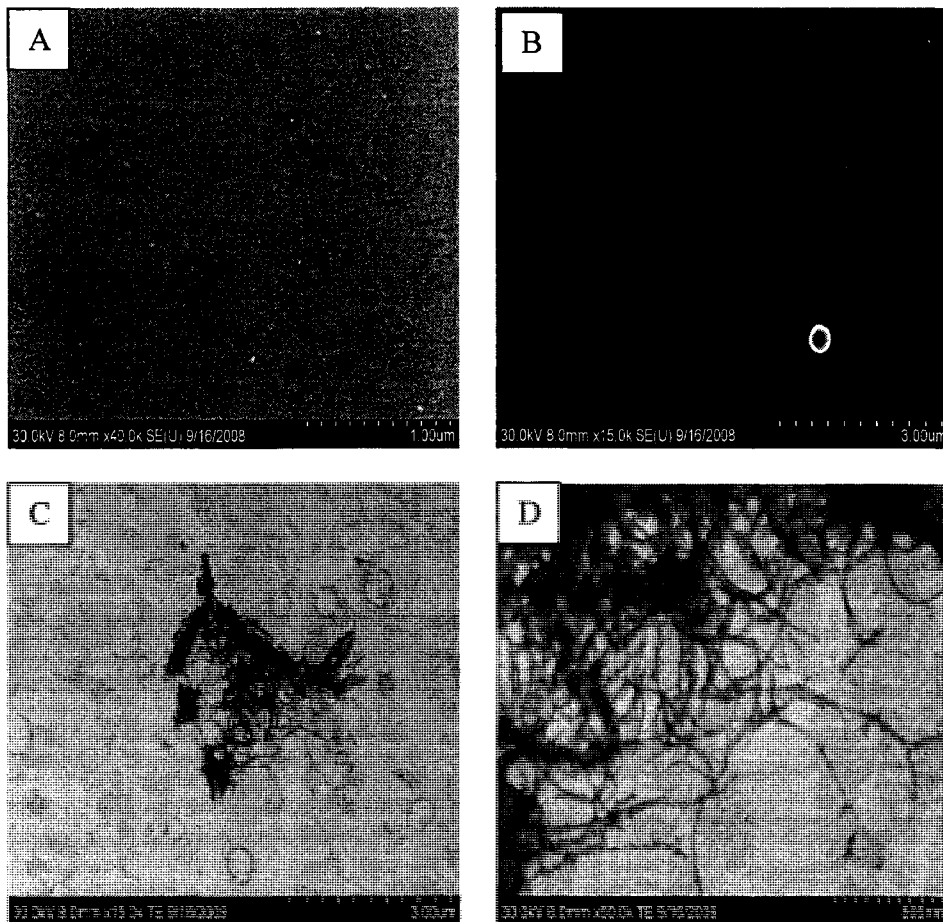


Figure 2.6. Representative SEM micrographs of biotin RNTs complexed with streptavidin (FITC) in water – PBS buffer, pH = 7.4 (A & B) filtered sample (C & D) unfiltered sample.

SEM studies of the two mixtures (filtered and unfiltered) revealed that no tubes were present in the filtered mixture (Fig 2.6.A & B); while the unfiltered mixture showed what appeared to be aggregation of streptavidin over bundles of RNTs (Fig 2.6.C & D). The molecular cut off 100 KDa caused excess streptavidin filtered out as well as nanotubes coated with streptavidin.

2.4. Conclusion and Future Work

We have demonstrated that the twinbase motif, **39**, dissolves completely at 1 mg.mL⁻¹ in water and self-assembles instantaneously to form long RNTs. This makes the twinbase motif an attractive scaffold for the synthesis of RNTs functionalized for biological applications. The G[^]C twinbase motif, **38**, was functionalized successfully with FITC; however, an alternative route was used to synthesize biotin functionalized RNTs. The solubility of the G[^]C motif in water was reduced when functionalized with hydrophobic moieties (FITC and D-(+)-biotin). This problem can be alleviated by using small molecular weight PEG (mw < 200 g.mol⁻¹) linkers to connect the hydrophobic moieties to the G[^]C motif.

Investigations into cellular internalization of FITC and biotin-streptavidin RNTs by mammalian cells is currently under investigation. Molecular modeling of biotin RNTs and RNTs functionalized with the biotin-streptavidin complex are also being carried out. If these systems are shown to be internalized by mammalian cells, then research must be conducted to establish their toxicological profiles. Once this is done, their potential for biomedical applications can be determined.

2.5. Experimental Section

2.5.1 General Information

All reagents and solvents are commercially available from Aldrich, NovaBiochem, Acros, Genscript, Fisher Scientific, Fluka and Advanced ChemTech, and were used without further purification. Reagent grade CH₂Cl₂, THF, CH₃OH, 1,2-DCE, Et₂O were purified on an M Braun solvent purification system. All reactions are carried out under N₂ or Argon unless otherwise stated. Cambridge Isotope Laboratories solvents were used for NMR analysis as received. Chromatographic supports for flash chromatography were Silicycle ultra pure silica gel (4 – 63 μm). Silica coated TLC plates were used to monitor reaction progress and visualization were made under UV light or by chemical staining (KMnO₄ / dH₂O or Ninhydrin / *n*-BuOH / AcOH).

All NMR characterizations were performed on Varian Inova NMR spectrometers (600, 500 or 400 MHz) with solvents as internal references. The NMR data is presented as follows: chemical shift, multiplicity, coupling constant and integration. Chemical shifts are reported in parts per million and first order coupling constants, *J*, are reported in Hertz. High resolution mass spectra were obtained from the Mass Spectrometry Laboratory at the Department of Chemistry, University of Alberta and nominal mass spectra were obtained using an Agilent 1100 series LC / MSD. UV-vis spectra were recorded on an Agilent 8453 spectrometer and DLS on a Malvern Zetasizer Nano S. Melting points were measured using a Büchi capillary melting point apparatus (model B-545). All weighing were carried out on a Mettler Toledo balance-AG285 and FTIR spectra recorded on a FTS 7000 series from Digilab.

Physical Studies

Sample preparation for microscopy studies (AFM, SEM and TEM)

1 mg / mL solutions of samples were prepared in vials using d H₂O, followed by

heating to boiling and then sonicating for ~ 3 min; this was repeated for a second time. Solutions were allowed to age for one week at room temperature after which microscopy studies were carried out. The pHs of these one week old, 1 mg / mL, solutions were recorded using an Orion 3 star benchtop pH meter (Thermo electric corporation).

TEM and SEM Imaging

A droplet of the sample (1 mg / mL) was deposited on to a carbon-coated 400-mesh copper grid for ~ 30 seconds; excess sample was blotted away by gently touching the outer edge of the grid with filter paper. Staining was accomplished by depositing a drop of uranyl acetate (2% in water) onto the grid for ~ 20 seconds and blotting as mentioned above. The grid was then dried at 100 °C under vacuum prior to imaging. TEM imaging was performed using a JOEL 2010 microscope or a Hitachi HF 3300, operating at 200 kV. The dimensions of nanotubes were obtained by randomly measuring individual assemblies using Adobe Photoshop and calculating the average.

SEM images of nanotubes on carbon-coated 400 mesh copper grids (without staining) were recorded using a high resolution Hitachi S-4800 cold field emission SEM operating at an accelerating voltage of 5 kV and a working distance of ~ 3.0 mm.

AFM imaging

AFM samples were prepared by depositing ~ 50 μ L of 1 mg / mL solution onto 10 x 10 mm² of freshly peeled Mica grade V-4 (SPI supplies) substrate. AFM measurements were performed in tapping mode (TM-AFM) at a rate of 2 Hz per line using a Digital Instrument/Veeco Instrument Multimode nanoscope IV equipped with an E scanner. Silicon cantilevers (Mikros Masch USA, Inc) with spring constants of 40 N/m were used.

CD spectroscopy

Stock solution of 1 mg in 1 mL of water (limited solubility) and 1 mg in 1 mL of DMSO were prepared by heating to boiling and sonicating as mentioned above. 50 μ L of each solution was diluted to 2.0 mL with water and DMSO respectively each week, over a six week period, and their CD spectra were recorded on a Jasco J-810 CD spectrometer.

2.5.2. Synthetic Procedures

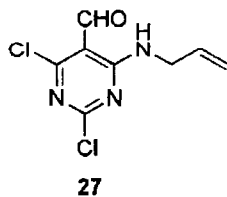


26

To a stirred solution of POCl₃ (235 mL, 393.63 g, 2.57 mol) was added barbituric acid (50 g, 390 mmol) and *N,N*-dimethylformamide (30 mL, 28.32 g, 387 mmol) at room temperature under an atmosphere of nitrogen. The mixture was heated at reflux for 15 h, then cooled to room temperature. Excess POCl₃ was then removed by simple distillation, and the resulting dark viscous material was gently added to crushed ice (~700 g) while being stirred vigorously. The resulting pale brown precipitate was then filtered, washed with dH₂O (2 L) and dried under high vacuum. The desired compound was obtained as a yellow crystalline compound **26** (C₅HCl₃N₂O, 44 g, 54%), after recrystallization from acetone. *R*_f = 0.41 (SiO₂, 10% EA/Hex]. mp = 129 °C.

¹H NMR (500 MHz, CDCl₃) δ (ppm): 10.51 (s, 1H).

¹³C NMR (500 MHz, CDCl₃) δ (ppm): 185.5, 164.70, 123.1.



27

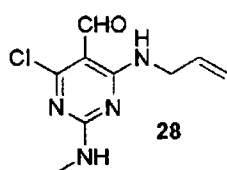
Allylamine (15.16 g, 19.92 mL, 272 mmol) was added to a stirred solution of **26** (44 g, 210 mmol) in CH₂Cl₂ at -78 °C under an atmosphere of nitrogen. The resulting mixture was held at -78 °C for 4 h and allowed to warm up for one hour. The reaction was then quenched with dH₂O and extracted with CH₂Cl₂. The

organic layers were combined and washed with dH₂O (60 mL), brine (30 mL), and then dried over anhydrous Na₂SO₄. The solution was filtered and the solvent was evaporated to yield a crude yellow liquid as product, which was subsequently purified by silica gel column chromatography (0-2% EA/Hex). The desired compound **27** (C₈H₇Cl₂N₃O, 34.10 g, 70%) was obtained as a clear viscous liquid. R_f = 0.33 (SiO₂, 10% EA/Hex).

¹H NMR (500 MHz, CDCl₃) δ (ppm): 10.12 (s, 1H), 9.37 (s, br, 1H), 5.90-5.61 (m, 1H), 5.15-5.07 (m, 2H), 4.13-4.25 (m, 2H).

¹³C NMR (500 MHz, CDCl₃) δ (ppm): 189.2, 167.4, 163.6, 161.1, 132.5, 118.0, 107.5, 43.8.

LRMS (ESI): Calcd mass for (M + H)⁺ / z = 232.00, found 232.1.

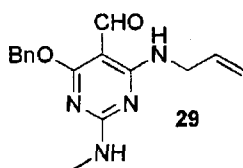


Methylamine (2.0 M solution in THF, 10.61 mL, 9.13 g, 294 mmol) was added to a stirred solution of **27** (34.10 g, 147 mmol) in THF at 0 °C under an atmosphere of nitrogen. The reaction mixture was stirred at 0 °C for 1 h, then for 6 h at room temperature. The reaction was quenched with saturated aqueous NH₄Cl and the organic layer separated and removed by reduced pressure (rotovap). The crude product was recrystallized from CH₂Cl₂ to yield a white crystalline solid **28** (C₉H₁₁N₄O, 23.26 g, 70%). R_f = 0.20 (SiO₂, 10% EA/Hex). mp = 156 °C.

¹H NMR (400 MHz, CDCl₃) δ (ppm): 10.11 (s, 1H), 9.37 (br, s, 1H), 6.80 (br, s, 1H), 6.07-5.81 (m, 1H), 5.33-5.10 (m, 2H), 4.21 (t, ³J = 5.4 Hz, 2H), 3.08 (d, ³J = 4.8 Hz, 3H).

^{13}C NMR (500 MHz, CDCl_3) δ (ppm): 187.6, 166.1, 162.6, 162.2, 133.4, 116.9, 101.9, 43.0, 28.7.

HRMS (ESI): Calcd mass for $(\text{M} + \text{H})^+ / z = 226.0621$, found 226.0624.

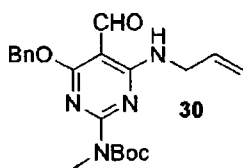


To a stirred solution of NaH (5.69 g, 237 mmol) in THF, at room temperature and under nitrogen, was added benzyl alcohol (22.28 g, 21.32 mL, 206 mmol). After 15 min, the solution was cooled to 0 °C, then a solution of **28** (23.26 g, 103 mmol) in THF was added. The mixture was warmed to room temperature and heated at reflux for 22 h, after which it was then cooled to 0 °C and quenched by the addition saturated NH_4Cl . The organic layer was separated and removed under reduced pressure (rotovap), and the residual solid was dissolved in diethylether (Et_2O), washed with dH_2O (50 mL), then brine (30 mL) and finally dried over anhydrous Na_2SO_4 . Filtration, followed by solvent evaporation under reduced pressure (rotovap) and subsequent silica gel chromatography (0-5% EA/Hex) yielded **29** ($\text{C}_{16}\text{H}_{18}\text{N}_4\text{O}_2$, 22.40 g, 73%) as a mild yellow solid. $R_f = 0.49$ (SiO_2 , 30% EA/Hex). mp = 56 °C.

^1H NMR (400 MHz, CDCl_3) δ (ppm): 10.30 (s, 1H), 9.35 (s, br, 1H, major isomer), (because of the possible hydrogen bond between the oxygen atom of the aldehyde and the hydrogen atom of the allylic nitrogen, this compound displays two sets of peaks for certain protons). 9.35 (s, br, 1H, minor isomer), 7.42-7.34 (m, 5H), 6.00-5.86 (m, br, 1H), 5.41-5.10 (m, 4H), 4.25 (s, br, 2H, major isomer), 4.09 (s, br, 2H, minor isomer), 3.07 (d, $^3J = 8.5$ Hz, 3H).

^{13}C NMR (400 MHz, CDCl_3) δ (ppm): 187.0, 172.2, 162.9, 163.3, 136.8, 134.0, 129.1, 128.8, 127.6, 116.2, 93.4, 68.1, 43.4, 28.7.

HRMS (ESI): Calcd mass for $(\text{M} + \text{H})^+ / z = 298.1430$, found 298.1424.

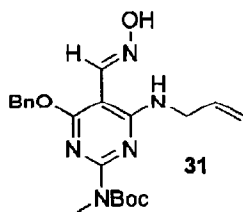


4-*N,N*-dimethylaminopyridine (4.60 g, 37.6 mmol) and triethylamine (22.82 g, 31.44 mL, 225 mmol) were added to a stirred solution of compound **29** (22.40 g, 75.20 mmol) in THF at room temperature and under nitrogen. After 5 min of stirring, Boc_2O (19.70 g, 90.4 mmol) was added and the reaction mixture was stirred for 20 h. The reaction was quenched with dH_2O (50 mL), and the organic layer was separated and removed under reduced pressure (rotovap). Ethyl acetate (1.0 L) was used to dissolve the residual dark brown oil, which was washed with 10% citric acid (100 mL), dH_2O (80 mL), 5% aqueous NaHCO_3 (100 mL), and brine (100 mL). The organic layer was dried over anhydrous Na_2SO_4 , filtered, and the solvent was removed under reduced pressure (rotovap). The dark yellow / brown residue was purified by silica gel chromatography (0 - 5% EA/Hex). The desired compound **30** ($\text{C}_{21}\text{H}_{26}\text{N}_4\text{O}_4$, 26.93 g, 90%) was obtained as mild yellow solid. $R_f = 0.35$ (SiO_2 , 10% EA/Hex). mp = 55 °C.

^1H NMR (500 MHz, CDCl_3) δ (ppm): 10.11 (s, 1H), 9.16 (t, br, $^3J = 5.7$ Hz, 1H), 7.38-7.31 (m, br, 5H), 5.92-5.82 (m, 1H), 5.61 (s, 2H), 5.31-5.14 (m, br, 2H), 4.21 (t, $^3J = 4.8$ Hz, 2H), 3.39 (s, 3H), 1.66 (s, 9H).

^{13}C NMR (500 MHz, CDCl_3) δ (ppm): 188.5, 172.2, 163.2, 162.6, 154.0, 136.3, 134.6, 129.2, 128.8, 128.5, 116.7, 94.7, 82.4, 68.7, 43.5, 35.2, 28.7.

LRMS (ESI): Calcd for $(\text{M} + \text{H})^+ / z = 399.20$, found 399.00.



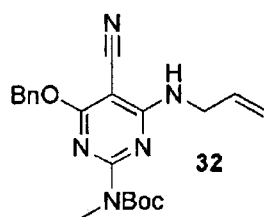
Compound **30** (26.93 g, 67.67 mmol) was dissolved in anhydrous methanol (50 mL), KHCO_3 (27 g, 270 mmol) and hydroxylamine hydrochloride (9.49 g, 135.3 mmol) was then added at rt under an atmosphere of nitrogen. The resulting slurry was heated at reflux for 3 h then cooled to rt and quenched with dH_2O (10 mL). The solvent was removed (rotovap) and the

residual solid was dissolved in EA (200 mL), washed with dH₂O (10 mL) and brine (10 mL). The organic layer was dried over anhydrous Na₂SO₄, filtered, and evaporated to dryness (rotavap) to yield compound **31** (C₂₁H₂₇NO₄, 25 g, 90%) as a yellow liquid. This material was used in the next step without further purification. *R_f* = 0.50 (SiO₂, 30% EA/Hex).

¹H NMR (400 MHz, CDCl₃) δ (ppm): 8.47 (s, 1H), 8.10 (t, ³*J* = 6.5 Hz, 1H), 7.60 (s, br, 1H), 7.46-7.34 (m, 5H), 6.06-5.80 (m, 1H), 5.49 (s, 2H), 5.28-5.10 (m, 2H), 4.25-4.13 (m, 2H), 3.41 (s, 3H), 1.89 (s, 9H).

¹³C NMR (500 MHz, CDCl₃) δ (ppm): 167.3, 161.1, 159.5, 155.0, 146.4, 137.2, 135.3, 128.9, 128.7, 116.1, 88.5, 82.0, 68.6, 43.8, 35.3, 28.8.

HRMS (ESI): Calcd for (M + H)⁺ / *z* = 413.2063, found 413.2050.



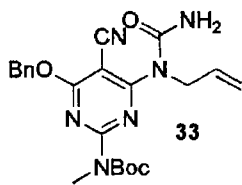
Compound **31** (25 g, 60.9 mmol), Et₃N (25.0 mL, 18.5 g, 182 mmol), and THF (20 mL) were cooled to 0°C, then trifluoroacetic anhydride (12.70 mL, 19.20 g, 91.3 mmol) was slowly added. After stirring for 15 min, the mixture was allowed to warm to rt then it was heated at reflux for 5 h. After cooling to rt, the reaction was quenched with dH₂O (15 mL) and the solvent was removed under reduced pressure (rotovap). The residual solid was dissolved in EA (180 mL), washed with dH₂O (2 x 30 mL), 10% aqueous citric acid (20 mL), dH₂O (30 mL), 5% aqueous NaHCO₃ (20 mL), and brine (20 mL). The organic layer was dried over anhydrous Na₂SO₄, filtered, and evaporated to dryness under reduced pressure (rotavap). Compound **32** (C₂₁H₂₅N₅O₃, 19.70 g, 82%) was obtained as a mild yellow solid after silica gel chromatography (3% EA/Hex). *R_f* = 0.64 (SiO₂, 30% EA/Hex). mp = 68 °C.

Optimization: To 5 mL of DMF was added 4.46 g (24.2 mmol) of 2,4,6-Trichloro-1,3,5-triazine (TCT) at rt. After the formation of a white salt (vilsmeier salt), the reaction was monitored by TLC until there was no more TCT. Then, 10 g of the oxime **31** (24.2 mmol) in 80 mL DMF was added and the reaction was stirred at rt for 24 h. After the reaction was completed (TLC), it was quenched by the addition of 35 mL dH₂O, and extracted with 200 mL of EA. The organic phase was washed with 30 mL saturated Na₂CO₃ followed by 20 mL of brine. The nitrile compound, **32**, was recrystallized from hexanes as a yellow solid with a yield of 82%.

¹H NMR (400 MHz, CDCl₃) δ (ppm): 7.49-7.35 (m, 5H), 5.91-5.83 (m, 1H), 5.78 (t, ³J = 5.6 Hz, 1H), 5.51 (s, 2H), 5.27 (d, ³J = 17.1 Hz, 1H), 5.19 (d, ³J = 10.1 Hz, 1H), 4.18 (d, ³J = 5.7 Hz, 2H), 3.40 (s, 3H), 1.58 (s, 9H).

¹³C NMR (400 MHz, CDCl₃) δ (ppm): 170.6, 164.3, 161.0, 153.8, 136.3, 134.1, 128.7, 128.4, 128.3, 117.2, 115.1, 82.3, 69.1, 68.8, 43.9, 34.9, 28.4.

HRMS (ESI): Calcd for (M + H)⁺ / z = 395.1957, found 395.1961.



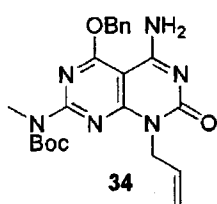
To a solution of compound **32** (19.7 g, 49.9 mmol) in CH₂Cl₂ (120 mL), *N*-Chlorocarbonylisocyanate (10.53 g, 8 mL, 99.8 mmol) was added dropwise at 0 °C over a period of 15 min under an atmosphere of nitrogen. After stirring for 2 h at 0 °C, the mixture was allowed to warm to rt and was stirred for an additional 3 h. The reaction mixture was cooled to 0 °C and carefully quenched with dH₂O (30 mL, exothermic reaction) followed by 5% aqueous NaHCO₃ (20 mL). The product was extracted with chloroform (500 mL) and the resulting organic layer was washed with dH₂O (2 x 50 mL) and brine (50 mL) and dried over anhydrous Na₂SO₄. Filtration and evaporation of the organic solvents under reduced pressure

(rotavap) yielded **33** (C₂₂H₂₆N₆O₄, 19.89 g, 91%) as a viscous liquid, which was used in the next step without further purification. *R_f* = 0.16 (SiO₂, 30% EA/Hex).

¹H NMR (400 MHz, CDCl₃) δ (ppm): 7.46 (m, br, 5H), 5.94-5.75 (m, 1H), 5.51 (s, 2H), 5.18 (t, ³*J* = 21.2 Hz, 2H), 4.92 (d, ³*J* = 5.4 Hz, 2H), 3.41 (s, 3H), 1.54 (s, 9H).

¹³C NMR (500 MHz, CDCl₃) δ (ppm): 172.5, 163.5, 159.1, 155.9, 152.9, 135.7, 133.8, 129.1, 128.9, 128.2, 117.3, 114.4, 86.5, 83.9, 70.1, 48.5, 35.0, 28.5.

HRMS (ESI): Calcd mass for (M + H)⁺ / *z* = 438.2016, found 438.2027.

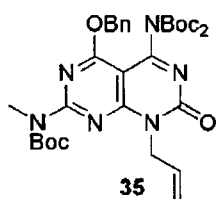


Compound **33** (19.89 g, 45.4 mmol) was stirred in 7 M NH₃ CH₃OH (35 mL) under an atmosphere of nitrogen at rt for 3 h. Excess CH₃OH was removed under reduced pressure (rotovap) and the desired compound **34** (C₂₂H₂₆N₆O₄, 16.15 g, 81%) was obtained as a white solid after silica gel chromatography (30-100% Hex/EA). *R_f* = 0.26 (SiO₂, EA). mp = 192 °C.

¹H NMR (500 MHz, CDCl₃) δ (ppm): 8.00 (s, br, 1H), 7.51-7.41 (m, 5H), 7.15 (s, 1H), 6.02-5.91 (m, br, 1H), 5.66 (s, 2H), 5.27 (d, ³*J* = 17.2 Hz, 1H), 5.18 (d, ³*J* = 10.2 Hz, 1H), 4.87 (d, ³*J* = 5.6 Hz, 2H), 3.47 (s, 3H), 1.61 (s, 9H).

¹³C NMR (500 MHz, CDCl₃) δ (ppm): 167.0, 161.7, 161.1, 160.8, 156.4, 153.5, 135.6, 133.0, 129.3, 129.1, 117.8, 86.6, 83.0, 70.3, 45.0, 35.3, 28.6.

HRMS (ESI): Calcd mass for (M + H)⁺ / *z* = 439.2094, found 439.2096.

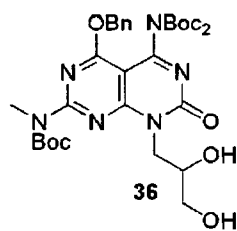


4-*N,N*-dimethylaminopyridine (4.49 g, 36.8 mmol), Et₃N (30.6 mL, 22.3 g, 220 mmol) in THF (20 mL) and Boc₂O (24.1 g, 100.4 mmol) were added to a stirred solution of compound **34** (16.15 g, 36.8 mmol) in 200 mL THF, under an atmosphere nitrogen. After stirring at rt for 36 h, the reaction was quenched by the addition dH₂O (30 mL) and the solvent was removed under reduced pressure (rotovap). The residual solid was dissolved in EA (300 mL), washed with dH₂O (25 mL), 10% aqueous citric acid (25 mL), dH₂O (2 x 30 mL), 5% aqueous NaHCO₃ (20 mL), and brine (20 mL), then dried over anhydrous Na₂SO₄. After filtration and removal of the solvent under reduced pressure (rotavap) the residual solid was purified by silica gel chromatography (5-20% EA/Hex) to yield compound **35** (C₃₂H₄₂N₆O₈, 20.89 g, 89%) as a white foam. *R_f* = 0.66 (SiO₂, 50% EA/Hex). mp = 78 °C.

¹H NMR (400 MHz, CDCl₃) δ (ppm): 7.41-7.37 (m, 5H), 6.07-5.87 (m, 1H), 5.58 (s, 2H), 5.24 (t, ³*J* = 12.4 Hz, 2H), 4.94 (d, ³*J* = 9.2 Hz, 2H), 3.46 (s, 3H), 1.59 (s, 9H), 1.35 (s, 18H).

¹³C NMR (500 MHz, CDCl₃) δ (ppm): 166.0, 161.4, 161.1, 160.7, 155.6, 152.9, 149.4, 135.2, 131.5, 128.9, 128.7, 118.3, 93.1, 83.8, 83.2, 70.4, 45.5, 35.2, 28.3, 28.1.

HRMS (ESI): Calcd for (M + H)⁺ / z = 638.3064, found 638.3057.

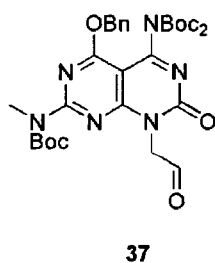


To a stirred solution of compound **35** (20.89 g, 32.7 mmol) in acetone / dH₂O (8:1, 60 mL) was added 50% aqueous *N*-methylmorpholine *N*-oxide (15.2 g, 31.1 mL, 65.5 mmol) at rt. After stirring for 5 min, OsO₄ (0.1 M solution in *t*-BuOH, 16.3 mL, 1.64 mmol) was added dropwise over a period of 5 min. The resulting brown solution was stirred at rt for 23 h then quenched with aqueous sodium sulfite until all the excess OsO₄ was destroyed (brown solution turns colorless). Diol **36** was extracted in CHCl₃ (150 mL) and washed with dH₂O (2 x 10 mL) and brine (15 mL). The organic layer was dried over anhydrous Na₂SO₄, filtered, and evaporated to dryness under reduced pressure (rotavap). Crystallization from EA yielded compound **36** (C₃₂H₄₄N₆O₁₀, 18.26 g, 83%) as a white solid. *R*_f = 0.15 (SiO₂, 50% EA/Hex). mp = 136 °C.

¹H NMR (500 MHz, CDCl₃) δ (ppm): 7.46 (m, br, 5H), 5.61 (s, 2H), 4.63 (d, ³*J* = 4.5 Hz, 2H), 4.18 (m, 1H), 4.09 (d, ³*J* = 5.6 Hz, 1H), 3.60 (m, 2H), 3.51 (s, 3H), 3.28 (t, ³*J* = 7.2 Hz, 1H), 1.62 (s, 9H), 1.39 (s, 18H).

¹³C NMR (500 MHz, CDCl₃) δ (ppm): 166.3, 162.2, 161.3, 160.0, 157.4, 152.8, 149.7, 149.6, 135.1, 129.1, 128.5, 93.8, 84.5, 84.3, 71.2, 70.8, 63.8, 45.9, 35.2, 28.5, 28.3.

HRMS (ESI): Calcd mass for (M + H)⁺ / *z* = 672.3119, found 672.3131.



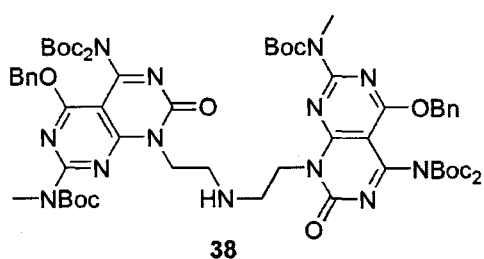
A solution of compound **36** (18.26 g, 27.1 mmol) in CH₂Cl₂ / dH₂O (4:1, 150 mL) and sodium periodate (11.62 g, 54.4 mmol) was stirred at rt for 36 h. The mixture was then filtered through a pad of celite and washed with CH₂Cl₂ (2 x 200 mL). Separation and evaporation of the organic layer under reduced

pressure (rotavap) followed by silica gel chromatography (5-30% EA/Hex) yielded compound **37** (C₃₁H₄₀N₆O₉, 13.7 g, 79%) as a white foam. $R_f = 0.48$ (SiO₂, 30% EA/Hex). mp = 152 °C.

¹H NMR (400 MHz, CDCl₃) δ (ppm): 9.58 (s, 1H), 7.39-7.29 (m, br, 5H), 5.53 (s, 2H), 5.09 (s, 2H), 3.34 (s, 3H), 1.49 (s, 9H), 1.27 (s, 18H).

¹³C NMR (400 MHz, CDCl₃) δ (ppm): 194.0, 165.8, 161.2, 161.2, 160.9, 155.6, 152.5, 149.2, 134.9, 128.8, 128.8, 128.6, 93.0, 84.0, 83.4, 70.4, 52.2, 35.1, 28.2, 27.9.

HRMS (ESI): Calcd for (M + H)⁺/z = 641.2935, found 641.2945.

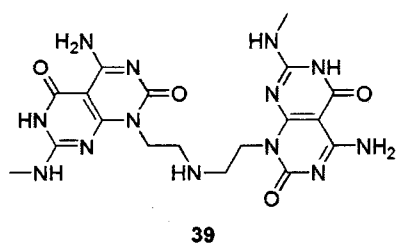


To a stirred solution of compound **37** (5.0 g, 7.81 mmol) in 30 mL of 1,2-dichloroethane was added 0.5M NH₃ in dioxane (62.5 mL, 31.25 mmol) and NaBH(OAc)₃ (3.8 g, 17.96 mmol) and the mixture was stirred rt for 24 h. The reaction was quenched by the addition of dH₂O (20 mL) and the organic phase was separated, washed with brine (10 mL), dried over anhydrous Na₂SO₄ and the solvent was removed under reduced pressure (rotavap) to yield a yellow oil that was purified by silica gel chromatography to give compound **38** (C₆₂H₈₃N₁₃O₁₆, 4.20 g, 85%) as a yellow solid. $R_f = 0.2$ (SiO₂, EA). mp = 97-98°C.

¹H NMR (400 MHz, CDCl₃) δ (ppm): 7.45-7.25 (m, 10H), 5.56 (s, 4H), 4.43-4.40 (t, ³J = 7.0 Hz, 4H), 3.47 (s, 6H), 3.11-3.07 (t, ³J = 7.0 Hz, 4H), 1.55 (s, 18H), 1.27 (s, 36H).

^{13}C NMR (600 MHz, CDCl_3) δ (ppm): 165.6, 161.1, 160.2, 155.6, 152.4, 149.2, 139.2, 134.9, 128.5, 127.8, 92.8, 83.6, 82.8, 69.8, 50.4, 41.0, 34.8, 31.2, 27.9.

HRMS (ESI): Calcd mass for $(\text{M} + \text{H})^+ / z = 1266.6153$, found 1266.6150.



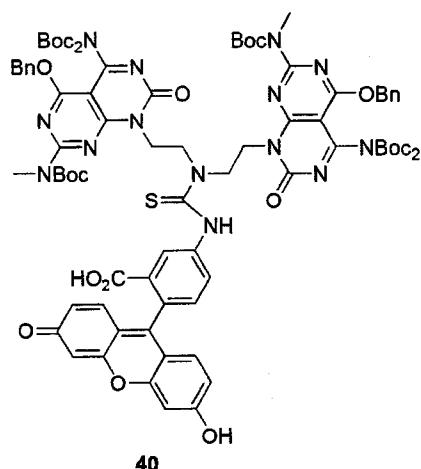
To 200 mg of **38** (0.158 mmol) was added 3 mL of 4M HCl / dioxane at rt under an atmosphere of nitrogen. The reaction was monitored by TLC and by the presence of the precipitated product **39** as an HCl salt. After 8 h the excess HCl /

dioxane was removed under reduce pressure (rotovap), and the precipitated soild was washed with Et_2O and DCM, and dried uner high vacuum. Compound **39** was otained as a white solid. Elemental analysis was not done on this compound, hence no yield was reported, since the purpose of synthesizing this compound was to investigate if the twinbase motif, **39**, would form nanotubes. mp = 325 °C (decomposed).

^1H NMR (500 MHz, $\text{DMSO}-d_6$) δ (ppm): 9.17 (s, 2H), 9.07 (d, 1H), 8.81 (s, 2H), 4.35 (t, $^3J = 5.3$ Hz, 4H), 4.23 (s, br, 1H), 3.26 (t, $^3J = 5.3$ Hz, 4H), 2.96 (s, 6H).

^{13}C NMR (600 MHz, $\text{DMSO}-d_6$) δ (ppm): 161.3, 160.5, 156.7, 156.1, 148.7, 83.01, 46.3, 39.3, 28.4.

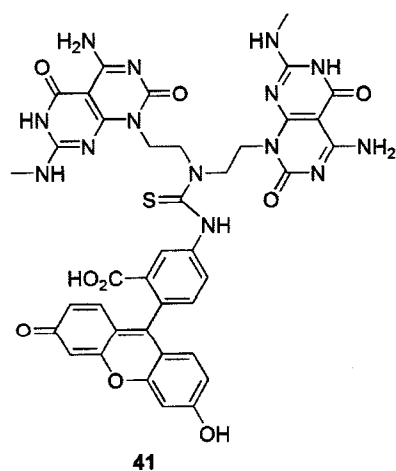
HRMS (ESI): Calcd mass for $(\text{M} + \text{H})^+ / z = 486.2069$, found 486.2066.



Compound **38** (500 mg, 0.395 mmol) was dissolved in 5.0 mL of EtOH and Fluorescein (5)-6-isothiocayante (138 mg, 0.355 mmol) and *N,N'*-diisopropylamine (102 mg, 137 μ L, 0.79 mmol) were added. The reaction was stirred overnight in the dark. EtOH was removed under reduce pressure (rotovap) and the residual yellow oil was taken up in EA (100 mL), washed with 0.5 M HCl (2 x 15 mL), dH₂O (20 mL), brine (20 mL) and purified by silica gel chromatography (1 % Acetic acid/EA) to afford compound **40** (C₈₃H₉₆N₁₄O₂₁S, 435 mg, 74%) as a yellow oil. R_f = 0.45 (SiO₂, 1% Acetic acid/EA).

¹H NMR (400 MHz, CDCl₃) δ (ppm): 9.75 (s, 1H), 8.31 (s, 1H), 7.79 (s, br, 1H), 7.46-7.27 (m, 10H), 6.92 (m, 1H), 6.68 (s, 2H), 6.59 (m, 2H), 6.40 (m, 2H), 5.6 (s, 4H), 4.59 (s, br, 4H), 4.10 (s, br, 4H), 3.56 (s, 6H), 1.56 (s, 18H), 1.29 (s, 36H).

HRMS (ESI): Calcd mass for (M + Na)⁺ / z = 1678.6298, found (M + Na)⁺ / z 1678.6292.



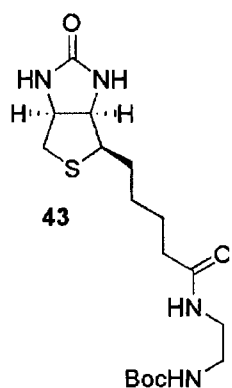
Compound **40** (200 mg, 0.120 mmol) was dissolved in 5.0 mL of 4.0 M HCl/dioxane and was stirred for 5 h. HCl and dioxane were removed under reduced pressure (rotovap) to afford a dark yellow oil, to which diethyl ether was added to precipitate compound **41** (C₄₁H₃₄N₁₄O₉S - 3HCl - 3H₂O - C₄H₁₀O, 120 mg, 86%) as a yellow solid. mp = 290 °C (decomposed).

^1H NMR (600 MHz, $\text{DMSO-}d_6$) δ (ppm): 12.19 (s, 2H) 10.38-10.00 (s, br, 1H), 9.50 (s, 1H), 9.19-9.14 (m, 2H), 8.7-8.6 (m, 2H), 8.18-8.12 (m, 2H), 7.83 (s, 1H), 7.62 (s, 1H), 7.27 (s, 1H), 6.7-6.5 (m, 6H), 4.37 (s, br, 4H), 4.17 (s, 4H), 2.96 (s, 6H).

^{13}C NMR (600 MHz, $\text{DMSO-}d_6$): 182.0, 170.1, 168.5, 168.2, 167.6, 161.2, 160.8, 160.0, 155.8, 151.9, 147.7, 142.4, 135.9, 130.8, 129.1, 128.5, 128.3, 127.7, 127.2, 126.1, 123.4, 120.1, 118.7, 112.9, 109.7, 102.2, 82.1, 46.9, 46.1, 27.7.

HRMS (MALDI): Calcd mass for $(\text{M} + \text{H})^+ / z = 875.2426$, found 875. 2427.

Elemental analysis: Calcd for $[\text{C}_{39}\text{H}_{34}\text{N}_{14}\text{O}_9\text{S} - 3\text{HCl} - 3\text{H}_2\text{O} - \text{C}_4\text{H}_{10}\text{O}]$: C 46.43, H 4.80, N 17.63, Cl 9.56, S 2.88. Found: C 46.58, H 4.43, N 17.63, S 3.17.



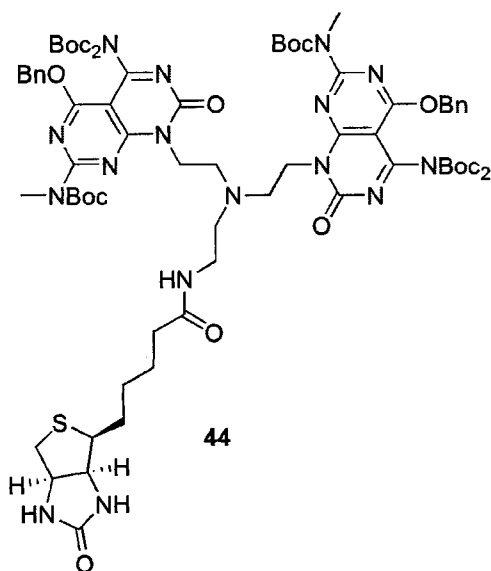
131 mg of mono Boc-protected diaminoethane (0.817 mmol), D-(+)-biotin (200 mg, 0.817 mmol), HBTU (341 mg, 0.900 mmol) and 0.43 mL of Et_3N (0.314 mmol) were dissolved, via sonication, in 5 mL of DMF. The reaction was stirred at rt for 4 h, and was monitored by LCMS. The product was precipitated by the addition of Et_2O and was washed with Et_2O and DCM to give **43** ($\text{C}_{17}\text{H}_{30}\text{N}_4\text{O}_4\text{S}$, 275 mg, 87%) as a white solid. mp = 171.5-172.6 $^\circ\text{C}$.

^1H NMR (600 MHz, $\text{DMSO-}d_6$) δ (ppm): 7.72 (s, br, 1H), 6.71 (s, br, 1H), 6.38 (s, 1H), 6.31 (s, 1H), 4.28 (t, $^3J = 6.5$ Hz, 1H), 4.10 (m, 1H), 3.07-3.0 (m, 1H), 3.01 (q, $^3J = 6.2$ Hz, 2H), 2.92 (q, $^3J = 6.2$ Hz, 2H), 2.78 (m, 1H), 2.01 (t, $^3J = 7.5$ Hz, 2H), 1.59 (m, 1H), 1.45 (m, 3H), 1.34 (s, 9H), 1.27 (m, 1H), 1.21 (m, 2H).

^{13}C NMR (600 MHz, $\text{DMSO-}d_6$) δ (ppm): 172.6, 163.2, 156.1, 78.1, 61.5, 59.6, 55.8, 40.3, 40.0, 40.0, 39.1, 35.6, 28.6, 28.5, 25.6.

HRMS (ESI) Calcd mass for $(M + Na)^+ / z = 409.1880$, found 409.1877.

The Boc protecting group of **43** was removed by treatment with 30% TFA/DCM for ~ 4 h. LCMS was used to monitor the reaction. The TFA ammonium salt of **43** was precipitated by the addition of Et₂O.



Compound **43** (100 mg, 0.348 mmol) was deprotected, see above, and dissolved in 10 mL of DMF which was treated with 36 μ L of DIEA (2.08 mmol). The mixture was stirred for about 10 min and 445 mg of compound **37** (0.697 mmol) was added to this mixture and stirred for ~ 15 min, then 295 mg of NaBH(OAc)₃ (1.39 mmol) was added and the mixture was stirred for 24 h at rt. TLC and LCMS was used

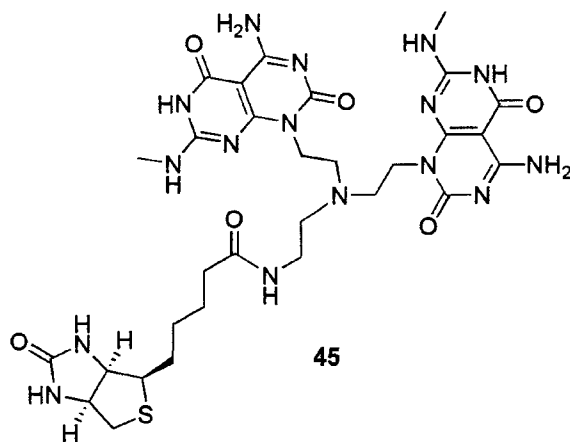
to monitor the reaction. After the reaction was completed, the solvent was removed under reduced pressure (rotovap) and the yellow residue was dissolved in MeOH and adsorbed onto silica gel. Purification by silica gel chromatography (0-10% MeOH/DCM) afforded **44** (C₇₄H₁₀₂N₁₆O₁₈S, 253 mg, 64%) as a pale yellow solid. $R_f = 0.48$ (SiO₂, 10% MeOH/DCM). mp = 94.6-95.8 °C.

¹H NMR (600 MHz, CDCl₃) δ (ppm): 7.42-7.29 (m, 10H), 6.99 (s, br, 1H), 5.54 (s, 4H), 4.45 (s, br, 2H), 4.30 (s, br, 5H), 3.46 (s, 6H), 3.31 (s, br, 2H), 2.91-2.82 (m, 7H), 2.66 (d, ³J = 12.4 Hz, 1H), 2.39 (s, 1H), 2.83 (t, ³J = 6.0 Hz, 2H), 1.66 (m, 3H), 1.55 (s, 18H), 1.44 (m, 3H), 1.36 (m, 1H), 1.27 (s, 36H).

^{13}C NMR (600 MHz, CDCl_3) δ (ppm) : 173.6, 165.6, 164.0, 161.3, 160.8, 160.4, 156.0, 152.4, 149.2, 134.8, 128.6, 128.5, 128.5, 93.0, 83.8, 83.0, 70.1, 61.9, 60.2, 55.3, 52.6, 51.6, 44.6, 41.7, 40.7, 37.6, 35.5, 35.0, 28.2, 27.9, 27.7, 25.5.

HRMS (MALDI) Calcd mass for $(\text{M} + \text{H})^+ / z = 1535.7352$, found 1535.7334.

Elemental analysis: Calcd for $[\text{C}_{74}\text{H}_{102}\text{N}_{16}\text{O}_{18}\text{S} - \text{CH}_2\text{Cl}_2 - \text{CH}_3\text{OH}]$ C 55.23, H 6.59, N 13.56, S 1.94. Found C 55.15, H 6.59, N 13.12, S 1.90.



300 mg of compound **44** (0.195 mmol) was dissolved in 5 mL of 95% TFA/thioanisole and 5 ml of DCM and was allowed to stir at room temperature for 4 h, after which the reaction was stopped. The product was precipitated by the addition of Et_2O and was purified by washing extensively

with Et_2O and DCM to afford **45** as a white solid. mp = 315 $^\circ\text{C}$ (decomposed).

^1H NMR (600 MHz, $\text{DMSO}-d_6$) δ (ppm) : 12.35 (s, br, 2H), 9.20 (s, br, 2H), 8.15 (s, br, 2H), 4.49-4.40 (m, 3H), 4.38-4.33 (m, 1H), 4.31-4.28 (m, 1H), 4.2-4.15 (m, 1H), 3.63 (s, br, 4H), 3.42 (s, br, 4H), 3.08 (s, br, 1H), 2.92 (s, br, 6H), 2.84 (s, 1H), 2.65-2.54 (d, 1H), 2.1-2.02 (m, 2H), 1.61-1.55 (m, 1H), 1.5-1.4 (m, 3H), 1.36-1.30 (m, 3H).

^{13}C NMR (600 MHz, $\text{DMSO}-d_6$) δ (ppm): 174.6, 163.7, 161.6, 160.3, 156.5, 156.0, 148.7, 82.9, 63.3, 61.9, 60.2, 55.7, 50.0, 43.2, 39.9, 39.8, 35.3, 28.5, 28.5, 28.2, 25.4.

HRMS (MALDI) Calcd mass for $(M + H)^+ / z = 755.3266$, found 755.3265.

Elemental analysis: Calcd for $[C_{30}H_{42}N_{16}O_6S - (CF_3COOH)_{3.25} - 0.25 C_4H_{10}O]$ C 39.37, H 4.21, N 19.59, S 2.80. Found: C 39.41, H 4.43, N 19.28, S 3.03.

Complexation of Streptavidin (FITC) to Biotin functionalized RNTs.

500 μ L of biotin functionalized RNT solution (0.5 $\text{mg}\cdot\text{mL}^{-1}$, limited solubility), 500 μ L of PBS buffer, pH = 7.4 and 20 μ L of streptavidin (FITC) [1 $\text{mg}\cdot\text{mL}^{-1}$] were mixed in a vial. After 4 h a sample was casted onto a carbon grid and analyzed using SEM.

2.6. References

1. F. D. Emerich, C. G. Thanos, "Targeted nanoparticle-based drug delivery and diagnosis," *J. Drug Target*, **2007**, 15, 163.
2. V. Wagner, A. Dullaart, A-K. Bock and A. Zweck, "The emerging nanomedicine landscape," *Nat. Biotechnol.* **2006**, 24, 1211.
3. (a) C. M. Henry, *Chem. Eng. News*, **2004**, 82, 37. (b) D. A. Smith and H. van de Waterbeemd, "Pharmacokinetics and metabolism in early drug discovery," *Curr. Opin. Chem. Biol.* **1999**, 3, 373. (c) G. Bendas, "Immunoliposomes: A promising approach to targeting cancer therapy," *Bio. Drugs*, **2001**, 15, 4, 215.
4. (a) S. Iijima, "Helical microtubules of graphitic carbon," *Nature*, **1991**, 354, 56. (b) Special issues on carbon nanotubes, *Acc. Chem. Res.* **2002**, 35, 997.
5. W. Wu, S. Wieckowski, G. Pastorin, M. Benincasa, C. Klumpp, J-P. Briand, R. Gennaro, and M. Prato, A. Bianco, "Targeted delivery of amphotericin B to cells by using functionalized carbon nanotubes," *Angew. Chem. Int. Ed. Engl.* **2005**, 44, 6358.
6. (a) M. Bruchez, Jr., M. Moronne, P. Gin, S. Weiss, and A. P. Alivisatos, "Semiconductor nanocrystals as fluorescent biological labels," *Science*, **1998**, 281, 2013. (b) W. C. W. Chan and S. Nie, "Quantum Dot bioconjugates for ultrasensitive nonisotopic detection," *Science*, **1998**, 281, 2016. (c) Y. Cui, Q. Wei, H. Park, and C. M. Lieber, "Nanowire nanosensors for highly sensitive and selective detection of biological and chemical species," *Science*, **2001**, 293, 1289. (d) B. F. Erlanger, B-X Chen, M. Zhu, and L. Brus, "Binding of an anti-fullerene IgG monoclonal antibody to single wall carbon nanotubes," *Nano Lett.* **2001**, 1, 465.
7. (a) N. W. Shi Kam, M. O'Connell, J. A. Wisdom, and H. Dai, "Carbon nanotubes as multifunctional biological transporters and near-infrared agents for selective cancer cell destruction," *Proc. Natl. Acad. Sci. USA.* **2005**, 102, 11600. (b) N. W. Shi Kam, Z. Liu, and H. Dai, "Carbon

- Nanotubes as intracellular transporters for proteins and DNA: An investigation of the uptake mechanism and pathway,” *Angew. Chem. Int. Ed. Engl.* **2006**, 45, 577. (c) D. Pantarotto, J-P. Briand, M. Prato and A. Bianco, “Translocation of bioactive peptides across cell membranes by Carbon nanotubes,” *Chem. Commun.* **2004**, 16.
8. (a) D. Pantarotto, R. Singh, D. McCarthy, M. Erhardt, J-P. Briand, M. Prato, K. Kostarelos, and A. Bianco, “Functionalized carbon nanotubes for plasmid DNA gene delivery,” *Angew. Chem. Int. Ed.* **2004**, 43, 5242. (b) R. Singh, D. Pantarotto, D. McCarthy, O. Chaloin, J. Hoebeke, C. D. Partidos, J-P. Briand, M. Prato, A. Bianco, and K. Kostarelos, “Binding and condensation of plasmid DNA onto functionalized carbon nanotubes: Toward the construction of nanotube-based gene delivery vectors,” *J. Am. Chem. Soc.* **2005**, 127, 4388.
 9. Z. Liu, W. Cai, L. He, N. Nakayama, K. Chen, X. Sun, X. Chen and H. Dai, “In vivo biodistribution and highly efficient tumour targeting of carbon nanotubes in mice,” *Nature Nanotech.* **2007**, 2, 47.
 10. (a) Y. Liu, D-C. Wu, W-D. Zhang, X. Jiang, C-B. He, T. Chung, S. H. Goh, and K. W. Leong, “Polyethylenimine-grafted multiwalled carbon nanotubes for secure noncovalent immobilization and efficient delivery of DNA,” *Angew. Chem. Int. Ed.* **2005**, 44, 4782. (b) N. W. Shi Kam, Z. Liu, and H. Dai, “Functionalization of carbon nanotubes via cleavable disulfide bonds for efficient intracellular delivery of siRNA and potent gene silencing,” *J. Am. Chem. Soc.* **2005**, 127, 12492.
 11. (a) D. Lison and J. Muller, “Lung and systemic responses to carbon nanotubes (CNT) in mice,” *Toxicol. Sci.* **2008**, 101, 179. (b) L. A. Mitchell, J. Gao, R. V. Wal, A. Gigliotti, S.W. Burchiel, and J. D. McDonald, “Pulmonary and systemic immune response to inhaled multiwalled Carbon Nanotubes,” *Toxicol. Sci.* **2007**, 100, 203. (c) D. B. Warheit, B. R. Laurence, K. L. Reed, D. H. Roach, G. A. M. Reynolds, and T. R. Webb, “Comparative pulmonary toxicity assessment of single-

- wall carbon nanotubes in rats,” *Toxicol. Sci.* **2004**, *77*, 117. (d) C-W. Lam, J. T. James, R. McCluskey, and R. L. Hunter, “Pulmonary toxicity of single-wall carbon nanotubes in mice 7 and 90 days after intratracheal instillation,” *Toxicol. Sci.* **2004**, *77*, 126. (e) V. L. Colvin, “The potential environmental impact of engineered nanomaterials,” *Nat. Biotechnol.* **2003**, *21*, 1166. (f) Yuliang Zhao, Gengmei Xing and Zhifang Chai, “Are carbon nanotubes safe?” *Nature Nanotech.* **2008**, *3*, 191. (g) C. S. Sharma, S. Sarkar, A. Periyakaruppan, J. Barr, K. Wise, R. Thomas, B. L. Wilson, and G. T. Ramesh, “Single-walled carbon nanotubes induces oxidative stress in rat lung epithelial cells”, *J. Nanosci Nanotech.* **2007**, *7*, 2466. (h) L. Guo, A. Von Dem Bussche, M. Buechner, A. Yan, A. B. Kane and R. H. Hurt, “Adsorption of essential micronutrients by carbon nanotubes and the implications for nanotoxicity testing”, *Small*, **2008**, *4*, 6, 721.
12. (a) N. W. Shi Kam, T. C. Jessop, P. A. Wender, and H. Dai, “Nanotube molecular transporters: internalization of carbon nanotube-protein conjugates into mammalian cells,” *J. Am. Chem. Soc.* **2004**, *126*, 6850. (b) N. W. Shi Kam and H. Dai, “Carbon Nanotubes as intracellular protein transporters: generality and biological functionality,” *J. Am. Chem. Soc.* **2005**, *127*, 6021. (c) A. Bianco, K. Kostarelos, C. D. Partidos and M. Prato, “Biomedical applications of functionalised carbon nanotubes,” *Chem. Commun.* **2005**, 571. (d) G. Pastorin, W. Wu, S. Wieckowski, J-P. Briand, K. Kostarelos, M. Prato and A. Bianco, “Double functionalisation of carbon nanotubes for multimodal drug delivery,” *Chem. Commun.* **2006**, 1182.
13. (a) H. Fenniri, Bo-Liang Deng, A. E. Ribbe, K. Hallenga, J. Jacob and P. Thiyagaran, “Entropically driven self-assembly of multichannel rosette nanotubes,” *Proc. Natl. Acad. Sci. USA.* **2002**, *99*, 6487. (b) H. Fenniri, Bo-Liang Deng and A. E. Ribbe, “Helical rosette nanotubes with tunable chiroptical properties,” *J. Am. Chem. Soc.* **2002**, *124*, 11064.

14. J. G. Moralez, J. Ruez, T. Yamazaki, R. K. Motkuri, A. Kovalenko and H. Fenniri, "Helical rosette nanotubes with tunable stability and heirarchy," *J. Am. Chem. Soc.* **2005**, 127, 8309.
15. (a) L. J. Prins, E. E. Neuteboom, V. Paraschiv, M. Crego-Calama, P. Timmerman and D. N. Reinhoudt, "Kinetic stabilities of double, tetra-, and hexarosette hydrogen-bonded assemblies," *J. Org. Chem.* **2002**, 67, 4808. (b) M. G. J. Ten- cate, M. Omerovic, G. V. Oshovsky, M. Crego-Calama and D. N. Reinhoudt, "Self-assembly and stability of double nanostructures with biological functionalities," *Org. Biomol. Chem.* **2005**, 3, 3727. (c) V. Paraschiv, M. Crego-Calamas, R. H. Fokkens, C. J. Padberg, P. Timmerman and D. N. Reinhoudt, "Nanostructures via noncovalent synthesis: 144 hydrogen bonds bring together 27 components," *J. Org. Chem.* **2001**, 66, 8297.
16. (a) R. J. Bergeron and J. S. McManis, "Reagents for the stepwise functionalization of Spermine," *J. Org. Chem.* **1988**, 53, 3108. (b) H. Newman, "Trifluoroacetyl as a protecting group for 1-Halosugars," *J. Org. Chem.* **1965**, 30, 1287.
17. L. De Luca, G. Giacomelli and A. Porcheddu, "Beckman rearrangement of oximes under very mild conditions," *J. Org. Chem.* **2002**, 67 (17), 6272.
18. S. L. Hussey and B. R. Peterson, "Efficient delivery of streptavidin to mammalian Cells: Clathrin-mediated endocytosis regulated by a synthetic ligand," *J. Am. Chem. Soc.* **2002**, 124, 626 (and references there in).
19. P. S. Stayton, S. Freitag, L. Klumb, A. Chilkoti, V. Chu, J. Penzotti, R. To, D. Hyre, L. Le Trong, I. Lybrand and R. Stenkamp, "Streptavidin-biotin binding energetic," *Biomol. Eng.* **1999**, 16, 39.
20. F. J. Green, "Sigma-Aldrich handbook of stains dyes and indicators", **1990**, p 377.
21. R. Sjöback, J. Nygren and M. Kubista, "Absorption and fluorescence of fluorescein," *Spectrochimica Acta part A*, 51(1995), L7.

22. C. R. Cantor and P. R. Schimmel, "Biophysical chemistry", 1980, Freeman: New York.
23. (a) A. Kovalenko. Three-dimensional RISM theory for molecular liquids and solid-liquid interfaces, in: *Molecular Theory of Solvation*, F. Hirata (ed) Series: *Understanding Chemical Reactivity*, vol. 24, P. G. Mezey (ed.) Kluwer Academic Publisher, Dordrecht, 2003, pp. 169 – 275. (b) A. Kovalenko and F. Hirata, "Self-consistent description of a metal-water interface by the Kohn-Sham density functional theory and the three-dimensional reference interaction model site model," *J. Chem. Phys.* 1999, 110, 10095. (c) A. Kovalenko and F. Hirata, "Potential of mean force of simple ions in ambient aqueous solution II. Solvation structure from the three-dimensional reference interaction site model approach, and comparison with simulations," *J. Chem. Phys.* 2000, 112, 10391.
24. J. G. Moralez, J. Ruez, T. Yamazaki, R. K. Motkuri, A. Kovalenko and H. Fenniri, "Helical rosette nanotubes with tunable stability and Hierarchy," *J. Am. Chem. Soc.* 2005, 127, 8307.
25. R. S. Johnson, T. Yamazaki, A. Kovalenko and H. Fenniri, "Molecular basis for water-promoted supramolecular chirality inversion in helical rosette nanotubes," *J. Am. Chem. Soc.* 2007, 129, 5735.
26. A. Yu. Kasumov, D. V. Klinov, P-E. Roche, S. Guéron and H. Bouchiat, "Thickness and low temperature conductivity of DNA molecules," *Appl. Phys. Lett.* 2004, 84, 6, 1007.
27. M. Reches and E. Gazit, "Biological and chemical decoration of peptide nanostructures via Biotin-Avidin Interactions," *J. Nanosci. Nanotech.* 2007, 7, 2239.

Chapter 3: Radioactive Rosette Nanotubes

3.1. Introduction

Research into the delivery and targeting of therapeutics with nanoparticle agents is at the forefront of nanomedicine.¹ Suitable nanoparticulate delivery systems need to offer the desired biodistribution, an effective delivery of the cargo to the target, and adequate rate of clearance from the host. Our research group has shown that helical rosette nanotubes (HRNTs) are a promising orthopaedic implant material.² These findings, along with the recent investigation into the use of CNTs for the delivery of drugs,³ proteins, peptides,⁴ and nucleic acids⁵ led us to investigate the suitability of our RNTs for biomedical applications, more so, the delivery of drugs. In light of these potential biomedical applications of our RNTs their *in vivo* behavior needs to be elucidated. More specifically, the *in vivo* toxicological and pharmacological profiles of RNTs have to be established. Early research into the *in vitro* cytotoxicity of RNTs have shown that they neither reduce cell viability at moderate doses nor do they induce a time-dependent inflammatory response in pulmonary epithelial cells.⁶ The objective of this chapter is to synthesize RNTs that will be used to investigate their biomedical suitability and establish their pharmacological profile.

Recently, radioactive tracers have been used to determine the biocompatibility of nanoparticles.⁷ Thus, we decided to synthesize a radiolabeled derivative of our G[^]C motif which will subsequently be self-assembled into radioactive NTs. The renal imaging agent mercaptoacetyltriglycine (MAG₃) was chosen as the chelating ligand for the radioactive element.⁸ The MAG₃ ligand will be used to functionalize our G[^]C motif, then the self-assembly of the MAG₃-G[^]C conjugate will be studied to see if it forms RNTs (Fig 3.1). Once it is established that the MAG₃-G[^]C conjugate forms NTs, we will then proceed to label it with the radioactive element (^{99m}Tc) and study its self-assembly under physiological conditions. If radioactive NTs are formed, then *in vivo* biological studies will be

conducted to investigate the biodistribution and pharmacological profile of RNTs. The secondary objective of this chapter is to investigate what sort of effect, if any, would the hydrophobic characteristics of our RNTs have on the renal uptake of MAG_3 .

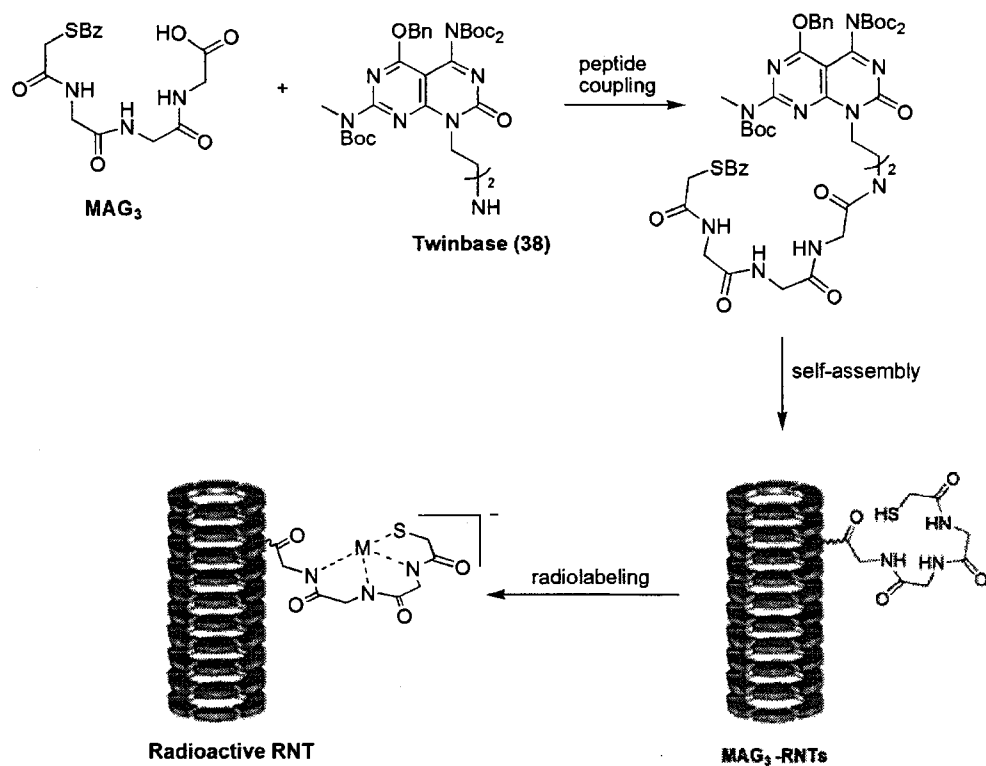


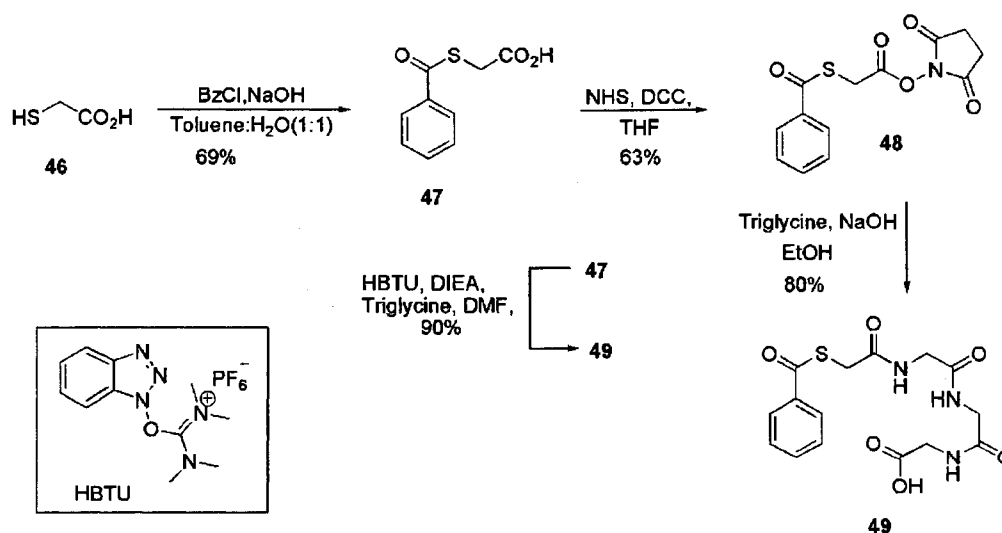
Figure 3.1. Scheme depicting the synthesis of radioactive RNTs.

3.2. Results and Discussion

3.2.1. Synthesis of MAG₃(49)

The MAG₃ complex was first synthesized by Fritzberg et al., at the University of Utah in 1986, as a potential replacement for radioiodinated *o*-iodohippuric acid (OIH) in renal function studies.⁸ It is currently commercially available in a kit formulation. Taylor et al.⁹ reported an alternative synthetic pathway for the synthesis of MAG₃ (Scheme 3.1).

The synthesis of the chelator **49** (MAG₃) began with the protection of the thiol functionality of commercially available thioglycolic acid, **46**, with benzoyl chloride to yield **47** (Scheme 3.1). The carboxylic acid functional group of **47** was converted to an NHS-activated ester using DCC and NHS to afford **48**. The terminal primary amine functionality of triglycine was coupled to the activated carboxyl group of **48** to afford MAG₃ (**49**) with a yield of 80%. This synthesis was optimized by simply reacting **47** with triglycine in the presence of HBTU and DIEA to afford **49** in 90% yield.¹⁰ This synthetic pathway avoids the generation of dicyclohexylurea (DCU), which is difficult to remove.



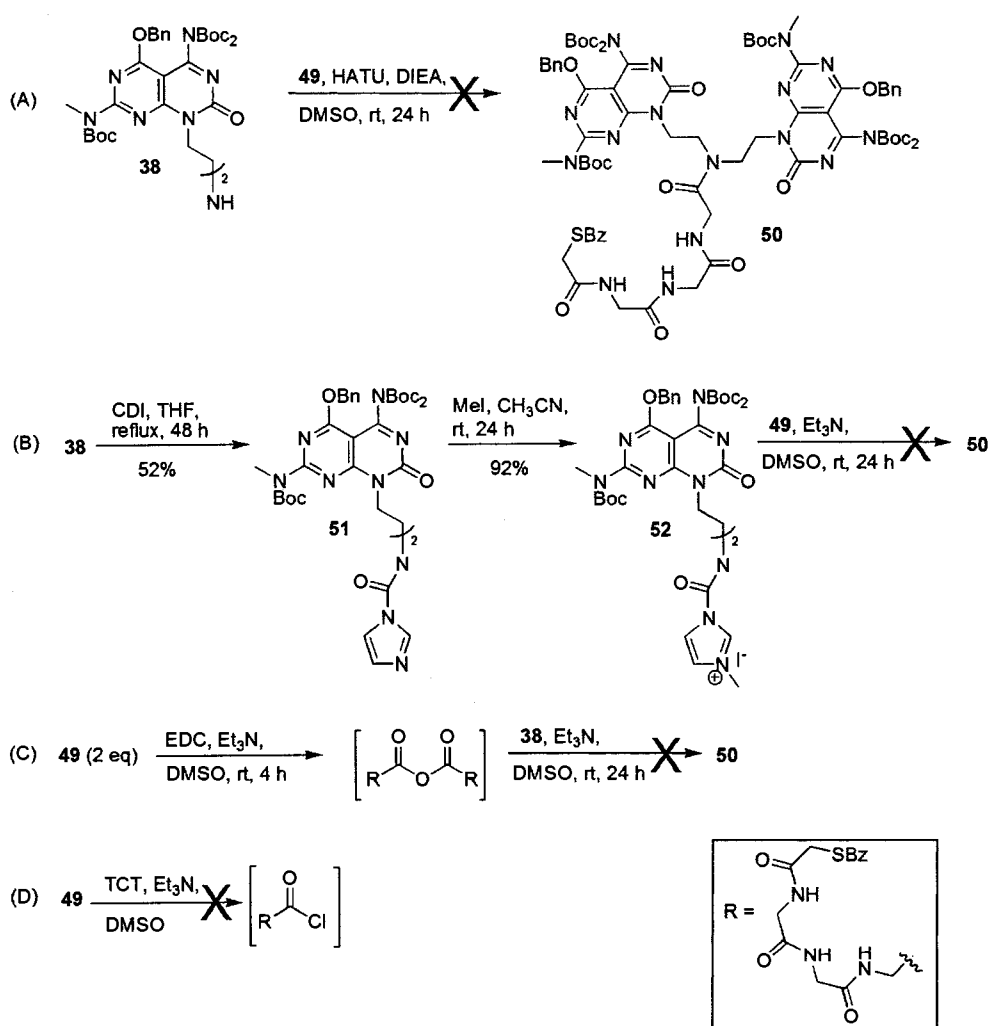
Scheme 3.1. Synthesis of Mercaptotriglycine (MAG₃) ligand, **49**.

3.3.2. Conjugation of MAG₃ (49) to Twinbase (38)

As mentioned previously, we first began by exploring the coupling of the G[^]C base **38** with the acid functionality of **49**. We soon discovered this to be quite a challenge as the synthesis of tertiary amides are much more difficult than those of secondary amides. A survey of the literature revealed that HATU is the most used reagent for the coupling of sterically hindered secondary amines with carboxylic acids.¹¹ Attempts to couple **38** and **49** in the presence of HATU were not successful; **38** was recovered after allowing the reaction to go for 24 h (Scheme 3.2). Heating the reaction to 50 °C for the same period of time did not change the outcome. LCMS revealed that **49** had reacted with HATU to form the activated ester intermediate; this would indicate that the secondary amino functionality of **38** was sterically hindered.

Batey et al., have reported that tertiary amides can be formed by employing carbamoylimidazolium salts.¹² This methodology entails converting the secondary amine to the electrophilic carbamoylimidazolium salt, and then to the tertiary amide by reaction with the carboxylate salt of the acid. The reaction of **38** with CDI under reflux for 2 days yielded only 51% of the target imidazole derivative, **51**, (Scheme 3.2.B), with the remaining starting material being recovered. Allowing the reaction to go for 5 days showed no improvement in the yield of product. The twinbase-imidazole derivative, **51**, was successfully methylated, producing the electrophilic carbamoylimidazolium salts **52**. Coupling of **49** and **52** was not successful; both were detected by LCMS after 24 h. Heating the reaction at 50 °C resulted in the same outcome as when the reaction was carried out at rt. The outcome of this reaction is somewhat perplexing, because the sterically hindered secondary amine **38** reacted with CDI, but the highly electrophilic carbamoylimidazolium salt, **52**, did not react with the carboxylate. The only plausible explanation for this observation is that triethylamine was not a strong enough base to deprotonate the carboxylic acid. In hindsight, a stronger, non-aqueous base should have been employed.

Increasing the reactivity of the carboxyl group of **49** was investigated as a way of forcing the reaction between **38** and **49**. To this end, attempts were made to convert the carboxylic acid functional group to the more reactive anhydride (symmetrical) or the even more reactive acyl chloride derivative (Scheme 3.2.C & D). The symmetric anhydride of **49** was generated by reacting 2 equivalents of **49** with 1-ethyl-3(3'-dimethylamino) carbodiimide HCl salt (EDC).¹³ Attempts to react the anhydride (not isolated) with **38** were not fruitful, **38** was recovered even after the reaction was heated for 24 h at 50 °C.



Scheme 3.2. Conjugation of MAG₃ to twinbase **38**.

The common method of generating acyl chlorides is to use thionyl or oxalyl chloride with a catalytic amount of DMF.¹⁴ These methodologies were not utilized because they produce HCl as a by-product, which would deprotect the Boc groups of **38**. It was reported that TCT in the presence of triethylamine converts carboxylic acids to acyl chlorides under basic condition.¹⁵ Reacting **49** with TCT to generate the acyl chloride derivative was not successful. It is very likely that the acyl chloride was not formed since attempts to trap it with butylamine showed no adduct. All of the above reactions were conducted in DMSO (Scheme 3.2) because of the insolubility MAG₃ in most common organic solvents (polar and non-polar). This may have had a small impact on the outcome of the forementioned reactions, however it is very likely that sterics was the main reason why coupling between **38** and **49** was not successful.

Attempts to conjugate MAG₃ to the twinbase, **38**, were eventually abandoned. We reasoned that the steric hindrance of **38** can be alleviated by appending amine linkers onto the G⁺C motif. To this end, two twinbase derivatives (**53** and **55**)

functionalized with *N*-Fmoc ethyl and butyl amino linkers were synthesized (Scheme 3.3). We also expected that the terminal primary amine should enhance the probability of reactivity. Unfortunately, coupling of the free amines of **53** and **55** with **49** in the presence of the coupling agent HBTU failed to yield the expected targets, **54** and **56**. Similar results were obtained when peptide coupling with HBTU was attempted

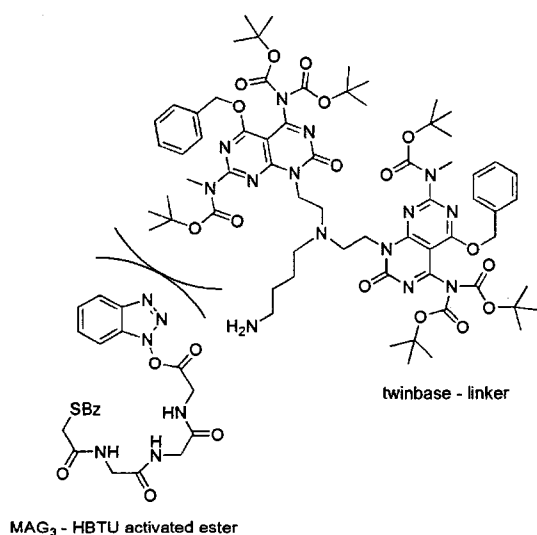
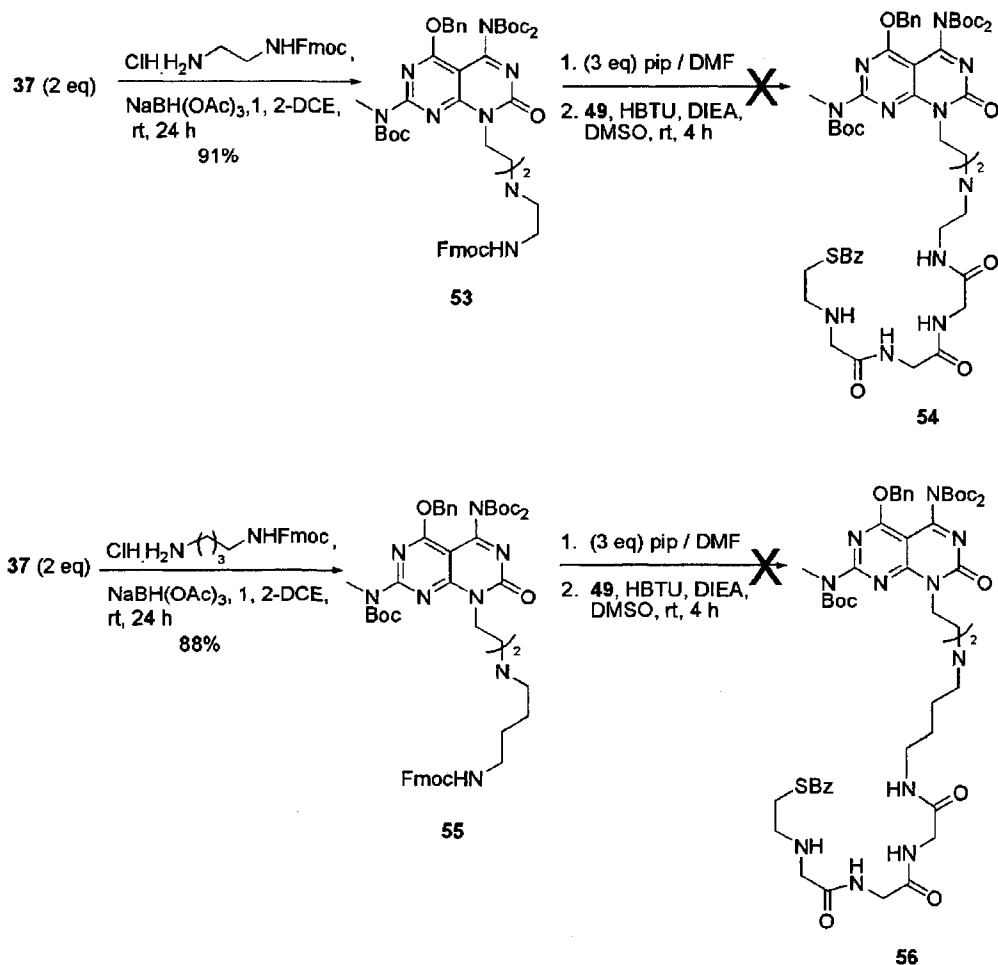


Figure 3.2. Steric interaction between twinbase and MAG₃ - HBTU activated ester.

with a twinbase motif functionalized with a hexylamino linker. We hypothesized that steric interactions between the twinbase G⁺C motif and the activated ester

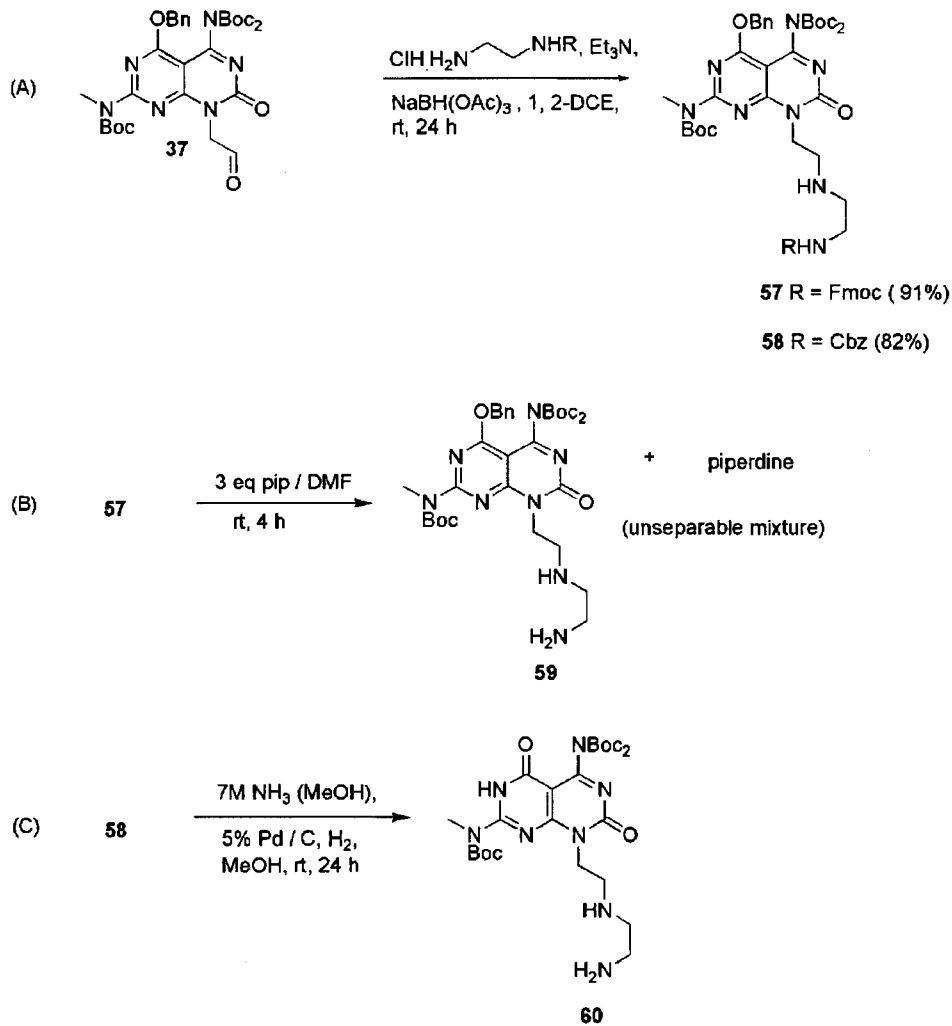
formed by reacting **49** with HBTU were responsible for the lack of reactivity (Fig 3.2). To test this hypothesis we decided to investigate whether MAG_3 would react with the free amine of a monobase derivative.



Scheme 3.3. Conjugation of MAG_3 to twinbases with amino linkers.

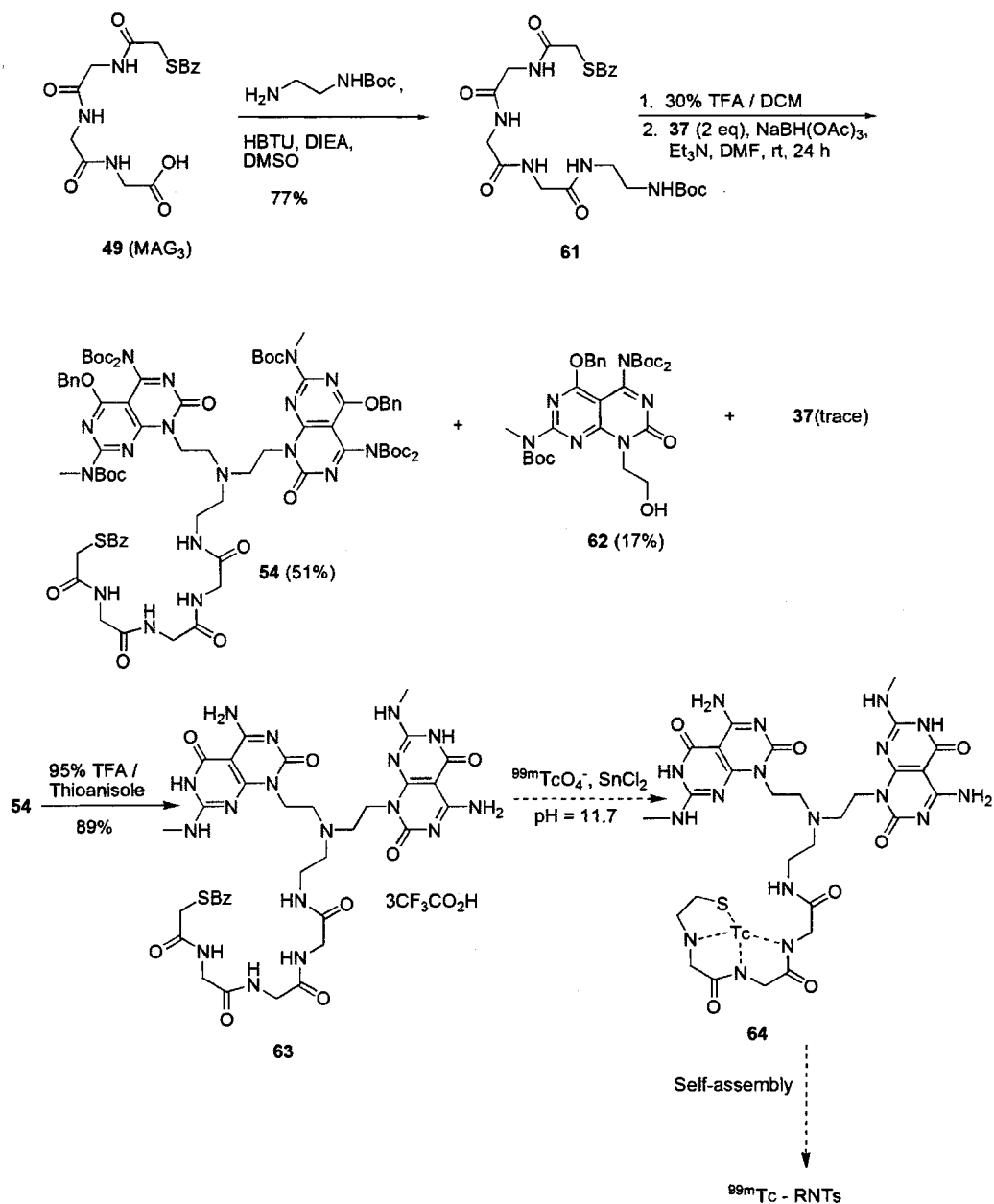
3.2.3. Conjugation of MAG_3 (49) to Monobase G[^]C derivatives

The synthesis of a monobase G[^]C derivative of **54** was attempted several times, but remained unsuccessful (Scheme 3.4). Chromatographic isolation of the free amine of the monobase derivative was extremely difficult. The problem was compounded by the inability to selectively remove the Cbz protecting group of the ethylamine linker without affecting the other protecting groups of the G[^]C motif (Scheme 3.4.C).



Scheme 3.4. Synthesis of the monobase G[^]C derivative of **54**.

We then suspected that if the ethylamino linker was appended onto MAG₃ then we could attach it to the G[^]C motif yielding a MAG₃-G[^]C monobase adduct. This adduct could then be coupled *in situ*, via reductive amination, to a second equivalent of G[^]C aldehyde (**37**) to afford the MAG₃ derivatized twinbase target, **54**, (Scheme 3.5).



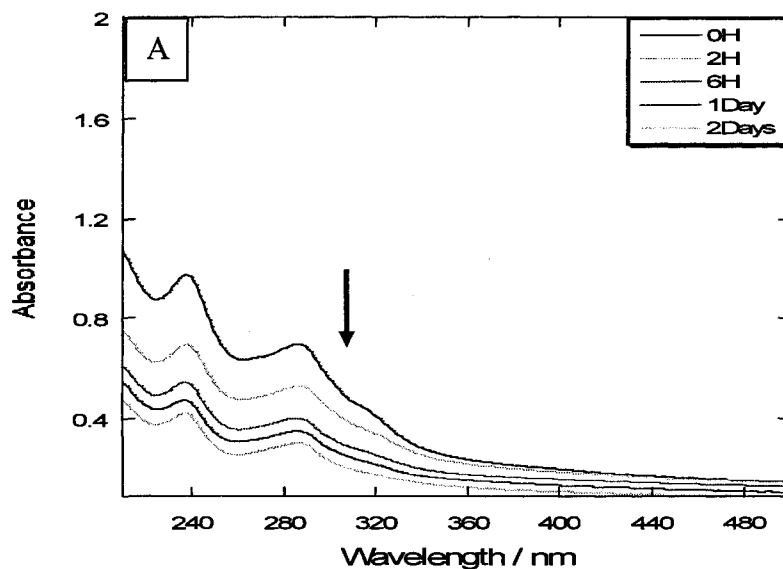
Scheme 3.5. Synthesis of radioactive nanotubes.

N-Boc diamoethane was successfully coupled to MAG₃ using HBTU in the presence of Hunig's base. The insolubility of the MAG₃ motif in most common organic solvents led us to purify **61** (Scheme 3.5) by precipitation with diethylether. The Boc group was deprotected quantitatively with 30% TFA/DCM,

and the ammonium salt was reacted with two equivalents of the G[^]C aldehyde (37) to afford the twinbase-MAG₃ adduct 54 in a yield of 51%. The successful coupling of MAG₃ to *N*-Boc diaminoethane and reaction of the MAG₃-G[^]C intermediate with a second equivalent of G[^]C aldehyde supports our hypothesis of steric hinderance of the free amino functionality of twinbase G[^]C motifs. The protected twinbase-MAG₃ derivative (54) was cleanly deprotected with 95% TFA/thioanisole to afford 63. The self assembly and characterization of 63 was then studied.

3.3. Microscopic characterization of unchelated RNTs (compound 63)

The MAG_3 metal chelator motif (49) showed very limited solubility in all solvents except DMF and DMSO, thus we anticipated that it would reduce the solubility of the G[^]C motif in water. However, once it is labeled, the resulting compound (64) would have a net negative charge making the resulting RNTs water soluble, thus facilitating biological studies. The self-assembly of compound 63 was studied by dissolving 1 mg in 1 mL of water (solubility limited) and 1 mL of DMSO separately. The 1 mg.mL⁻¹ water sample produce very poor SEM images because of small undissolved particulate matter which was distributed over most of the SEM grid. However, RNTs were visualized (Fig 3.3.B). DMSO proved to be a better solvent for characterization, thus 50 μL of a 1 mg.mL⁻¹ solution was diluted to 1 mL with DMSO and was used for electron microscopy studies. SEM provided visual evidence of RNT formation in DMSO, but more importantly in water. Self-assembly of RNTs were also studied by UV-vis spectroscopy, which revealed two characteristic maxima at 238 and 287 nm along with a hypochromic effect which indicates π - π stacking interactions between rosettes.



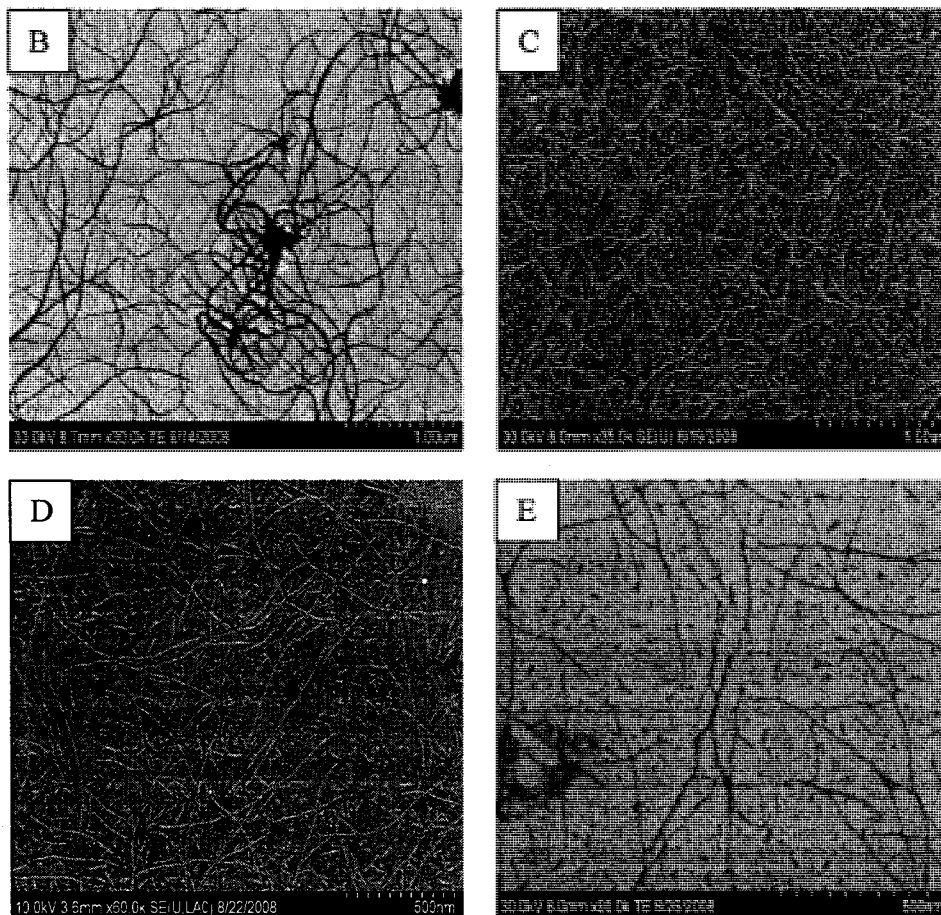


Figure 3.3. Non-representative SEM micrograph of compound **63** in water (A) time dependent UV-vis study in water. (B) 1mg.mL^{-1} after 2 days. Representative SEM micrographs from a 0.05 mg.mL^{-1} in DMSO (C) after 3 days (D) after 1 week (E) after 1 week stained with ua.

RNT diameter was found to be $3.2 \pm 0.3\text{ nm}$ and $3.8 \pm 0.1\text{ nm}$ using TM-AFM and TEM, respectively. The height profile (inset Fig 3.4.G) is in agreement with the measured diameter from TM-AFM. As stated in the previous chapter TM-AFM measurements are slightly less than TEM because of the compression from the AFM tip. The AFM data shows that all the NTs are about the same height.

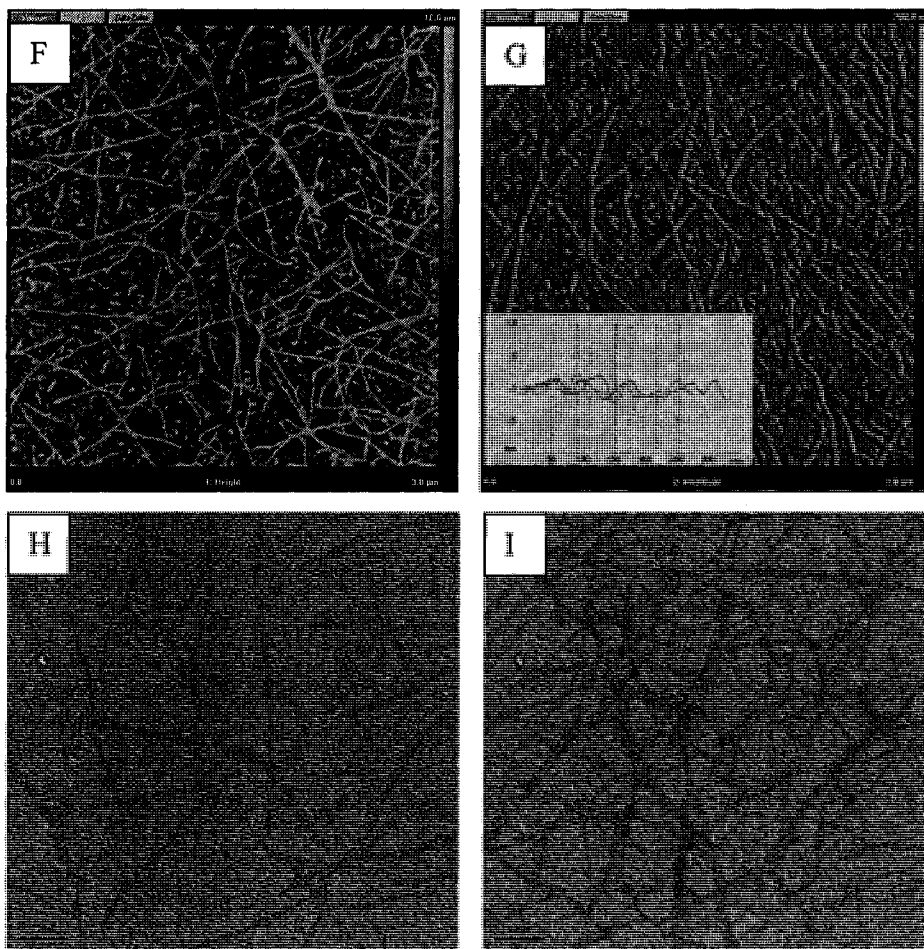
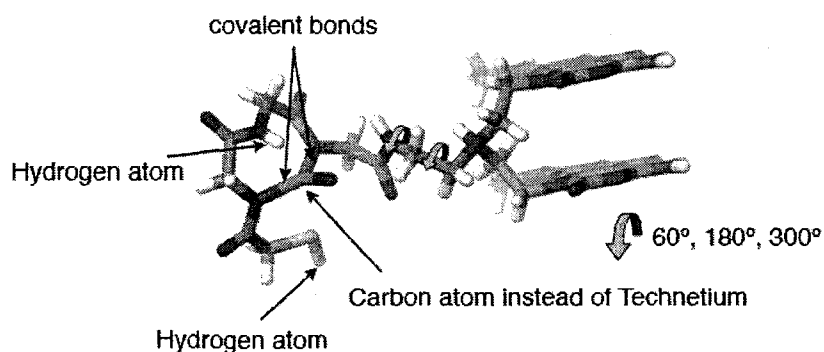


Figure 3.4. Representative TM-AFM (F and G with height profile inset) and TEM micrographs (H and I) of compound **63** ($0.05 \text{ mg}\cdot\text{mL}^{-1}$ DMSO, 1 week old solution). Scale bar = 50 nm.

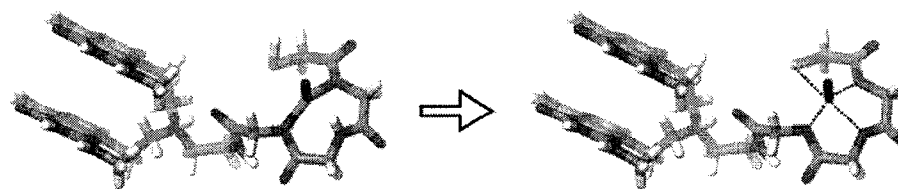
Once compound **63** was shown to self-assemble in water, the next step is to chelate the radioactive metal into the MAG_3 motif. A sample of compound **63** was submitted to our collaborators at the Cross Cancer Institute, University of Alberta for radioactive labeling, we are currently awaiting their findings. However, molecular modeling of the radioactive labeled G⁺C motif (**64**) was done to gain some insight about the physical parameters of the radioactive nanotubes. The calculated diameter was not expected to be too different from the experimental value of compound **63**, since chelation does not extend the molecular length of the MAG_3 component. Molecular modeling was conducted for **64** using macromodel

8.5. The following model (65) was used, since the motif includes a radioactive metal whose molecular parameters (Leonard-Jones sigma and epsilon) are not available in the literature.



65

In the above model, a carbon atom was connected to the three nitrogen and sulphur atoms instead of technetium, thus the total charge of the MAG_3 unit would change from -1 to 0. It is assumed that the MAG_3 orientation is determined mainly by the steric interaction in the nanotube; thus by changing the two dihedral angles indicated by the arrows, the MAG_3 group was sampled and optimized. During this conformational sampling the MAG_3 group was fixed according to x-ray conformation¹⁶ and the $\text{G}^{\wedge}\text{C}$ motif was also fixed according to previous modeling.¹⁷ The resulting 9 conformers were multiplied and arranged to form rosette nanotubes consisting of 7 double-rosette stacks. The energies of 9 RNTs in GB/SA water model were calculated and compared to obtain the most stable one. As a result, the following conformer (66) was found to be most stable.



motif conformation forming
the most stable RNT

66

The following is a representation of a radioactive rosette and nanotube as described by the modeling above. The covalent bonds between the carbon atom replacing the technetium and two nitrogen atoms are omitted, and the hydrogen atoms attached to the sulphur and nitrogen atoms are also omitted. The calculated diameter is about 1.0 nm greater than experimental measurement of 63.

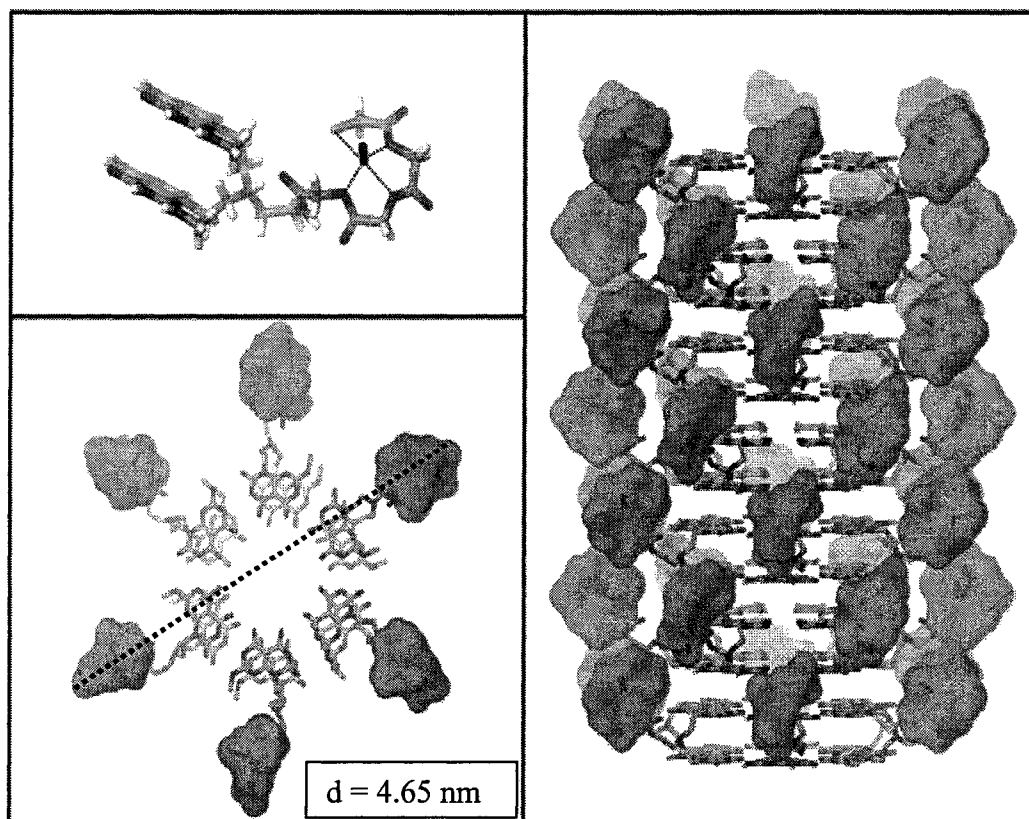


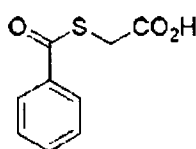
Figure 3.5. Molecular model of rosette and a RNT formed from radioactive labeled G^C motif (compound 64).

This was not expected, however this may be rationalized by the fact that some assumptions were made concerning the Leonard-Jones parameters of 64. TEM analysis of the actual radioactive NTs may provide measurements that are more in line with molecular modeling.

3.4. Conclusion and Future Work

We have demonstrated that **63**, the unchelated precursor of compound **64**, is capable of forming RNTs in water, thus we anticipate that the chelation of radioactive metals (^{188}Re and $^{99\text{m}}\text{Tc}$) should lead to the formation of radioactive RNTs under physiological conditions. It would be interesting to see what impact chelation would have upon the self-assembly and stability of the RNTs. Biological studies (*in vivo*) will provide us with very important pharmacokinetic data (biodistribution, toxicity, mechanism of cellular uptake) about our systems, and will define future biological applicability and limits of our systems. By mixing this system with other functionalize G[^]C motifs we may be able to self-assemble RNTs that are tagged with the radio-marker thus facilitating the monitoring of RNTs.

3.5. Experimental: Synthetic Procedures



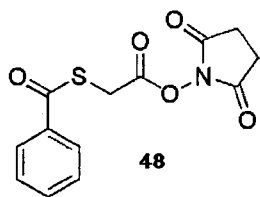
47

Sodium hydroxide, 8.8 g (0.22 mol) and 9.2 g (0.1 mol) thioglycolic acid were dissolved in a mixture of 75 mL toluene and 75 mL water and cooled in an ice bath to about 10 °C. Benzoyl chloride, 14.05 g (0.1 mol) was added over 30 min and stirring was continued for 30 min at 10 °C and an additional 30 min at room temperature. The organic layer was separated, washed four times with distilled water, and the combined aqueous layers were acidified to pH = 1.5 by the addition of concentrated hydrochloric acid. The precipitated product was filtered and dried under vacuum. Recrystallization from ethyl acetate gave compound 47 as white crystalline solid (C₉H₈O₃S, 13.30 g, 69%). mp = 102.8-103.6 °C (lit: 102-103 °C).¹⁸

¹H NMR (500 MHz, DMSO-*d*₆) δ (ppm): 7.93-7.60 (m, 5H), 3.9 (s, 2H).

¹³C NMR (500 MHz, DMSO-*d*₆) δ (ppm): 190.1, 169.5, 135.7, 134.1, 129.2, 126.8, 39.6, 39.0, 31.3.

HRMS (EI): Calcd mass for (M + H)⁺ / z = 196.0194, found (M + H)⁺ / z 196.0196 (3%), (M + H - OBz)⁺ / z 105.0340 (100%), (M + H - benzyl)⁺ / z 77.0394 (48.24%).



48

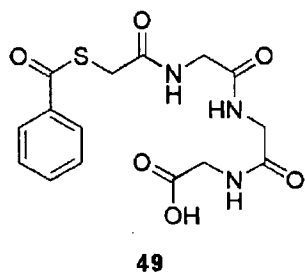
9.8 g (0.05 mol) of *S*-benzoylthioglycolic acid, 47, and 5.75 g (0.05 mol) of *N*-hydroxysuccinimide were dissolved in 60 mL of dry tetrahydrofuran and then cooled to -5 °C. Then 12.38 g (0.06 mol) of dicyclohexylcarbodiimide, dissolved in 20 mL of THF, was added over a period of 20 min. The reaction mixture was then stirred continuously for 2 h at -5 °C, then at room temperature for 13 h. Glacial acetic acid (0.2 mL) was then added

and the mixture was stirred for an additional hour, after which the product was separated from *N,N'*-dicyclohexylurea and the residue extracted twice with boiling THF. The combined filtrate was evaporated to dryness and the colorless residue was recrystallized from ethyl acetate to obtain compound **48** as colorless needles (C₁₃H₁₁NO₅S, 9.23 g, 63%). mp = 134.1-135.3 °C (lit: 135-137 °C).¹⁸

¹H NMR (500 MHz, DMSO-*d*₆) δ (ppm): 7.96-7.57 (m, 5H), 4.41 (s, 2H), 2.80 (s, 4H).

¹³C NMR (500 MHz, DMSO-*d*₆) δ (ppm): 189.0, 169.8, 165.3, 135.1, 134.5, 129.3, 127.0, 28.1, 25.4.

HRMS (ESI) Calcd mass for (M + Na)⁺ / z = 316.0250, found 316.0249.



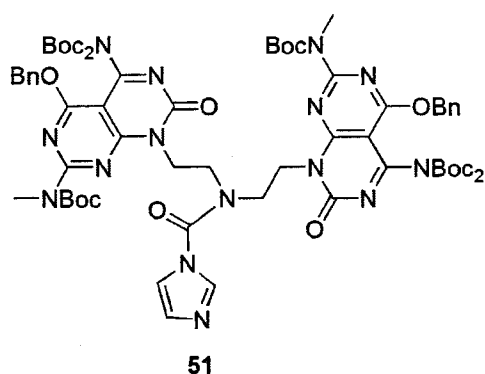
Triglycine, 2.83 g (15 mmol), was dissolved in 13 mL of water by the dropwise addition of 1 N NaOH. This solution was then added in one portion to a warm solution (~ 55 °C) of **48** (5.86 g, 20 mmol) in 120 mL of ethanol. The mixture was heated at reflux for 2.5 h and then stirred at room temperature for 12 h. The solvent was removed by evaporation (rotovap), and the colourless residue was extracted twice with boiling acetonitrile and recrystallized twice from 20% water in methanol to afford **49** (C₁₅H₁₇N₃O₆S, 4.30 g, 80%). mp = 194.2-195.4 °C (lit: 195-196 °C).¹⁸

Optimization: 100 mg of **47** (0.510 mmol), 196 mg of HBTU (0.510 mmol) and 71 μL of Et₃N (0.510 mmol) were dissolved in 5 mL of DMSO and stirred for 2 h. To this mixture was added 96.5 mg of triglycine (0.510 mmol) and the mixture was stirred for 24 h. Compound **49** was precipitated as a white solid using Et₂O in a yield of 90%.

^1H NMR (500 MHz, $\text{DMSO-}d_6$) δ (ppm) : 8.53 (t, $^3J = 5.9$ Hz, 1H), 8.22 (t, $^3J = 5.9$ Hz, 1H), 7.97 (t, $^3J = 5.6$ Hz, 1H), 7.93 (m, 2H), 7.68 (m, 1H), 7.55 (m, 2H), 3.87 (s, 2H), 3.77 (d, $^3J = 5.9$ Hz, 2H), 3.72 (d, $^3J = 5.9$ Hz, 2H), 3.63 (d, $^3J = 5.6$ Hz, 2H).

^{13}C NMR (500 MHz, $\text{DMSO-}d_6$) δ (ppm): 190.3, 171.2, 168.8, 168.6, 167.1, 135.9, 134.0, 129.1, 126.9, 42.4, 41.8, 41.5, 32.4.

HRMS (ESI) Calcd mass for $(\text{M} + \text{Na})^+ / z = 390.0730$, found 390.0729.

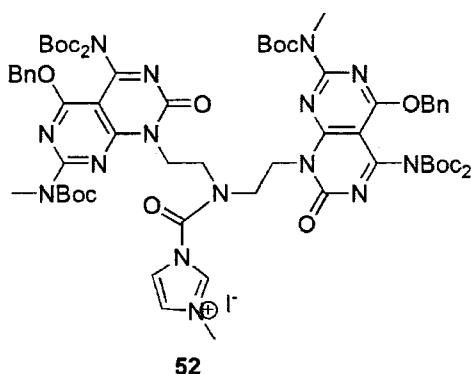


200 mg (0.158 mmol) of compound **38** and 28 mg (0.173 mmol) of N,N' -carbonyldiimidazole was dissolved in 30 mL of dry THF and was refluxed for 48 h. The reaction was quenched with distilled water, solvent removed under reduced pressure, and the residue was taken up in EA. The organic layer was separated, washed with brine and dried over anhydrous Na_2SO_4 . Filtration, followed by silica gel chromatography afford compound **51** as a yellow solid ($\text{C}_{66}\text{H}_{85}\text{N}_{15}\text{O}_{17}$, 159 mg, 74%). $R_f = 0.38$ (SiO_2 , 5% MeOH/ Et_2O), mp = 87°C .

^1H NMR (500 MHz, CDCl_3) δ (ppm): 7.55 (s, 1H), 7.43-7.30 (m, 10H), 7.05 (s, 1H), 6.71 (s, 1H), 5.55 (s, 4H), 4.55 (s, br, 4H), 4.07 (s, br, 4H), 3.41 (s, 6H), 1.57 (s, 18H), 1.27 (s, 36H).

^{13}C NMR (500 MHz, CDCl_3) δ (ppm): 165.5, 161.0, 160.8, 152.1, 149.1, 134.8, 128.5, 128.3, 125.5, 93.0, 83.8, 83.0, 70.1, 67.9, 65.8, 40.8, 34.8, 30.3, 29.6, 28.1, 27.7, 25.6, 15.2.

HRMS (ESI) Calcd mass for (M + H)⁺ / z = 1360.6318, found 1360.6321.



52

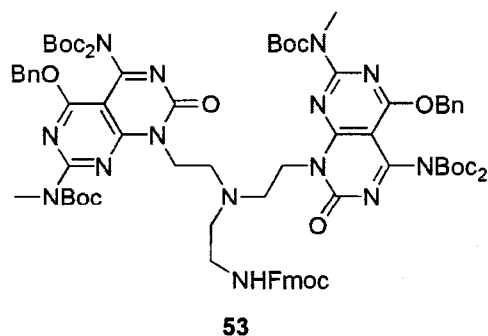
159 mg (0.117 mmol) of compound **51** was dissolved in 5 mL of acetonitrile and 36 μ L (0.585 mmol) of iodomethane was added and the reaction was allowed to stir for 24 h at room temperature. The solvent along with residual iodomethane were removed under vacuum (rotovap) to afford **52** as a viscous yellow oil (C₆₇H₈₈N₁₅O₁₇I, 148 mg, 92%).

159 mg (0.117 mmol) of compound **51** was dissolved in 5 mL of acetonitrile and 36 μ L (0.585 mmol) of iodomethane was added and the reaction was allowed to stir for 24 h at room temperature. The solvent along with residual iodomethane were removed under vacuum (rotovap) to afford **52** as a

¹H NMR (400 MHz, DMSO-*d*₆) δ (ppm) : 9.43 (s, 1H), 7.85 (s, 1H), 7.68 (s, 1H), 7.41-7.30 (m, 10H), 5.58 (s, 4H), 4.55 (s, br, 2H), 4.35 (s, br, 2H), 3.89 (s, br, 5H), 3.74 (s, br, 2H), 3.41 (s, 6H), 1.51 (s, 18H), 1.26 (s, br, 36H).

HRMS (ESI) Calcd mass for (M + H)⁺ / z = 1374.6475, found 1374.6477.

148 mg (0.108 mmol) of compound **52**, 40 mg of **49** (0.108 mmol) and 30 μ L of Et₃N (0.220 mmol) were dissolved in 5 mL of DMSO via sonication and stirred for 24 h. TLC and LCMS analysis revealed that the expected target, **50**, was not produced.



53

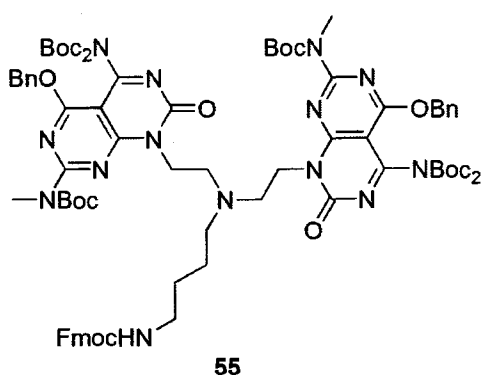
25 mg of *N*-Fmoc-ethylenediamine hydrochloride (0.078 mmol) and 22.0 μ L of Et₃N (0.156 mmol) were mixed in 10 mL of 1, 2-DCE for ~ 10 min, after which 50 mg of **37** (0.078 mmol) and 21.5 mg of NaBH(OAc)₃ (0.101 mmol) were added, and the reaction was allowed to stir over night. After TLC and LCMS showed that the reaction was completed another

equivalent of **37** and 1.3 equivalents of NaBH(OAc)₃ were then added and the reaction was stirred for another 24 h at rt. The reaction was quenched by adding 10 mL dH₂O and the solvent was removed under reduced pressure, and the resulting yellow residue was taken up in 20 mL Et₂O, washed with 10 mL of brine and dried over anhydrous Na₂SO₄. Filtration, followed by silica gel chromatography (10% MeOH /DCM) yielded **53** (C₇₉H₉₈N₁₄O₁₈, 109 mg, 91%) as a pale yellow solid. R_f = 0.79 (SiO₂, 10% MeOH/DCM).

¹H NMR (400 MHz, CDCl₃) δ (ppm) : 7.71-7.28 (m, 19H), 5.78 (s, br, 1H), 5.57 (s, 4H), 4.39 (t, ³J = 7.2 Hz, 4H), 4.33 (d, ³J = 7.3 Hz, 2H), 4.23 (t, ³J = 7.3 Hz, 1H), 3.47 (s, 6H), 3.31 (t, ³J = 5.6 Hz, 2H), 2.96 (t, ³J = 7.2 Hz, 4H), 2.88 (t, ³J = 5.6 Hz, 2H), 1.54 (s, 18H), 1.32 (s, 36H).

¹³C NMR (600 MHz, CDCl₃) δ (ppm): 165.6, 161.2, 161.0, 160.3, 156.5, 155.6, 152.5, 149.3, 144.1, 141.2, 134.9, 128.5, 128.5, 128.5, 127.5, 127.0, 125.2, 119.8, 92.8, 83.7, 82.9, 70.1, 66.5, 60.37, 53.8, 50.8, 47.3, 41.2, 34.9, 28.1, 27.8.

HRMS (ESI) Calcd mass for (M + H)⁺ / z = 1531.7256, found 1531.7253.



54.2 mg of *N*-Fmoc-butylenediamine hydrochloride (0.156 mmol) and 217 μL of Et₃N (1.25 mmol) were mixed in 15 mL of 1,2-DCE for ~ 10 min, after which 100 mg of **37** (0.156 mmol) and 43.06 mg of NaBH(OAc)₃ (0.203 mmol) were added, and the reaction was stirred over night. TLC and LCMS showed that the reaction was completed, then another equivalent of **37** and 1.3 equivalents of NaBH(OAc)₃ were added and the mixture was allowed to stir for another 24 h at rt. The reaction was quenched by the addition of 10 mL of dH₂O, solvent was

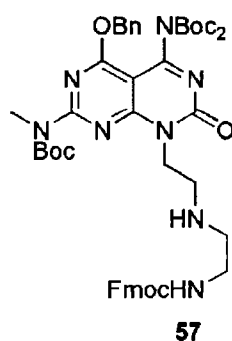
removed under reduced pressure and the yellow residue was taken up in Et₂O, washed with brine and dried over anhydrous Na₂SO₄. Filtration, followed by silica gel chromatography (0-10% MeOH/DCM) afforded compound **55** (C₈₁H₁₀₂N₁₄O₁₈, 214 mg, 88%) as a pale yellow solid. R_f = 0.45 (SiO₂, 5% MeOH /DCM).

¹H NMR (500 MHz, CDCl₃) δ (ppm) : 7.74-7.28 (m, 18H), 5.57 (s, 4H), 4.41 (t, ³J = 7.3 Hz, 4H), 4.34 (d, ³J = 7.2 Hz, 2H), 4.21 (t, ³J = 7.2 Hz, 1H), 3.48 (s, 6H), 3.17 (s, br, 2H), 2.93 (t, ³J = 7.3 Hz, 4H), 2.70 (s, br, 2H), 1.56 (s, 18H), 1.48 (m, 5H), 1.31(s, 36H).

¹³C NMR (500 MHz, CDCl₃) δ (ppm): 165.6, 161.2, 161.0, 160.3, 156.5, 155.6, 152.5, 149.3, 144.1, 141.2, 134.9, 128.5, 128.5, 128.5, 127.5, 127.0, 125.2, 119.8, 92.8, 83.7, 82.9, 70.0, 66.5, 60.4, 53.8, 50.8, 47.3, 41.2, 35.0, 28.1, 27.8, 27.5, 24.9.

HRMS (ESI) Calcd mass for (M + H)⁺ / z = 1559.7569, found 1559.7576.

Deprotection of **53** and **55** were successful carried out with 3 equivalents of piperidine and their respective free amines were isolated by silica gel chromatography using (0-10% MeOH/DCM). Coupling of 1 equivalent of the free amines of **53** and **55** with 1 equivalent of **49** in the presence of HBTU were not successful, the free amines were recovered after 24 h.



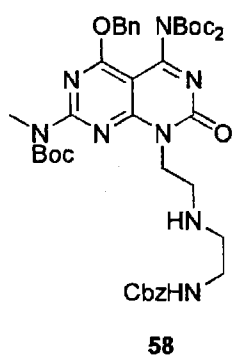
25 mg of *N*-Fmoc-ethylenediamine hydrochloride (0.078 mmol) and 22.0 μL of Et₃N (0.156 mmol) were mixed in 10 mL of 1,2-DCE for ~ 10 min, after which 50 mg of **37** (0.078 mmol) and 21.5 mg of NaBH(OAc)₃ (0.101 mmol) were added and the reaction was allowed to stir overnight.

TLC and LCMS were used to monitor the reaction progress. The reaction was quenched by adding 10 mL dH₂O and the solvent was removed under reduced pressure, and the resulting yellow residue was taken up in 20 mL Et₂O, washed with 10 mL of brine and dried over anhydrous Na₂SO₄. Filtration, followed by silica gel chromatography (10% MeOH/DCM) yielded **57** (C₄₈H₅₈N₈O₁₀, 64 mg, 91%) as a pale yellow solid. R_f = 0.36 (SiO₂, 10% MeOH/DCM).

¹H NMR (600 MHz, CDCl₃) δ (ppm) : 7.75-7.28 (m, 13H), 5.55 (s, 2H), 5.31 (s, br, 1H), 4.45 (t, ³J = 5.9 Hz, 2H), 4.34 (d, ³J = 6.8 Hz, 2H), 4.20 (t, ³J = 6.8 Hz, 1H), 3.44 (s, 6H), 3.25 (s, br, 2H), 3.02 (s, br, 2H), 2.79 (s, br, 2H), 1.52 (s, 9H), 1.26 (s, 18H).

¹³C NMR (600 MHz, CDCl₃) δ (ppm) : 170.4, 165.8, 165.8, 165.6, 165.6, 165.2, 159.8, 159.4, 157.8, 157.7, 154.3, 154.0, 152.7, 150.3, 140.2, 133.5, 133.1, 133.0, 97.4, 97.2, 88.8, 88.6, 88.0, 87.9, 74.8, 66.9, 66.3, 39.9, 39.8, 32.8, 32.7, 32.6.

LRMS (ESI) Calcd mass for (M + H)⁺ / z = 904.43, observed 906.40



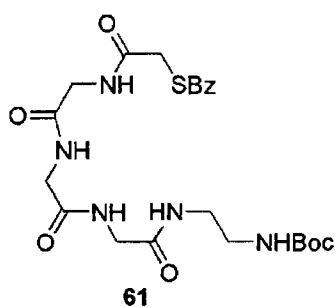
86.5 mg of *N*-Cbz ethylenediamine (0.373 mmol) and 86 μL of Et₃N (0.625 mmol) were mixed in 15 mL of THF for ~ 10 min. 200 mg of **37** (0.312 mmol) and 132 mg of NaBH(OAc)₃ (0.625 mmol) were then added to the mixture and stirred overnight. TLC and LCMS showed that the reaction was completed. The reaction was quenched with dH₂O, solvent removed under reduced pressure, and

the residue was taken up in Et₂O. The organic phase was washed with brine and dried over anhydrous Na₂SO₄. Filtration, followed by silica gel chromatography (0-10% MeOH/DCM) afforded **58** (C₄₁H₅₄N₈O₁₀, 209 mg, 82%) as a viscous yellow oil. R_f = 0.44 (SiO₂, 10% MeOH/DCM).

^1H NMR (600 MHz, CDCl_3) δ (ppm) : 7.40-7.27 (m, 10H), 5.83 (s, 2H), 5.02 (s, 2H), 4.47 (t, $^3J = 5.6$ Hz, 2H), 3.42 (s, 3H), 3.30 (t, $^3J = 2.5$ Hz, 2H), 3.09 (t, $^3J = 5.6$ Hz, 2H), 2.87 (s, br, 2H), 1.53 (s, 9H), 1.30 (s, 18H).

^{13}C NMR (600 MHz, CDCl_3) δ (ppm) : 165.7, 161.2, 160.9, 160.5, 156.7, 155.9, 152.5, 149.4, 136.6, 134.8, 128.5, 128.5, 128.4, 128.2, 128.0, 127.9, 93.1, 83.8, 83.2, 70.1, 66.5, 48.5, 46.6, 42.1, 39.7, 34.8, 28.0, 27.6.

HRMS (ESI) Calcd mass for $(\text{M} + \text{H})^+ / z = 819.4039$, found 819.4036.



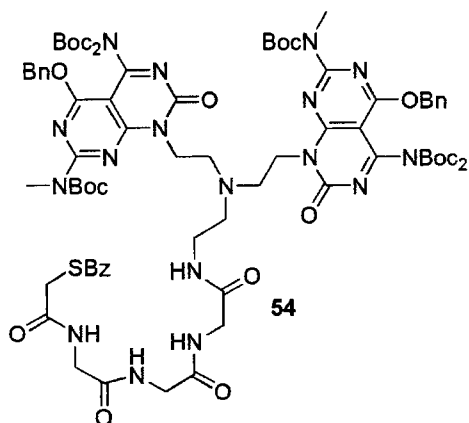
44 mg of *N*-Boc ethylenediamine (0.273 mmol), 100 mg of **49** (0.273 mmol), 103 mg of HBTU (0.273 mmol) and 72 μL of Et_3N were dissolved in 4 mL of DMSO and stirred at rt for 4 h. LCMS was used to monitor the reaction. Addition of Et_2O precipitated **61** ($\text{C}_{22}\text{H}_{31}\text{N}_5\text{O}_7\text{S}$, 107 mg, 77%) as a white solid, which was subsequently washed with DCM. mp = 223.2 $^\circ\text{C}$ (decomposed).

^1H NMR (500 MHz, $\text{DMSO}-d_6$) δ (ppm): 8.47 (t, $^3J = 5.3$ Hz, 1H), 8.21 (t, $^3J = 6.6$ Hz, 1H), 8.08 (t, $^3J = 5.9$ Hz, 1H), 7.94 (m, 2H), 7.70 (m, 1H), 7.56 (m, 2H), 7.78 (t, $^3J = 5.7$ Hz, 1H), 6.78 (t, $^3J = 5.6$ Hz, 1H), 3.88 (s, 2H), 3.77 (d, $^3J = 5.6$ Hz, 2H), 3.74 (d, $^3J = 5.7$ Hz, 2H), 3.65 (d, $^3J = 5.9$ Hz, 2H), 3.06 (td, $J = 6.2$ Hz, 2H), 2.95 (td, $J = 6.2$ Hz, 2H), 1.36 (s, 9H).

^{13}C NMR (600 MHz, $\text{DMSO}-d_6$) δ (ppm): 190.8, 169.6, 169.5, 169.3, 167.7, 156.1, 136.4, 134.5, 129.6, 127.3, 78.2, 43.0, 42.6, 42.4, 39.2, 32.9, 28.6.

HRMS (ESI) Calcd mass for $(\text{M} + \text{H})^+ / z = 532.1836$, found 532.1834.

Quantitative deprotection of the Boc group was accomplished with 30 TFA / DCM over a 4 h period. Addition of Et₂O precipitated the ammonium salt of **61**, which was washed with DCM to afford a mild pink solid.



163 mg of the TFA salt of **61** (0.313 mmol) and 132 μ L of Et₃N (0.964 mmol) were dissolved in 10 mL DMF via sonication. To this mixture was added 400 mg of **37** (0.625 mmol) and the solution was stirred for ~ 10 min, after which 272 mg of NaBH(OAc)₃ (1.28 mmol) was added and the mixture was stirred at rt for

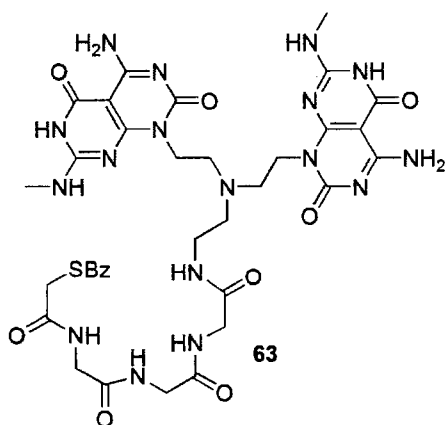
24 h. TLC and LCMS were used to monitor the reaction. DMF was removed under reduce pressure and the viscous yellow residue was dissolved in EA, washed with dH₂O, brine, and dried over anhydrous Na₂SO₄. Filtration, followed by silica gel chromatography (0-5% MeOH/DCM) afforded **54** (C₇₉H₁₀₃N₁₇O₂₁S – CH₃OH, 269 mg, 51%) and **62** (C₃₁H₄₂N₆O₉, 68 mg, 17 %) with trace amount of unreacted aldehyde, **37**. R_f = 0.42 (SiO₂, 5% MeOH/DCM). mp = 88.8-89.3 °C.

¹H NMR (600 MHz, CD₃OD) δ (ppm) : 7.88-7.31 (m, 15H), 5.60 (s, 4H), 4.32 (t, ³J = 7.3 Hz, 4H), 3.92 (s, br, 4H), 3.85 (s, br, 4H), 3.44 (s, 6H), 3.29 (m, 2H), 2.97 (s, 2H), 2.93 (t, ³J = 7.0 Hz, 4H), 2.86 (s, 2H), 2.82 (t, ³J = 7.3 Hz, 4H), 1.54 (s, 18H), 1.28 (s, 36H).

¹³C NMR (600 MHz, CD₃OD) δ (ppm) : 190.8, 170.8, 170.6, 170.1, 169.8, 165.7, 161.55, 160.8, 160.5, 156.3, 152.5, 149.3, 136.3, 136.1, 135.0, 133.7, 128.6, 128.3, 128.3, 126.9, 92.9, 84.2, 83.0, 70.1, 51.3, 42.9, 42.5, 42.2, 41.5, 37.6, 35.5, 34.3, 32.1, 27.1, 26.7.

HRMS (ESI) Calcd mass for (M + H)⁺ / z = 1658.7308, found 1658.7315.

Elemental analysis: Calcd for $[C_{79}H_{103}N_{17}O_{21}S - CH_3OH]$ C 56.83, H 6.38, N 14.08, S 1.90. Found: C 56.51, H 6.29, N 13.95, S 1.94.



200 mg (0.121 mmol) of **54** was dissolved in 5 mL of 95% TFA/thioanisole and stirred at room temperature for 4 h. LCMS analysis revealed that the reaction was completed. Addition of Et_2O precipitated the product which was purified by extensive washing with Et_2O and DCM, to afford **63** ($C_{35}H_{44}N_{17}O_9S - (CF_3COOH)_3 - H_2O$, 132 mg, 89%) as a white solid. mp = decomposed at 287 °C.

1H NMR (600 MHz, $DMSO-d_6$) δ (ppm) : 12.38 (s, br, 1H), 9.16 (s, 2H), 9.04 (s, br, 1H), 8.50 (m, 2H), 8.33-8.22 (m, 3H), 8.13 (m, 1H), 7.90 (m, 3H), 7.70 (m, 2H), 7.55 (m, 3H), 4.40 (s, br, 4H), 4.30 (s, 1H), 3.87 (s, 4H), 3.78-3.65 (m, 8H), 3.45-3.30 (m, 4H), 2.88 (s, br, 6H).

^{13}C NMR (600 MHz, $DMSO-d_6$) δ (ppm): 190.7, 170.3, 169.8, 167.8, 161.7, 160.2, 156.5, 156.0, 148.7, 136.3, 134.5, 129.5, 127.3, 82.8, 49.9, 42.7, 42.6, 40.4, 36.8, 32.9, 28.4.

HRMS (MALDI) Calcd mass for $(M + H)^+ / z = 878.3223$, found 878.3224.

Elemental analysis: Calcd for $[C_{35}H_{44}N_{17}O_9S - (CF_3COOH)_3 - H_2O]$ C 39.78, H 3.91, N 19.23, S 2.59. Found: C 39.77, H 3.97, N 18.88, S 2.87.

3.6. References

1. D. F. Emerich; C. G. Thanos, "Targeted nanoparticle-based drug delivery and diagnosis," *J. Drug. Target.* **2007**, 15, 163.
2. (a) A. Chung, J. G. Morales, T. J. Webster and H. Fenniri, "Helical rosette nanotubes: A biomimetic coating for orthopaedics?" *Biomaterials*, **2005**, 26, 7304. (b) A. Chung, J. G. Morales, T. J. Webster and H. Fenniri, "Helical rosette nanotubes: A more effective orthopaedic implant material," *Nanotechnology*, **2004**, 15, S234.
3. W. Wu, S. Wieckowski, G. Pastorin, M. Benincasa, C. Klump, J-P. Briand, R. Gennaro, M. Prato, A. Bianco, "Targeted delivery of amphotericin B to cells by using functionalized carbon nanotubes," *Angew. Chem. Int. Ed. Engl.* **2005**, 44, 6358.
4. B. F. Erlanger, B-X. Chen, M. Zhu and L. Brus, "Binding of an anti-fullerene IgG monoclonal antibody to single wall carbon nanotubes," *Nano. Lett.* **2001**, 1, 465.
5. N. W. Shi Kam, Z. Liu and H. Dai, "Carbon nanotubes as intracellular transporters for proteins and DNA: An investigation of the uptake mechanism and pathway," *Angew. Chem. Int. Ed. Engl.* **2006**, 45, 577.
6. W. S. Journey, S. S. Suri, J. G. Morales, H. Fenniri and B. Singh, "Low inflammatory activation by self-assembling rosette nanotubes in human calu-3 pulmonary epithelial cells," *Small*, **2008**, 4, 6, 817.
7. a) D. W. Cagle, S. J. Kennel, S. Mirzadeh, J. M. Alford, and L. J. Wilson, "In vivo studies of fullerene-based materials using endohedral metallofullerene radiotracers," *Proc. Natl. Acad. Sci. USA.* **1999**, 96, 5182. (b) R. Singh; D. Pantarotto; L. Lacerda; G. Pastorin; C. Klump; M. Prato; A. Bianco and K. Kostarelos, "Tissue biodistribution and blood clearance rates of intravenously administered carbon nanotube radiotracers," *Proc. Natl. Acad. Sci. USA.* **2006**, 103, 3357. (c) E. J. Petersen; Q. Huang and W. J. Webber, "Ecological uptake and depuration

- of carbon nanotubes by lumbriculus variegates,” *Environ. Health perspective*, **2008**, 4, 496. (d) J. Guo; X. Zhang; Q. Li and W. Li, “Biodistribution of functionalize multiwall carbon nanotubes in mice,” *Nucl. Med. Biol.* **2007**, 34, 579.
8. A. R. Fritzberg, S. Kasina, D. Eshima and D. L. Johnson, “Synthesis and biological evaluation of technetium-99m MAG3 as a hippuran replacement,” *J. Nucl. Med.* **1986**, 27(1), 111.
 9. W. Brandau, B. Bubeck, M. Eisenhut and D. M. Taylor, “Technetium-99m labeled renal function and imaging agents: III. Synthesis of ^{99m}Tc – MAG₃ and biodistribution of by-products,” *Appl. Radiat. Isot.* **1988**, vol. 39, # 2, 121.
 10. L. A. Carpino, A. El-Faham and F. Albericio, “Racemization studies during solid-phase peptide synthesis using azabenzotriazole base coupling reagents,” *Tetrahedron Lett.* **1994**, 35, 2279.
 11. (a) F. Albericio, J. M. Bofill, A. El-Faham and S. A. Kates, “Use of onium salt-bases coupling reagents in peptide synthesis,” *J. Org. Chem.* **1998**, 63, 9678. (b) L. A. Carpino, “1-hydroxy-7-azabenzotriazole. An efficient peptide coupling additive,” *J. Am. Chem. Soc.* **1993**, 115, 4397.
 12. (a) J. A. Grzyb and R. A. Batey, “Carbamoylimidazolium salts as diversification reagents: an application to the synthesis of tertiary amides from carboxylic acid,” *Tetrahedron Lett.* **2003**, 44, 7485. (b) R. A. Batey, C. Yoshima-Ishii, S. D. Taylor and V. Santhakumar, “A new protocol for the formation of carbamates and thiocarbamates using carbamoyl imidazolium salts,” *Tetrahedron Lett.* **1999**, 40, 2669.
 13. M. Mikolajczyk and P. Kielbasinski, “Recent development in the carbodiimide chemistry,” *Tetrahedron*, **1981**, 37, 233.
 14. (a) J. Wolfe, A. Muehldorf and J. Rebek, “Convergent functional groups create microenvironment for enolization catalysis,” *J. Org. Chem.* **1991**, 42, 1653. (b) P. L. White, D. M. Hegsted and J. Mayer, “Two complex

- salts of choline and copper and their activity as catalyst of fat oxidation,” *J. Am. Chem. Soc.* **1953**, 75, 2347.
15. (a) K. Venkataraman and D. R. Wagle, “Cyanuric chloride: a useful reagent for converting carboxylic acids into chlorides, esters, amides and peptides,” *Tetrahedron Lett.* **1979**, 20, 3037. (b) H. L. Rayle and L. Fellmeth, “Development of a process for triazine-promoted amidation of carboxylic acids,” *Org. Proc. Res. Dev.* **1999**, 3, 172.
16. G. Grummon, R. Rajagopalan, G. J. Palenik, A. E. Koziol, and D. L. Nosco, “Synthesis, Characterization and Crystal Structures of Technetium(V)-Oxo complexes useful in nuclear medicine. 1. Complexes of mercaptoacetylglycylglycylglycine (MAG3) and Its methyl ester derivative (MAG3OMe),” *Inorg. Chem.* **1995**, 34, 1764.
17. J. G. Moralez, J. Ruez, T. Yamazaki, R. K. Motkuri, A. Kovalenko, and H. Fenniri, “Helical rosette nanotubes with tunable stability and hierarchy,” *J. Am. Chem. Soc.* **2005**, 127, 8307.
18. R. F. Schneider, G. Subramanian, T. A. Field, J. G. McAfee, C. Zapf-Longo, E. Palladino and F. D. Thomas, “*N,N'*-bis(S-Benzoylmercaptoacetamido) ethylenediamine and propylenediamine ligands as renal function imaging agent: I. Alternate synthetic methods,” *J. Nucl. Med.* **1984**, 25, 233.